

# *Fabrication Procedures and Process Sensitivities for CdS/CdTe Solar Cells*

Doug H. Rose\*, Falah S. Hasoon, Ramesh G. Dhere, Dave S. Albin, Rosine M. Ribelin, Xiaonan S. Li, Yoxa Mahathongdy, Tim A. Gessert† and Pete Sheldon

*National Renewable Energy Laboratory, 1617 Cole Blvd, Golden, CO 80401, USA*

*This paper details the laboratory processes used to fabricate CdS/CdTe solar cells at the National Renewable Energy Laboratory. The basic fabrication technique includes low-pressure chemical vapor deposited SnO<sub>2</sub>, chemical-bath deposited CdS, close-spaced sublimated CdTe, solution-CdCl<sub>2</sub> treatment, and an acid-contact etch, followed by application of a doped-graphite paste. This paper also describes the results of a reproducibility study in which cells were produced by multiple operators with an average AM1.5 efficiency of 12.6%. And finally, this paper discusses process sensitivities and alternative cell fabrication procedures and reports the fabrication of a cell with an AM1.5 efficiency of 15.4%. Copyright © 1999 John Wiley & Sons, Ltd.*

## **INTRODUCTION**

Solar cells using CdTe absorber layers are one of the primary contenders for large-scale commercialization of thin-film photovoltaics.<sup>1</sup> Of the many possible methods of depositing the CdTe layer, close-spaced sublimation (CSS) has received the most attention recently because it is well-suited to large-scale manufacturing and has provided high efficiency for many different groups.<sup>2–7</sup> Although we have reported some of our discoveries in the area of CSS CdTe solar cells, we have not yet provided a description of our procedures with sufficient detail to allow interested groups to duplicate our work. This paper details our laboratory processes; it also describes the results of a reproducibility study, discusses process sensitivities and alternative cell fabrication procedures, and reports the fabrication of a cell with an AM1.5 efficiency of 15.4% as verified by the National Renewable Energy Laboratory.

## **SOLAR CELL FABRICATION**

The device structure and fabrication procedures described in this section were those used for the reproducibility study, the results of which are given later in this paper. The procedures were selected to reliably provide acceptable cell efficiency, not the maximum that can be achieved. Alternative procedures that we have found to be capable of producing higher efficiency are described later in this paper.

\* Correspondence to: Doug H. Rose, Solar Cells, Inc., 1702 N. Westwood Avenue, Toledo, OH 43607, U.S.A.

Contract/grant sponsor: U.S. Department of Energy; Contract/grant number: DE-AC36-83CH10093.

† E-mail: tim\_gessert@nrel.gov

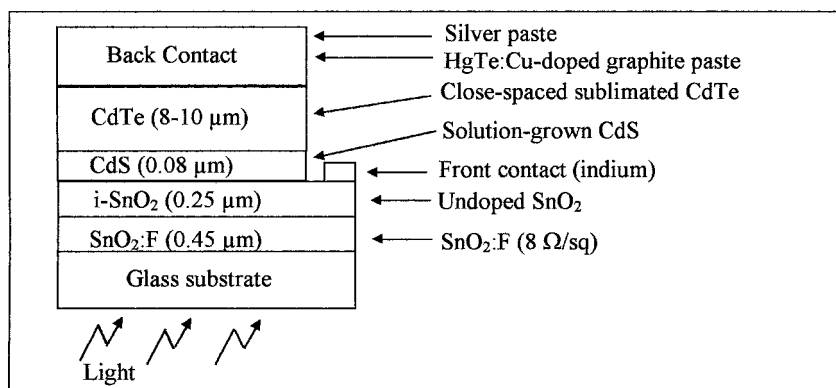


Figure 1. Solar cell device structure

### Device

Figure 1 shows the layers of the solar cell as fabricated for the reproducibility study. The fluorine-doped tin oxide layer ( $\text{SnO}_2\text{:F}$ , also called conductive tin oxide or  $\text{c-SnO}_2$ ) is the transparent contact that provides current collection from the front of the device. The undoped  $\text{SnO}_2$  layer (also called  $\text{i-SnO}_2$  for 'intrinsic' or 'insulating'- $\text{SnO}_2$ ) may help protect the open-circuit voltage of the device in some situations. The CdS layer serves as the window layer, and the CdTe layer serves as the absorber layer for the incident light. The HgTe:Cu-doped graphite layer produces an ohmic contact to the CdTe, and the silver layer decreases the lateral resistivity of the back contact.

### Substrate and front contact

The substrate we used was  $76 \times 76 \times 1.1$  mm Corning 7059 glass. The substrate is first cleaned by sonication in a 1% solution of Liquinox soap in hot deionized (DI) water, followed by five rinses/sonication in DI water (two of which are in hot DI water). The  $\text{SnO}_2\text{:F}$  layer was deposited by low-pressure chemical vapor deposition (LPCVD) at a total pressure of 60 torr and a substrate temperature of  $550^\circ\text{C}$ . Tetramethyltin (TMT) was used as the Sn precursor, and bromotrifluoromethane ( $\text{CBrF}_3$ ) was used as the fluorine dopant source. The TMT was delivered from a room-temperature liquid bubbler to the reactor using  $\text{N}_2$  as the carrier gas with a flow of 0.025 standard liters per minute (slpm). Other flow rates were as follows: 0.8 slpm of  $\text{CBrF}_3$ , 1.875 slpm of  $\text{O}_2$ , and 1.5 slpm of  $\text{N}_2$ . The films were typically deposited to a thickness of  $4500 \text{ \AA}$  in 8 min and had a sheet resistance of  $8 \Omega/\text{sq}$ . The  $\text{i-SnO}_2$  layer was then deposited with a thickness of approximately  $2500 \text{ \AA}$  using identical conditions except without any  $\text{CBrF}_3$  flow. The resistivity of the  $\text{i-SnO}_2$  layer is approximately  $1 \Omega\text{-cm}$ . The transmission and the absorbance of a bi-layer ( $\text{c-SnO}_2/\text{i-SnO}_2$ ) on glass are shown in Figure 2.

### CdS layer

The CdS layer is grown by chemical-bath deposition (CBD). Prior to deposition, the substrates are cut into  $38 \times 38$  mm pieces and cleaned by sonication in hot DI water. The reactor, a water-jacketed beaker, is covered and continuously-stirred. To deposit  $800\text{--}1000 \text{ \AA}$  of CdS, the constituents outlined in Table I are introduced into 550 ml of DI water in the reactor.

The substrates are placed, six at a time, in the bath in a quartz holder and 30 min are allowed to elapse so that the deposition temperature of  $88^\circ\text{C}$  is reached. The first three constituents of Table I are then added (the ammonia is put in slowly by pipette to minimize reaction). Ten minutes are allowed to elapse before the thiourea is added. To minimize homogeneous reaction, the thiourea is added by a computer-controlled titrator in four aliquots of 2 ml, 10 min apart. The total deposition time, after the first addition

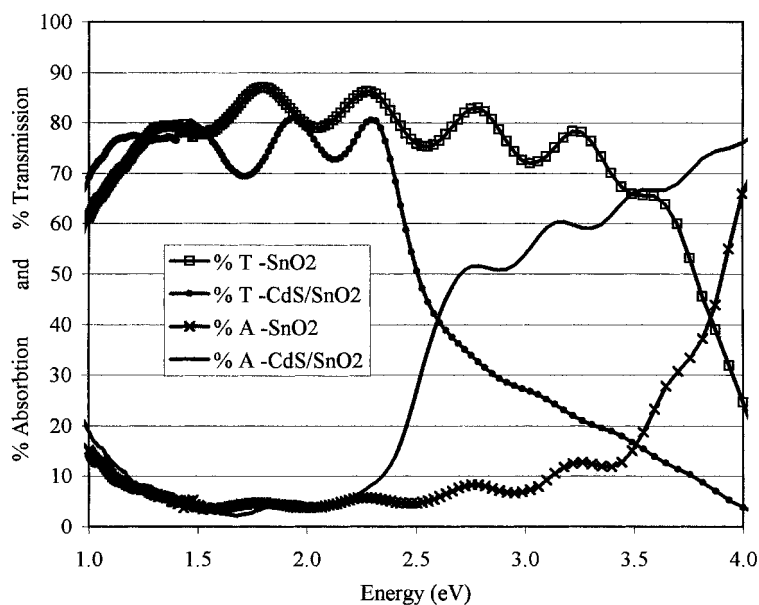


Figure 2. Transmission and absorption of glass/c-SnO<sub>2</sub>/i-SiO<sub>2</sub> and glass/CdS/i-SnO<sub>2</sub>/c-SnO<sub>2</sub> substrates

Table I. Constituents for CdS by chemical bath deposition

Chemical	Volume (ml)	Molarity (M)	Function
Cadmium acetate (CdAc <sub>2</sub> )	8 ml	0.033 M	Cadmium source
Ammonium acetate (NH <sub>4</sub> Ac)	4.6 ml	1 M	Buffer
Ammonia (NH <sub>4</sub> OH)	15 ml	15 M	Complexing agent
Thiourea (CS(NH <sub>3</sub> ) <sub>2</sub> )	8 ml	0.067 M	Sulfur source

of thiourea, is 38 min. The substrates are then removed from the bath, placed in warm DI water, and given three sonications (about 2 min each) to remove loosely adhered CdS particulates. The films are then blown dry with N<sub>2</sub> and stored in Fluoroware containers.

Deposition of CdS films in this manner primarily results in heterogeneous growth on the substrate. The CdS films are highly adherent, transparent, and conformal,<sup>8</sup> with an index of refraction around 2.4, which is close to the single-crystal CdS value of 2.5. However, impurity inclusions<sup>9</sup> and micro-pinholes<sup>10</sup> have also been identified. The CdS thickness can be measured by ellipsometry, near-bandgap absorption, or profilometry on etched islands. The transmission and the absorbance of the glass/c-SnO<sub>2</sub>/i-SnO<sub>2</sub>/CdS stack are shown in Figure 2 (along with the same substrate without the CdS layer).

After a CdS batch is completed, the remaining solution is put in a hazardous waste container, and the jacketed beaker and quartz holder are cleaned with 5 ml of HCl. After repeated rinses, the beaker and holder are reconditioned with hot water and 10 ml of NH<sub>4</sub>OH.

#### CdTe deposition

The CdTe is deposited by CSS following the examples of previous work.<sup>11–13</sup> The CdS layer is removed from the back of the substrate by wiping with a swab dipped in concentrated HCl. The substrate is then rinsed in DI water, dipped in a dilute HCl in DI water solution (1:40 HCl:DI H<sub>2</sub>O) for 5 s, rinsed again, and dried with N<sub>2</sub>. The substrate is then loaded in the deposition chamber as shown in Figure 3. The lamp susceptors, which absorb optical energy from the lamps and allow temperature control of the source and

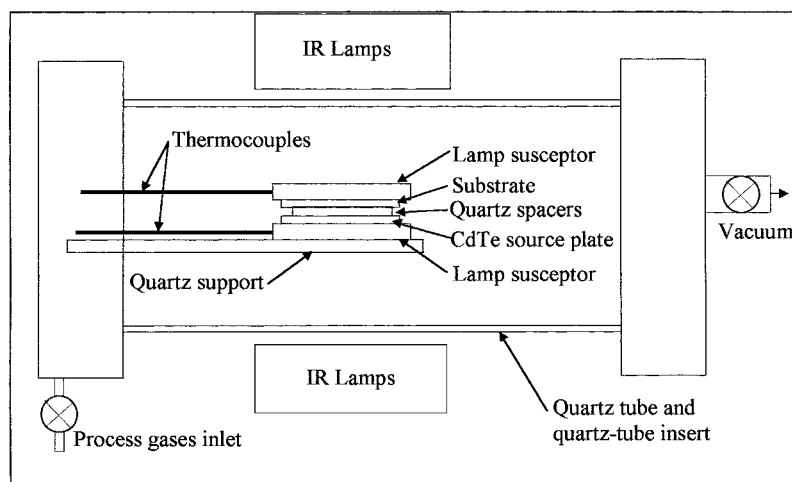


Figure 3. Close-spaced sublimation chamber

substrate, are coated with pyrolytic carbon (Fabmate<sup>®</sup> from Poco Graphite). The use of the coated susceptor is necessary to prevent the conversion of a large fraction of the oxygen in the chamber to CO and CO<sub>2</sub> during the CdTe deposition.<sup>14,15</sup>

The first stage of the deposition phase is an in-situ hydrogen anneal. Annealing the substrate at 400°C for 15 min in 30 torr H<sub>2</sub> is reported to reduce oxygen-related defects in the CdS and may produce a non-stoichiometric surface.<sup>7,16</sup> This step also causes some CdS recrystallization and cleans the surface in preparation for the CdTe deposition.

After cooling to 200°C, the CdTe deposition sequence is initiated. The chamber is pumped down to a background pressure of approximately 0.02 torr, and then He and O<sub>2</sub> are introduced. CSS of CdTe is based on the principle of reversible dissociation of CdTe at high temperatures. The elemental gases diffuse to the substrate,<sup>11</sup> which is in close proximity to the source plate. The gases recombine on the substrate, which is kept at a temperature lower than the source. Deposition process parameters include a 2 mm separation between the source and substrate, an oxygen partial pressure of 0.9 torr, and a helium partial pressure of 14.1 torr. The source and substrate are ramped together to 620°C, then the source temperature is ramped to 660°C in 30 s. The substrate and source are then kept at 620° and 660°C, respectively, for 3.25 min. For these conditions, the resultant CdTe thickness is 8–10 µm at the center of the substrate and 6.0–8.5 µm at the edge of the substrate.

The CdTe source plate used for the depositions consists of a piece of 7059 glass on which CdTe had previously been deposited using the same CSS system. Prior to insertion in the CSS system for fabrication of the source plate, the 7059 glass is cleaned with hot soap and DI water, rinsed, then given a 1-min etch in a 1 : 5 HF to DI water solution, then rinsed again. For source plate fabrication, CdTe is sublimated from a graphite boat packed with 99.999% pure CdTe powder (Alfa Aesar). Source plates are fabricated in 20-torr H<sub>2</sub>, with a boat temperature of 700°C, a substrate susceptor temperature of 600°C, 2 mm spacing, and a deposition time of 30 min. The resultant CdTe films are greater than 300 µm thick and have about 80% coverage of the glass substrate. After each use as a CdTe source, the CdTe source plate is blown off with N<sub>2</sub> to remove any loosely adhered oxides or CdTe particles.

Our group currently has three CSS systems with some design features common to all the systems. The deposition chamber consists of a quartz tube sealed against stainless-steel flanges with the lamp susceptors supported by a cantilevered quartz support (the environment was shown schematically in Figure 3). With this design, only quartz, the susceptors, and the source and substrate are located in the hot zone of the chamber. A quartz insert is located immediately inside the main quartz tube. Because the walls of the chamber are not heated, some CdTe condenses on the quartz during use of the system. The use of an insert allows for easy removal and cleaning (in a Teflon bath with 20 : 1 nitric acid : hydrochloric acid).

Temperature and pressure control of the system is provided by a Research Inc. controller. A personal computer with the program Micrihost PC (Research Inc.) is used for data logging and programming of the controller. Vacuum for the system is provided using a two-stage mechanical pump (Balzers) with Kytox 1514 oil. The deposition chamber is protected from pump oil contamination by a molecular sieve trap, a nitrogen cold trap, and a nitrogen purge which is kept on at the pump inlet except for brief periods when maximum vacuum in the chamber is desired.

#### *CdCl<sub>2</sub> anneal*

After CdTe deposition, a CdCl<sub>2</sub> anneal is performed. Cells made without the anneal generally have efficiencies between 6% and 10%, whereas cells made with the anneal are generally more than 12% efficient. The anneal does not produce bulk recrystallization in the CSS-deposited CdTe films<sup>17</sup> (the grain size is about 3 μm both before and after CdCl<sub>2</sub> treatment), but does increase  $V_{oc}$  and  $FF$ . Several mechanisms for these improvements have been proposed. These include the elimination of fast-recombination centers in the CdTe film,<sup>18</sup> reduction of recombination centers in the junction,<sup>19</sup> and the elimination of small grains at the grain boundaries.<sup>20</sup>

In preparation of the anneal, the 38 × 38 mm CdTe/CdS/i-SnO<sub>2</sub>/c-SnO<sub>2</sub>/glass substrates are scribed and broken into four equal pieces. The pieces are soaked in a 75%-saturated CdCl<sub>2</sub> in methanol solution (the saturated solution is 7.5 g CdCl<sub>2</sub> in 500 ml MeOH). The substrates are soaked for 15 min on a hot plate in a covered petri dish near the boiling point (55–60°C). After that soak, the pieces are taken out of the solution and immediately blown off with N<sub>2</sub>. The pieces are then placed on an aluminum plate in a tube furnace that is purged with He. The furnace is then set at 360°C and left on for 40 min with a flow of 100-sccm He and 25-sccm O<sub>2</sub>. From experiments with thermocouples attached to CdTe devices, we believe the temperature of the devices during the anneal is actually 400°C—this is the temperature we report when no further information is given. After cooling to a maximum of 50°C, the pieces are rinsed in DI water to remove any excess CdCl<sub>2</sub>. While CdCl<sub>2</sub> is not typically found on the surface of the CdTe after the anneal,<sup>21</sup> CdCl<sub>2</sub> can be found on the glass side and should be removed for safe handling.

#### *Back-contact formation*

A variety of contact preparation steps can be performed, but we used the following sequence in the reproducibility study. These procedures were developed following the examples of previous work.<sup>22,23</sup> The first step is to use Kapton tape (3M 5413 polyimide film) to mask a portion of the CdTe surface approximately 1 × 1 cm. The cells are then etched in 88:1:35 phosphoric acid:nitric-acid:DI-water (NP etch) to provide a clean, Te-rich surface.<sup>21,24</sup> The samples are held in the etch 4 seconds past the point when the CdTe surface is completely covered with small bubbles (total time in the etch is about 35 s). The bubbles are likely to be NO and NO<sub>2</sub>;<sup>25</sup> the bubble formation may indicate that the initial oxide layer on the CdTe has been penetrated,<sup>25</sup> or it may be an indication of a transition to hydrophobic behavior after the Te layer is formed. Immediately on removal from the acid, the samples are rinsed with DI water. HgTe:Cu-doped graphite is then brushed on the cell as the back contact. The paste is made by stirring 4 g HgTe:Cu (which is about 2 atomic% Cu) powder into 10 g graphite paste (Acheson Electrodag 114). The paste is thinned as needed with methyl ethyl ketone (MEK) as it thickens between uses.

Next, the contact is annealed by placing the device in a tube furnace at 280°C with a 100 sccm He flow for 30 min. A thin layer of silver paste (Acheson Electrodag 6S-33C) is then applied to the back contact. The device is then placed in an oven at 100°C for 1 h to cure the silver paste.

#### *Cell definition*

The Kapton tape is removed from the cell. To expose the front contact, a clean razor blade is used to scrape CdTe off the substrate around the cell. The total area of the CdTe (including that outside the Ag/HgTe:Cu-graphite area) is counted as the cell area for  $I$ – $V$  measurement purposes. A razor blade can

be used to scribe through the edge of the contact area to minimize nonactive area of the cell, but care must be taken not to create shorting at the scribe. And finally, using an ultrasonic soldering iron, indium is melted to the transparent conducting oxide layer around the cell.

## REPRODUCIBILITY STUDY

A study was done to determine the reproducibility of our cell fabrication process when multiple operators are involved. For the study set, 38 cells were made by a total of seven people over the course of two weeks. The set included three CdS depositions, 10 CdTe depositions, two CdTe sources, and three batches of post-deposition processing. The  $I$ - $V$  results (average and standard deviation) with AM1.5 illumination are shown in Table II. The  $I$ - $V$ s were taken on an unverified system, then adjusted based on a four cells that were sent for NREL-verified  $I$ - $V$  measurement.

Table II. AM1.5  $I$ - $V$  results for 38 cell baseline set

	Efficiency	$V_{oc}$ (V)	$J_{sc}$ (mA/cm <sup>2</sup> )	FF (%)	Area (cm <sup>2</sup> )
Average	12.6%	820	21.8	70.6	0.86
Standard deviation	0.5%	8	0.4	2.0	0.39

The maximum efficiency in the set was 13.3%. The minimum was 11.3%. Not counted in the 38-cell baseline were four cells that had visible scribing problems—the average efficiency of those four cells was 11.6%.

## PROCESS SENSITIVITIES AND ALTERNATIVE PROCEDURES

### Front contact

The characteristics of the front conductive contact can influence cell performance in both obvious and not so obvious ways. An increase in the carrier mobility in the conductive TCO layer provides lower absorptivity and lower resistivity,<sup>26</sup> thus allowing increased photocurrent and decreased series resistance. We estimate the improved transmissivity and conductivity of the tetramethyltin-precursor SnO<sub>2</sub> provides an increase of about 1% (absolute AM1.5) compared to standard commercially-available SnO<sub>2</sub>. Less obvious, but of potentially greater significance, are the chemical properties and stability of the front-contact layers. Alternative TCOs, such as cadmium stannate, may necessitate a less vigorous cleaning procedure than sonication in soap and hot DI water. Other TCOs, such as ZnO, decompose under the basic-aqueous environment of the CBD CdS. And finally, we have found that some front-contact layers can decompose from normal process conditions. Room-temperature sputter-deposited i-SnO<sub>2</sub> layers (which were not used for the baseline set) were particularly susceptible to decomposition during the 400°C H<sub>2</sub> anneal and high temperature processing.<sup>7</sup>

Aside from the negative effects of the i-SnO<sub>2</sub> layer if that layer decomposes during cell fabrication, the impact of the layer is not well understood. We have found that when devices were produced without a CdS layer, a high-resistivity SnO<sub>2</sub> layer produced by a proprietary technique at Golden Photon Inc. improved CdTe adhesion and device performance. However, our standard i-SnO<sub>2</sub> appears to have a much more subtle effect, possibly providing marginal protection of  $V_{oc}$  for thin CdS layers.<sup>27</sup>

One portion of the fabrication procedure we found to have a large impact on device performance is the cleaning procedures of the glass and front-contact layers. In particular, the absence of a clean TCO surface immediately prior to CdS deposition results in nonuniform CdS deposition, potential adhesion problems, and poor device performance. For instance, if a TCO-coated substrate is purchased and soap is

then used to clean the substrate prior to CdS deposition, care must be taken to ensure removal of all soap residue (hot DI rinses/sonication are quite effective). Exposure of the TCO to an acid prior to the CdS deposition can also produce nonuniform CdS and poor device performance.

#### *CdS: deposition and treatments*

The thickness of the CdS layer can strongly affect device performance. We find that devices with a CdS layer of 600 Å typically have lower open circuit voltages, particularly for CdTe deposition conditions that cause excessive loss of CdS. Devices with CdS thicknesses over 1000 Å have reduced photocurrent due to absorption in the CdS and lower  $V_{oc}$  due to inferior CdS from the latter stages of CBD growth.

The 5-s dip of the substrate in dilute HCl prior to CdTe deposition is a step that we find to be marginally beneficial. One experimental set showed a benefit to efficiency of 0.3% (absolute AM1.5) from the dip. Another set showed that 5–10 seconds of the dip provided fewer CdTe pinholes for thin CdTe films compared to no dip or a 60 s dip. We thus believe that the short dip ensures a clean CdS surface, but is not essential for high efficiency.

We also find that the hydrogen anneal of the CdS (described in the solar cell fabrication section) is not essential for high-efficiency devices when using our normal CdTe deposition conditions. In fact, some experimental sets have shown that simply eliminating the anneal can produce higher efficiencies. For example, one set of six devices showed that cells produced without any anneal were 13.9% efficient, whereas cells produced with the standard 400°C anneal in hydrogen were 13.4% efficient. However, another experiment set showed the hydrogen anneal to be of comparable efficiency to other CdS conditioning techniques, but with greater reproducibility. The hydrogen anneal was thus selected for the baseline fabrication procedure.

Despite our decision to incorporate the hydrogen anneal in our standard procedures, our highest efficiencies have been obtained by replacing the anneal with a brief high-temperature exposure immediately preceding the CdTe deposition. This procedure, called a thermal etch, is similar to one reported by Anthony;<sup>28</sup> however, in our case it was used as a way to remove possible deleterious effects associated with H<sub>2</sub> anneals and to provide a means to clean the surface prior to CdTe growth.<sup>29</sup> The thermal etch could also alter the stoichiometry of the surface, raise the temperature at which nucleation begins, and produce a gas phase of S or S-compounds that could redeposit on the substrate. Because some CdS is sublimated from the substrate, the use of a thermal etch can result in poor performance when a thin CdS layer is used. We expect that the irreproducibility of this procedure will decrease as our understanding increases.

#### *CdTe*

One of the key variables in our CSS deposition of CdTe is the oxygen partial pressure.<sup>15</sup> We find that oxygen acts as a nucleation aid and that at least 0.2 torr oxygen is needed to ensure pinhole-free films when thin films are desired at substrate temperatures above 600°C. Oxygen also serves to increase  $V_{oc}$  by improving the quality of the CdS/CdTe interface. Another benefit of oxygen is that it protects against the harmful effects of TCO decomposition (which can result from high-temperature processing, particularly in H<sub>2</sub>) by ensuring uniform CdTe nucleation, converting free Sn to less harmful SnO<sub>x</sub>, and passivating donors if they are present. One deleterious effect of oxygen is excessive source oxidation for oxygen partial pressures above 2 torr (with 13 torr He). Another deleterious effect is the production of features on the surface of the CdTe film, such as hillocks and particles with diameters greater than 10 μm. The balance of these positive and negative effects of oxygen yields an optimum partial pressure of about 1 torr with the other deposition parameters fixed as described.

Another important deposition variable is the substrate temperature. High temperature encourages CdS/CdTe interdiffusion during growth, larger grain size, and generally provides higher  $V_{oc}$ .<sup>30</sup> We find that temperatures above 620°C can result in higher efficiencies, but generally lower the reproducibility of the process.

### *CdCl<sub>2</sub>*

The CdCl<sub>2</sub> concentration during the solution-CdCl<sub>2</sub> dip can have a strong impact on device performance. For example, with the CdS and CdTe deposition conditions used for the reproducibility study, the average efficiency using 60%, 75%, and 90% CdCl<sub>2</sub> concentrations (three cells per concentration) was 13.2%, 13.8%, and 7.8%, respectively. There was no adhesion failure on any of the cells. Exposure of CdTe films to too high of a CdCl<sub>2</sub> concentration coupled with too high of an annealing time/temperature profile can result in low efficiency, either by loss of film adhesion (at the TCO/CdS or CdS/CdTe interface) or by some other mechanism that is not visible and not completely understood.

An alternative to the solution-CdCl<sub>2</sub> procedure used for the reproducibility study is a vapor-CdCl<sub>2</sub> treatment. Using a CSS system with a CdCl<sub>2</sub> source and a source and substrate temperature of 400°C for 10 min, we found that we can achieve comparable efficiencies to the solution-CdCl<sub>2</sub> method. The dry-CdCl<sub>2</sub> shows promise of offering greater reproducibility once the procedure is better understood. One observation we offer at this time is that thin CdS is less reliant on the CdCl<sub>2</sub> anneal, and, at the same time, can tolerate higher CdCl<sub>2</sub> exposure without peeling of the films.

### *Back contact*

For our process, the age of the NP contact etch does not appear to affect device performance. Eight cells produced with a variety of graphite pastes had an average AM1.5 efficiency of 12.8% when the NP was mixed 3 days prior to use, whereas eight cells produced under the same conditions, except with an NP etch mixed 5 min prior to use, had an average efficiency of 12.4%.

However, we found that the nature of the contact paste used can significantly affect device performance. We observed that the efficiencies of devices produced from older pastes were better than from pastes prepared immediately prior to use. For example, a cell made with old contact paste had an efficiency of 13%, whereas one made with freshly-made paste was only 10.3% efficient. The deleterious effect of freshly-made paste was even more pronounced for cells that used no oxygen during the CdTe deposition. We then learned that the aging process could be done artificially by heating the paste to drive off most of the solvent, mixing vigorously, adding more solvent, and repeating. At present, we do not know if the artificial aging produces a change in the bonding of the constituents or if it simply homogenizes the mixture. We have also learned that for our normal CdTe deposition conditions, the efficiency of cells improved with the ratio of the HgTe:Cu to the graphite (up to a ratio of 4:10). However, at this time, we do not fully understand the interaction of the Cu-doped graphite paste with the remainder of the process variables, as illustrated by the fact that we have produced a cell with an efficiency of 12.3% that had no Cu or HgTe added to the graphite paste. While cells produced without Cu added to the paste are generally below 7% efficient (with low  $V_{oc}$  and low  $FF$ ), the 12.3% cell (with a  $V_{oc}$  of 786 mV and  $FF$  of 65.1%) stands as an existence proof that high Cu concentrations are not always required.

As an alternative to the standard NP etch described in the solar cell fabrication section, the CdTe surface can be cleaned (with HCl or ion-beam milling) and then a Te layer evaporated onto the CdTe surface. This procedure produces comparable efficiency to the standard NP etch.<sup>31</sup>

The standard scribing procedure described in the solar cell fabrication section has the disadvantage of producing ragged edges and CdTe outside the contact that counts in the cell area, but contributes little to the current. Official efficiency measurements cannot, however, be taken using the contact area as the cell area, since OBIC measurements have shown some collection from outside of the defined contact. As an alternative to scribing, the cell area can instead be defined by a light mask on the front glass side of the cell. This procedure provides a  $J_{sc}$  truly representative of the cell and, if the mask is just slightly smaller than the contact area, decreases  $V_{oc}$  by only a few mV.

### *High efficiencies from alternative processes*

As an illustration of the efficiency that can be achieved with a few modifications from our standard fabrication techniques, a cell with an AM1.5 efficiency of 15.4%, as confirmed by the National

Renewable Energy Laboratory, is offered. The cell has a  $V_{oc}$  of 830 mV,  $J_{sc}$  of 24.7 mA cm<sup>-2</sup>, and an  $FF$  of 74.8%.

The cell was produced under the same conditions as those described in the fabrication procedures section except that (i) the 400°C hydrogen anneal of the CdS was replaced by a 15-s thermal etch at 625°C while the source temperature was kept at 600°C, (ii) the CdTe deposition was done in 3.67 minutes with 1 torr O<sub>2</sub> and 14 torr He, (iii) the contact etch was made 10 min before use, (iv) an anti-reflection coating of 1100 Å MgF was applied to the glass, and (v) the area of the cell was defined by a light mask.

### Acknowledgements

This work was supported by the U.S. Department of Energy under contract DE-AC36-83CH10093.

### REFERENCES

1. K. Zweibel, 'Toward low cost CdTe PV', *International Journal of Solar Energy*, **12**, 285–292 (1992).
2. J. Britt and C. Ferekides, 'Thin-film CdS/CdTe solar cell with 15.8% efficiency', *Applied Physics Letters*, **62**, 2851–2852 (1993).
3. R. C. Powell, R. Sasala, G. Rich, M. Steele and K. Bihn, 'Stability testing of CdTe/CdS thin-film photovoltaic modules', *Proceedings of the Twenty-Fifth IEEE Photovoltaic Specialists Conference*, Alexandria, VA, 1996, pp. 785–788.
4. S. Kumazawa, S. Shibutani, T. Nishio, T. Aramoto, H. Higuchi, T. Arita, A. Hanafusa, K. Omura, M. Murozono and H. Takakura, '15.1% highly efficient thin film CdS/CdTe solar cell', *Solar Energy Materials and Solar Cells*, **49**(1–4), 205–212 (1997).
5. D. Bonnet, B. Henrichs and H. Richter, 'Some phenomena in CdTe/CdS thin film solar cells made by close-spaced sublimation', *International Journal of Solar Energy*, **12**, 133–136 (1992).
6. N. Romeo, A. Bosio, R. Tedeschi and V. Canevari, 'High efficiency and stable CdTe/CdS thin film solar cells on soda lime glass', *Proceedings of the 2nd IEEE World Photovoltaic Specialists Conference*, Vienna, Austria, 1998.
7. D. S. Albin, D. H. Rose, R. Dhere, D. Niles, A. Swartzlander, A. Mason, D. Levi, H. Moutinho and P. Sheldon, 'Tin oxide stability effects—their identification, dependence on processing and impacts on CdTe/CdS Solar Cell Performance', *14th NREL/SNL PV Program Review, AIP Proceeding No. 394*, Lakewood, CO, 1996, pp. 665–681.
8. T. L. Chu, S. S. Chu, C. Ferekides, C. Q. Wu, J. Britt and C. Wang, 'High efficiency CdS/CdTe solar cells from solution-grown CdS films', *Proceedings of the Twenty-Second IEEE Photovoltaic Specialists Conference*, Las Vegas, NV, 1991, pp. 952–956.
9. J. Webb, D. H. Rose, D. W. Niles, A. Swartzlander and M. M. Al-Jassim, 'FTIR, EPMA, Auger, and XPS analysis of impurity precipitates in CdS films', *Proceedings of the Twenty-Sixth IEEE Photovoltaic Specialists Conference*, Anaheim, CA, 1997, pp. 399–402.
10. F. S. Hasoon, D. H. Rose, A. Swartzlander and D. Albin, Unpublished results, 1996.
11. T. C. Anthony, A. L. Fahrenbruch, R. H. Bube, 'Growth of CdTe films by close-spaced vapor transport', *Journal of Vacuum Science & Technology A*, **2**, 1296–1302 (1984).
12. T. L. Chu, 'Thin film cadmium telluride solar cells by two chemical vapor deposition techniques', *Solar Cells*, **23**, 31–48 (1988).
13. K. W. Mitchell, C. Eberspacher, F. Cohen, J. Avery, G. Duran and W. Bottenberg, 'Progress towards high efficiency thin film CdTe solar cells', *Solar cells*, **23**, 45–57 (1988).
14. D. H. Rose, D. S. Albin, R. J. Matson, A. B. Swartzlander, X. Li, R. G. Dhere, S. Asher, F. S. Hasoon and P. Sheldon, 'Effect of oxygen during close-spaced sublimation of CdTe solar cells', *Materials Research Society Symposium Proceedings Volume 426, Thin Films for Photovoltaic and Related Device Applications*, San Francisco, CA, 1996, pp. 337–348.
15. D. H. Rose, 'The effect of oxygen on CdTe-absorber solar cells deposited by close-spaced sublimation', Ph.D. dissertation, University of Colorado at Boulder, 1997.
16. A. Rohatgi, 'A study of efficiency limiting defects in polycrystalline CdTe/CdS solar cells', *International Journal of Solar Energy*, **12**, 37–49 (1992).

17. R. G. Dhere, D. S. Albin, D. H. Rose, S. Asher, K. Jones, M. Al-Jassim, H. Moutinho and P. Sheldon, 'Intermixing at the CdS/CdTe interface and its effect on device performance', *Materials Research Society Symposium Proceedings Volume 426, Thin Films for Photovoltaic and Related Device Applications*, San Francisco, CA, 1996, pp. 361–366.
18. H. Moutinho, M. Al-Jassim, D. Levi, P. Dippo and L. Kazmerski, "Effects of CdCl<sub>2</sub> treatment on the recrystallization and electro-optical properties of CdTe thin films", *Journal of Vacuum Science and Technology A*, **16**(3), 1251–1257 (1998).
19. D. Bonnet, B. Henrichs and H. Richter, 'Some phenomena in CdTe/CdS thin film solar cells made by close-spaced sublimation', *International Journal of Solar Energy*, **12**, 133–136 (1992).
20. F. Abou-Elfotouh, H. Moutinho, F. Hasoon, R. Ahrenkiel, D. Levi and L. Kazmerski, 'Effects of processing on the properties of polycrystalline CdTe grown by various deposition techniques', *Proceedings of the Twenty-Third IEEE Photovoltaic Specialists Conference*, Louisville, KY, 1993, pp. 491–494.
21. D. M. Waters, D. Niles, T. A. Gessert, D. Albin, D. H. Rose and P. Sheldon, 'Surface analysis of CdTe after various pre-contact treatments', *Proceedings of the 2nd IEEE World Photovoltaic Specialists Conference*, Vienna, Austria, 1998.
22. T. L. Chu and S. S. Chu, 'High efficiency thin film CdS/CdTe solar cells', *International Journal of Solar Energy*, **12**, 121–132 (1992).
23. K. Kuribayashi, H. Matsumoto, H. Uda, Y. Komatsu, A. Nakano and S. Ikegami, 'Preparation of low resistance contact electrode in screen printed CdS/CdTe solar cell', *Japanese Journal of Applied Physics*, **22**, 1828–1831 (1983).
24. D. Niles, X. Li, P. Sheldon and H. Hochst, 'A photoemission determination of the band diagram of the Te/CdTe interface', *Journal of Applied Physics*, **77**, 1–5 (1995).
25. J. Sarlund, M. Ritala, M. Leskela, E. Siponmaa and R. Zilliacus, 'Characterization of etching procedure in preparation of CdTe solar cells', *Solar Energy Materials and Solar Cells*, **44**(2), 177–190 (1996).
26. T. Coutts, X. Wu, P. Sheldon and D. Rose, 'Development of high-performance transparent conducting oxides and their impact on the performance of CdS/CdTe solar cells', *To be published in the Proceedings of the 2nd IEEE World Photovoltaic Specialists Conference*, Vienna, Austria, 1998.
27. X. S. Li, D. H. Rose, R. G. Dhere, R. Ribelin and P. Sheldon, 'The effect of high resistance TCO layers on CdS/CdTe device performance', *Proceedings of the NCPV Program Review Meeting*, September 8–11, Denver, Colorado, 1998.
28. T. C. Anthony, 'Preparation and properties of CdTe films and junctions using close-spaced vapor', Ph.D. dissertation, Stanford University, 1984.
29. D. S. Albin, R. G. Dhere, A. Swartzlander-Guest, D. H. Rose, X. S. Li, D. Levi, D. W. Niles, H. Moutinho, R. Matson and P. Sheldon, 'Interface Reactions in CdTe Solar Cell Processing', *Material Research Society Symposium Proceedings Volume 485*, 1998, pp. 215–220.
30. X. S. Li, D. Albin, S. Asher, Moutinho, B. Keyes, R. Matson, F. Hasoon and P. Sheldon, 'The effect of substrate temperature on material properties and the device performance of close-spaced sublimation deposited CdTe/CdS devices', *13th NREL Photovoltaics Program Review, AIP Conference Proceedings No. 353*, Lakewood, CO, 1995, pp. 376–383.
31. D. W. Niles, X. S. Li, D. S. Albin, D. H. Rose, T. A. Gessert and P. Sheldon, 'Evaporated Te on CdTe: a vacuum-compatible approach to making back contact to CdTe solar cell devices', *Progress in Photovoltaics*, **4**, 225–229 (1996).

# Growth of polycrystalline CdS and CdTe thin layers for high efficiency thin film solar cells

N. Romeo, A. Bosio\*, R. Tedeschi, V. Canevari

INFN-Istituto Nazionale di Fisica della Materia, Dipartimento di Fisica, Università degli Studi di Parma, Parco Area delle Scienze 7/A, I-43100 Parma, Italy

## Abstract

Recently, conversion efficiencies close to 16% for thin film solar cells based on the CdS/CdTe heterojunction have been reported. These relevant results, however, have not yet solved the problems which arise when industrial production is undertaken as the demand for low cost imposes constraints which considerably limit the final efficiency of the cells. In this paper, we will show that very high conversion efficiencies can still be achieved even making use of low cost soda-lime glass as substrate. In fact, the Na contained in this kind of glass diffuses during the fabrication of the cell into the active layers of the device causing a substantial decrease of the fill factor and consequently of the efficiency of the cell. In particular, we will describe the methods and the magnetron sputtering techniques used to grow a polycrystalline CdS thin film with a controlled Na content. We will also describe the details of the growth via the close-spaced sublimation (CSS) technique of the CdTe polycrystalline film, which are crucial for the heterojunction and the back contact which has been fabricated exploiting the characteristics of  $\text{Sb}_2\text{Te}_3$  which is a low gap *p*-type semiconductor with a high conductivity. © 2000 Elsevier Science S.A. All rights reserved.

*Keywords:* II-VI semiconductors; Deposition methods; Thin film solar cells

## 1. Introduction

Cadmium telluride (CdTe) is a suitable photovoltaic material for solar cells because of its optimum energy gap (1.43 eV) and high absorption coefficient for visible solar radiation. To reduce production costs, it is necessary to fabricate the solar cells with polycrystalline thin films deposited onto low-cost substrate like soda-lime glass. Because of short optical absorption length in CdTe and the difficulty of forming a thin film shallow homojunction with a high conductivity surface layer, thin film CdTe solar cells are of the heterojunction configuration. To allow the formation of the heterojunction, a transparent conducting semiconductor is used as the CdTe partner. Cadmium sulphide (CdS) has been found to be the best suited for thin film CdTe heterojunction solar cells, and conversion efficiencies of higher than 12% have been reported for CdS/CdTe solar cells prepared by several techniques. In efficient solar cells, CdS films are prepared by spray-pyrolisis, vacuum evaporation, RF sputtering and close-spaced sublimation (CSS), and CdTe films are deposited by CSS, electrodeposition, spraying, screen printing and metal-organic chemical vapour deposition (MOCVD). Each technique has its own advantages. However, the best

CdTe based thin film solar cells have been fabricated using the CSS method [1].

In this work, efficient thin film CdS/CdTe heterojunction solar cells have been prepared from CdS deposited by RF sputtering technique, and CdTe deposited by CSS, both cost-effective scalable techniques. The solar cell is of the front-wall configuration, i.e. films of CdS, *p*-type CdTe, and an ohmic contact are subsequently deposited onto a transparent conducting oxide-coated soda-lime glass (Fig. 1).

The front transparent contact has been prepared by depositing in sequence films of  $\text{In}_2\text{O}_3$  90%: $\text{SnO}_2$  10% (ITO) and  $\text{SnO}_2$ , the first one to get a low sheet resistance and the second one to passivate the soda-lime glass against Na diffusion. Besides, CdS films deposited by RF sputtering and CdTe films deposited via CSS technique on the top of the CdS layer are separately treated in a saturated cadmium chloride ( $\text{CdCl}_2$ ) atmosphere at a temperature of 500 and 400°C, respectively. Following this process the CdS film is restructured, being made denser with enhanced grain size. This fact yields an improvement both in the intrinsic quality of the film (crystalline quality, grain boundaries, superficial roughness) and in its electro-optical properties. It is known that the heat treatment around 400°C with  $\text{CdCl}_2$  has been routinely used to significantly improve electronic characteristic of polycrystalline CdS/CdTe films. Generally,

\* Corresponding author.

E-mail address: bosio@fis.unipr.it (A. Bosio).

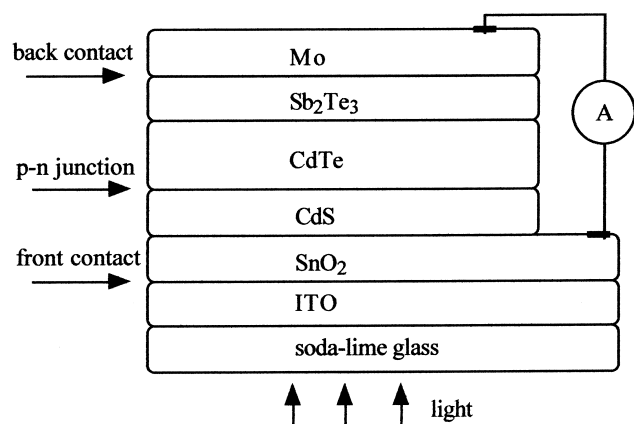


Fig. 1. CdS/CdTe thin film solar cell structure.

the  $\text{CdCl}_2$  treatment increase the average grain size of the CdS and CdTe films, prepared with several methods such as electrochemical or vacuum deposition, which usually grow with small grain size. In the case of high temperature deposition, such as the CSS method, the as-deposited average grain size is large ( $\geq 1 \mu\text{m}$ ) [2]. However, the  $\text{CdCl}_2$  heat treatment is still necessary to achieve good device characteristics. There is evidence that in large grain films the treatment promotes grain boundaries re-growth and small grains elimination. In either case,  $\text{CdCl}_2$  is believed to act as a flux agent that increases the atomic mobility of CdTe at the annealing temperature. The role of  $\text{CdCl}_2$  is not only that of re-crystallizing the CdTe film but also to dope it *p*-type. In fact, as-deposited CdTe films have shown to be *p*-type with a resistivity of  $10^4$ – $10^5 \Omega \text{cm}$ ; this kind of conductivity is probably due to stoichiometry native defects, like Cadmium vacancies ( $V_{\text{Cd}}$ ). After  $\text{CdCl}_2$  treatment, the same films are *p*-type conductivity again but with a resistivity as low as  $100 \Omega \text{cm}$ . The doping of CdTe by  $\text{CdCl}_2$  could be due to the formation of  $(V_{\text{Cd}}-\text{Cl})^-$  complexes which have an activation energy of 0.05 eV, that is a shallower energy level than that of Cadmium vacancies [3]. In the more efficient cells, as back contact a Cu-graphite layer is generally used. Since Cu is a highly diffusion element into CdTe, these cells, in the long period are destined to degrade. Recently, we have developed a new back-contact which does not contain any copper or any doping element that can diffuse into CdTe. This contact is made with a thin layer of  $\text{Sb}_2\text{Te}_3$ , which is a stable compound that exhibits a forbidden energy gap of 0.3 eV and is a degenerate *p*-type semiconductor with a resistivity of  $10^{-4} \Omega \text{cm}$ . The  $\text{Sb}_2\text{Te}_3$  layer is deposited by sputtering at a substrate temperature of 300–350°C. This high substrate temperature allows the formation of a  $p^+$   $\text{Sb}_2\text{Te}_3$  layer on top of CdTe film which assures, together with its low resistivity, the ohmic behaviour of the back contact. The best CdTe/CdS solar cell fabricated with these layers in our laboratory exhibits an efficiency of 14.6% that is very close to the maximum efficiency so far obtained (15.8%) [1].

## 2. Experimental procedure

### 2.1. Substrate preparation

The substrate used for the deposition is a 1 in.<sup>2</sup> soda-lime glass previously washed with a low-alkaline detergent and then carefully rinsed in deionized water. Finally, the substrate is rinsed again with acetone and propan-2-ol in an ultrasonic bath.

### 2.2. The transparent conducting oxide (TCO)

Due to its low cost, soda-lime glass is suitable for industrial production but this advantage is partially reduced because the sodium, contained in this type of glass, could diffuse during thermal treatments into the other layers which form the device. To avoid this problem, a passivating layer is often deposited on the soda-lime glass such as alumina ( $\text{Al}_2\text{O}_3$ ) or silica ( $\text{SiO}_2$ ). We are adopting a new scheme which consists in the deposition of a  $\text{SnO}_2$  layer that allows to control the Na diffusion. The front contact is set up with  $1 \mu\text{m}$  ITO ( $\text{In}_2\text{O}_3$  90%: $\text{SnO}_2$  10%) and a 0.1– $1 \mu\text{m}$   $\text{SnO}_2$  thick films. The ITO layer is deposited via magnetron RF sputtering, under an Argon pressure of  $1 \times 10^{-2}$  mbar, at a substrate temperature of 450°C with a deposition rate of  $5 \text{ \AA s}^{-1}$ . The ITO film exhibits a sheet resistance of  $R_s=1 \Omega \square^{-1}$ . This first deposition still allows the diffusion of sodium, from soda-lime glass, as it is evident by the appearance of NaCl crystallites when the surface of the ITO layer is treated in air at 500°C with  $\text{CdCl}_2$ . On top of this ITO film, we deposit in sequence the  $\text{SnO}_2$  layer with an  $\text{O}_2$  partial pressure of  $2 \times 10^{-4}$  mbar keeping all the other sputtering deposition parameters constant. Under these conditions,  $\text{SnO}_2$  grows in a very compact polycrystalline structure exhibiting a sheet resistance of  $R_s=10 \Omega \square^{-1}$ . This second layer, despite its greater resistance, does not modify the overall resistance, which keeps its minimum value, with the great advantage of controlling the Na diffusion by means of the  $\text{SnO}_2$  film thickness. Annealing these films with  $\text{CdCl}_2$ , as previously described, we do not observe any NaCl crystallite formation if the  $\text{SnO}_2$  layer is  $1 \mu\text{m}$  thick, while there are few small NaCl crystallites if the  $\text{SnO}_2$  film is  $0.5 \mu\text{m}$  thick. These TCO films exhibit a transparency of 85% in the region of visible spectrum of interest.

### 2.3. The CdS layer

The good quality of a thin film solar cell is strongly dependent on the proper interaction among the different layers which constitute the device. We consequently deposited, via magnetron RF sputtering, without removing the sample from the apparatus, a  $2000 \text{ \AA}$  thick layer of CdS at a substrate temperature of 200°C with a deposition rate of  $5 \text{ \AA s}^{-1}$  in an Ar pressure of  $1 \times 10^{-2}$  mbar. On top of the CdS film, a  $1500 \text{ \AA}$  thick layer of  $\text{CdCl}_2$  is then evaporated. Subsequently, the  $\text{CdCl}_2$  covered CdS film is annealed in

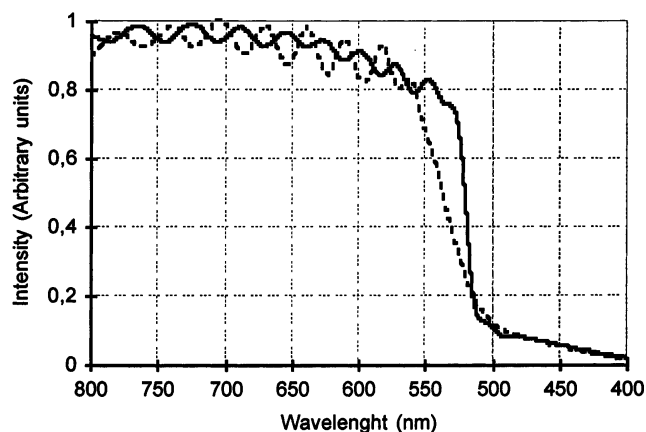


Fig. 2. Transmission spectrum of the CdS layer, before the CdCl<sub>2</sub> treatment (dash-dotted line) and after the treatment (solid line). The shift towards the right of the absorption edge proves the beneficial effect of the CdCl<sub>2</sub> treatment.

air in a two-step process, the first at 460°C and in sequence at 500°C, both steps for a duration of 20 min. The system is then washed in methanol to get rid of residual traces of CdCl<sub>2</sub>. The first important observation that we made is that the grain size of the CdS film after treatment depends strongly on the SnO<sub>2</sub> film thickness. A large grain size of CdS, in the order of 2000–3000 Å, is obtained for a lower SnO<sub>2</sub> thickness, while, by increasing the thickness of the SnO<sub>2</sub> layer, the grain size of the CdS film decreases. For a SnO<sub>2</sub> thickness of 1 μm, the grain size of the CdS film remains as it was before CdCl<sub>2</sub>-treatment (500 Å). We interpreted these results by taking into account the Na-diffusion from soda-lime glass; a larger grain size in the CdS film corresponds to a larger amount of Na present in the CdS film. We conclude that the Na-diffusion into the CdS film depends on the thickness of the SnO<sub>2</sub> layer and for a SnO<sub>2</sub> thickness on the order of 1 μm, the Na-diffusion is quite negligible. Anyhow, after CdCl<sub>2</sub> treatment, in the absence of Na, CdS films are denser and present a better crystalline quality than that of the not-treated samples [4]. This is put in evidence by observing the optical transmission spectra (Fig. 2). Besides, the X-ray diffractograms of the as-deposited CdS films show a mixture of cubic and hexagonal phase, while the post-treated films exhibit the hexagonal phase only (Fig. 3).

This unambiguously means that the CdCl<sub>2</sub> treatment is effective in recrystallizing the CdS film. The crystalline quality and compactness of CdS layer is an important parameter influencing the performance of CdTe/CdS solar cells: nanograins or a metastable crystalline phase (i.e. cubic phase), may enhance the formation of an interdiffused layer at the CdTe/CdS interface which influences the junction transport properties.

#### 2.4. The CdTe layer

The CdTe film is deposited via a CSS technique (Fig. 4) on top of the above described CdCl<sub>2</sub>-treated CdS film.

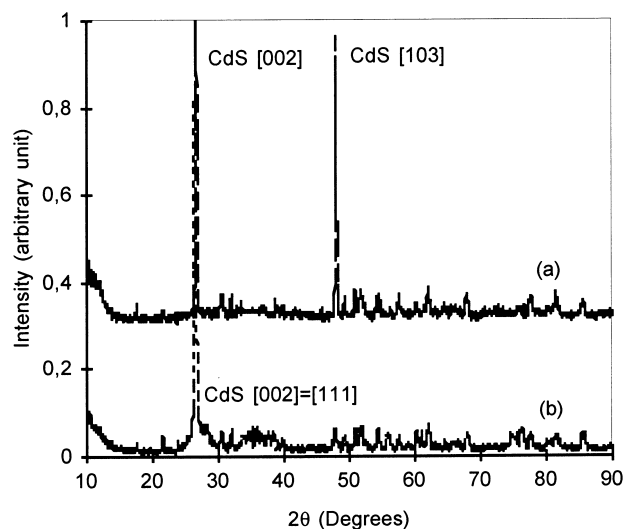


Fig. 3. (a) X-ray spectrum of the CdS layer before the CdCl<sub>2</sub> treatment; (b) X-ray spectrum of the CdS layer after the CdCl<sub>2</sub> treatment. To make the spectrum more legible we eliminated the peaks belonging to the ITO/SnO<sub>2</sub> layer.

First of all, the CdS film is treated in the CSS chamber under  $10^{-1}$  mbar hydrogen pressure and at 350°C substrate temperature for 20 min in order to remove the undesired presence of oxygen compounds (i.e. CdO) and any remaining traces of CdCl<sub>2</sub>. After that the CdTe deposition is carried out putting in a graphite crucible a sintered sputtering-like target. This target is a disk shaped with a 3.0 in. diam and is manufactured in this way: a 99.9999% purity CdTe powders provided by Cerac Inc. are placed into a graphite crucible inside an oven. Then under a 50 bar N<sub>2</sub> pressure, the temperature is risen up to 1200°C for 1 h, and therefore, slowly lowered at room temperature. As encapsulant, B<sub>2</sub>O<sub>3</sub> is used on top of CdTe. Using a sintered target as a CdTe source, any spitting of CdTe powders is inhibited and the substrate can be directly faced to the source. Besides, a 3 in. diam dimension ensures a very uniform deposition because of its wider size with respect to the substrate. The distance between source and substrate is typically 0.2 cm and

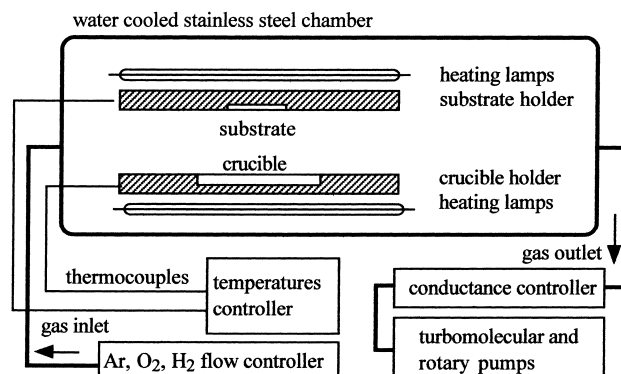


Fig. 4. Schematic diagram of our CSS system.

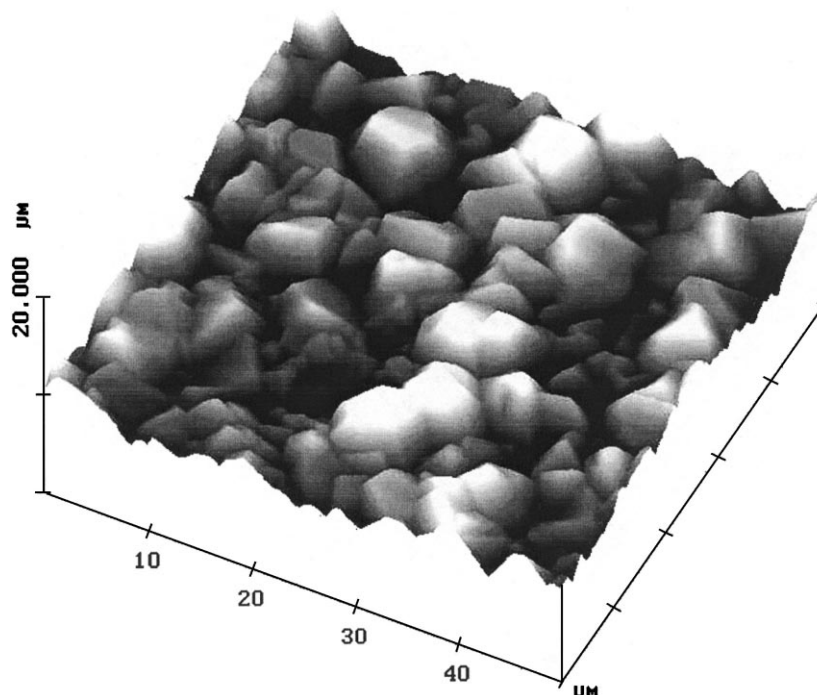


Fig. 5. AFM picture of the CdTe layer deposited at 500°C (on top of the CdCl<sub>2</sub>-treated CdS film) by CSS technique with an Ar pressure of 1 mbar and 650°C source temperature. Average grain size ≈10 μm.

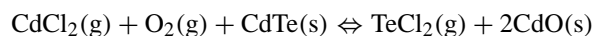
the temperature of source and substrate are 500 and 600°C, respectively. The deposition, is normally carried out in an Ar+O<sub>2</sub> atmosphere. A typical pressure during the deposition is 1 mbar and the content of oxygen is 1%. The role of O<sub>2</sub> is that to slow down the CdTe growth to allow the CdTe to grow with a smaller grain size and to have a better coverage of the CdS film. With these parameters a 5 μm thick CdTe film can be deposited in 5 min. The results of the AFM analysis on the surface of CdTe films are depicted in Figs. 5 and 6. In particular, a fast Fourier analysis has indicated that the average grain size changes from 10 μm for the film grown in Ar only, to 2–3 μm for the film grown with Ar+O<sub>2</sub>.

The CdTe film, covered by 0.3–0.5 μm thick CdCl<sub>2</sub> layer, is then treated in air for 20 min at 420–430°C. This treatment is needed in order to remove the structural defects and nanograins in the CdTe film and possibly to dope it with (V<sub>Cd</sub>-Cl)<sup>-</sup> complexes which behave as acceptor-like dopants.

### 2.5. The back contact

Contacts for thin film CdTe/CdS solar cells have always been a crucial problem because the presence of elements of the first group of the periodic table of elements limit the lifetime of the device. To solve this problem we use a stable material such as Sb<sub>2</sub>Te<sub>3</sub> [5]. This compound is a *p*<sup>+</sup> type low energy gap (0.3 eV) semiconductor with a resistivity of 10<sup>-4</sup> Ω cm. This material is deposited at a substrate temperature of 300–350°C by RF sputtering, using a 99.999%

pure target supplied by Cerac Inc., on top of a CdTe film previously etched in Br-methanol. This chemical etching is necessary in order to remove any oxygen compound and residual CdCl<sub>2</sub> from the surface of the CdTe film. In fact, during the CdCl<sub>2</sub>:O<sub>2</sub> vapour heating treatment, CdTe reacts with CdCl<sub>2</sub> and O<sub>2</sub> which results in the production of CdO on the surface of the CdTe grains according to the reaction (at 430°C)



further, CdTe and CdO react with Br<sub>2</sub> in methanol, according to the reactions



The product CdBr<sub>2</sub> is soluble in methanol and water and is removed from the surface by agitation and rinsing. The results is a Te-rich CdTe surface which can react with Sb during the subsequent sputtering deposition of the Sb<sub>2</sub>Te<sub>3</sub> back contact, forming a *p*<sup>+</sup> type layer inside the CdTe film. In fact, the deposition temperature of the Sb<sub>2</sub>Te<sub>3</sub> film, sputtered onto the Te-rich CdTe surface, is kept enough high to allow the re-evaporation of Te during the deposition, leaving then a Sb-rich Sb<sub>2</sub>Te<sub>3</sub> film. As a consequence, the Sb excess can react with the Te-rich CdTe surface. This *p*<sup>+</sup> CdTe region ensures an ohmic behaviour of Sb<sub>2</sub>Te<sub>3</sub> contact and Sb<sub>2</sub>Te<sub>3</sub>, being a stable compound, ensures the stability of the devices. Finally, the Sb<sub>2</sub>Te<sub>3</sub> is covered by 0.2 μm of Ta or Mo by RF sputtering in the same deposition chamber.

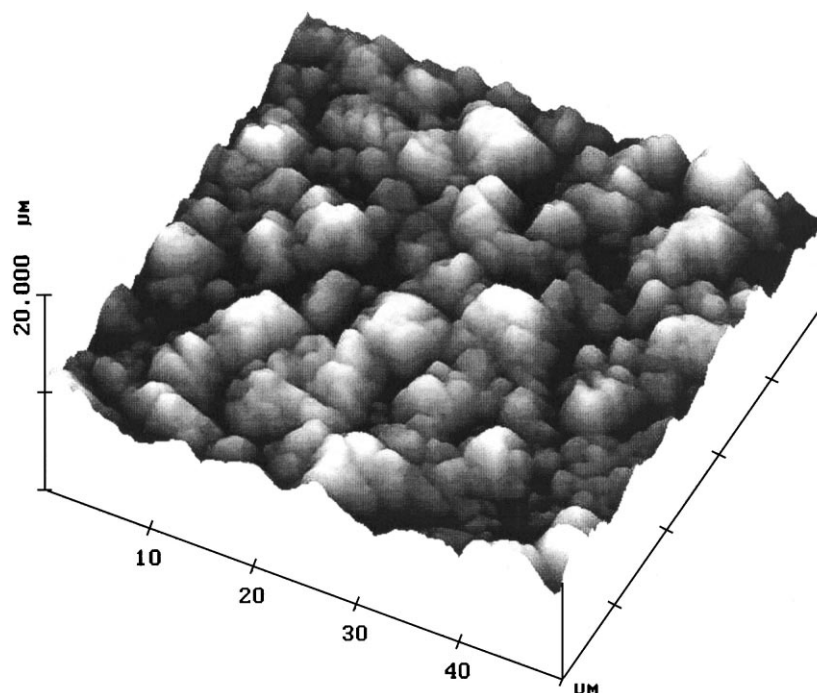


Fig. 6. AFM picture of the CdTe layer deposited at 500°C (on top of the CdCl<sub>2</sub>-treated CdS film) by CSS technique with an Ar pressure of 1 mbar+1% O<sub>2</sub> and 650°C source temperature. Average grain size ≈2–3 μm.

### 3. Results and conclusions

Our typical cell is fabricated without antireflecting coating with an area of 0.64 cm<sup>2</sup> and its characteristics were measured in the dark and under illumination. The  $J$  versus  $V$  characteristics of the cell, measured under the typical condition of 300 K, 100 mW cm<sup>-2</sup> and AM1.5 making use of a solar simulator supplied by Oriel Inc., are:  $V_{oc}$ =858 mV and  $J_{sc}$ =23 mA cm<sup>-2</sup> with a fill factor (ff) of 74% corresponding to a total area conversion efficiency of 14.6%. It is in our opinion that the results here reported are the consequence of two important factors which are the role of CdCl<sub>2</sub> in the fabrication of the CdS layer and the Sb<sub>2</sub>Te<sub>3</sub> back contact. Since CdS has a lattice mismatch with CdTe of 10%, a true abrupt heterojunction cannot work due to the high amount of interface defects. On the other hand, CdS mixes very easily with CdTe at the high deposition temperature of 500°C and this can remove the mismatch, and consequently, the interface energy states. This is due to the presence of a smooth transition through a mixed compound CdS<sub>1-x</sub>Te<sub>x</sub>. Unfortunately, the cell performance depends strongly on the thickness of this mixed layer. It is here that the role of CdCl<sub>2</sub> treatment of the CdS shows its great importance.

A very fine grained CdS film can easily mix with CdTe giving a too thick CdS<sub>1-x</sub>Te<sub>x</sub> mixed compound. This compound can form a buried homojunction which loses the good performance in photovoltage and photocurrent typical of the heterojunction.

On the contrary, if the CdTe grows on the surface of a CdS layer previously treated with CdCl<sub>2</sub>, then the good morphology and compactness of the polycrystalline film does not allow marked mixing, thus favouring the formation of a junction which develops in a few atomic layers still carrying a small amount of interface states. As a consequence of this reason, when we fabricate the device on soda-lime glass making use of a Na-free TCO covered by a CdS layer treated with CdCl<sub>2</sub> we observe a photovoltage consistently over 800 mV and a ff over 72% for all the solar cells prepared [6].

The quality of the Sb<sub>2</sub>Te<sub>3</sub> back contact has been investigated by studying the cell performances during a test period of six months, keeping the cell at 60°C under 10 suns in the open-circuit conditions. Under these conditions we did not notice any appreciable degradation of the cell performances, as resulted from the  $J$ - $V$  characteristics. During the test period, the cell showed a slight increase of  $V_{oc}$  (10–30 mV) while the ff suffered a decrease, which after repeated checks, was never >1%.

In conclusion, with the above described methods, very stable high efficiency CdS/CdTe polycrystalline thin films solar cells could be obtained.

### Acknowledgements

The authors gratefully acknowledge Dr. Lucio Zanotti, director of MASPEC Institute, for the supply of the sintered CdTe target, and Dr. Carlo Vignali from CIM for his techni-

cal support. This work has been partially supported by the European Commission under contract no. JOR3-CT98-0218 (DGXII-WSMN).

## References

- [1] J. Britt, C. Ferekides, *Appl. Phys. Lett.* 62 (22) (1993) 2851.
- [2] N. Romeo, A. Bosio, R. Tedeschi, A. Romeo, V. Canevari, D. Leone, in: *Proceedings of the 14th European Photovoltaic Solar Energy Conference*, 1997, pp. 2351–2354.
- [3] K. Zanio, *Cadmium Telluride, Semiconductors and Semimetals*, Vol. 13, Academic Press, New York, 1978, p. 148.
- [4] C. Ferekides, K. Dugan, V. Ceekala, J. Killian, D. Oman, R. Swamiwathan, D.L. Morel, in: *Proceedings of the IEEE First World Conference on Photovoltaic Energy Conversion*, Vol. 1, 1994, pp. 99–102.
- [5] N. Romeo, A. Bosio, R. Tedeschi, A. Romeo, V. Canevari, in: *Proceedings of the Second World Conference and Exhibition on Photovoltaic Solar Energy Conversion*, 1998, pp. 446–447.
- [6] N. Romeo, A. Bosio, R. Tedeschi, A. Romeo, V. Canevari, *Solar Energy Mater. Solar Cells* 58 (1999) 209–218.



ELSEVIER

Solar Energy Materials & Solar Cells 75 (2003) 185–192

Solar Energy Materials  
& Solar Cells

www.elsevier.com/locate/solmat

# Influence of CdS window layer on 2- $\mu\text{m}$ thick CdS/CdTe thin film solar cells

Kyotaro Nakamura\*, Masahiro Gotoh, Toshihiko Fujihara,  
Toshihiko Toyama, Hiroaki Okamoto

*Graduate School of Engineering Science, Department of Physical Science, Osaka University, Toyonaka,  
Osaka 560-8531, Japan*

## Abstract

Influence of the CdS window layer on the PV performances of 2- $\mu\text{m}$  thick CdS/CdTe solar cells has been studied as a function of the CdS thickness,  $d_{\text{CdS}}$ . With a reduction of  $d_{\text{CdS}}$  from 114 to 95 nm,  $J_{\text{SC}}$  increases due to an increase in blue response. While, at  $d_{\text{CdS}} < 85$  nm, the conversion efficiency largely decreases due to a decrease in  $V_{\text{OC}}$  and FF. The deterioration of the crystallinity of CdTe due to a decrease in the sulfur composition  $x$  of the CdTe $_{1-x}$ S $_x$  mixed-crystal layer is concluded to be the most possible mechanism for the large decreases in  $V_{\text{OC}}$  and FF. © 2002 Published by Elsevier Science B.V.

*Keywords:* CdTe; CdS; Crystallinity; Interface; CdTe $_{1-x}$ S $_x$  mixed-crystal layer

## 1. Introduction

For the CdS/CdTe thin film solar cells, a reduction of thickness of the photovoltaic (PV) active layer,  $d_{\text{PV}}$ , is one of the most important requests from a viewpoint of a reduction of the production cost as well as the harmful influence of Cd toxicity. We have attempted to fabricate highly efficient 2- $\mu\text{m}$  thick CdS/CdTe thin film solar cells, and already achieved the energy conversion efficiency,  $\eta$ , higher than 13% with  $d_{\text{PV}} = \sim 2 \mu\text{m}$  [1]. For the further improvement of the PV performances, the influence of the CdS layer, especially the thickness of the CdS layer,  $d_{\text{CdS}}$ , should be investigated because high efficiencies of  $\sim 16\%$  have been achieved with  $d_{\text{CdS}} = \sim 100$  nm for the CdS/CdTe solar cells with  $d_{\text{PV}} > 3 \mu\text{m}$  [2,3]. It is well known that (1) the CdS layer acts as the window layer which is related to the

\*Corresponding author.

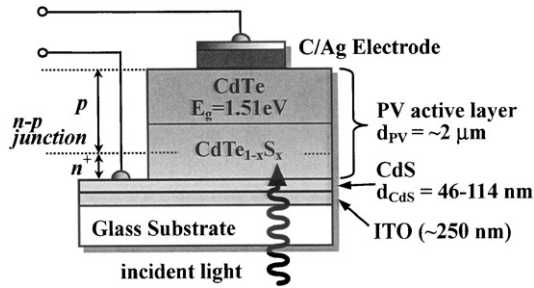


Fig. 1. Schematic configuration of CdS/CdTe thin film solar cell.

spectral response at short wavelength region, (2) crucial roles for the crystallinity of the CdTe layer and (3) for the formation of CdTe<sub>1-x</sub>S<sub>x</sub> mixed-crystal layer near the CdS/CdTe(S) interface.

In this paper, we report the PV performances of the 2- $\mu\text{m}$  thick CdS/CdTe thin film solar cells as a function of  $d_{\text{CdS}}$ , and discuss the influence of the reduction of  $d_{\text{CdS}}$  from the above viewpoints.

## 2. Experimental

The structure of the CdS/CdTe thin film solar cell is schematically displayed in Fig. 1. Fabrication procedure of the CdS/CdTe solar cells is as follows [1]. The CdS film was deposited by the metal organic chemical vapor deposition in air on indium tin oxide coated Corning 1737 glass. The thickness of the CdS film was changed by the deposition time, and confirmed by a stylus surface profiler and estimation from a phenomenological relationship between the optical transmissivity at a wavelength of 400 nm and  $d_{\text{CdS}}$ . Subsequently, the CdTe layer was deposited with a close-spaced sublimation technique, and  $d_{\text{PV}}$  was controlled to about 2  $\mu\text{m}$  by the source temperature and the deposition time, and measured by a stylus surface profiler (Sloan, Dektak<sup>3</sup>ST) after the deposition. After the growth of CdTe, the CdCl<sub>2</sub> treatment was performed. The films were coated with 0.3 M CdCl<sub>2</sub> aqueous solution and annealed in the 1 atm of oxygen and nitrogen mixed gas. The carbon electrode was formed by printing of Cu-doped carbon paste, and Cu was thermally diffused. Formation of silver back-contact completes the fabrication. The cell area was about 0.45 cm<sup>2</sup>.

## 3. Results and discussion

Fig. 2 shows the PV performances of 2- $\mu\text{m}$  thick cells as a function of  $d_{\text{CdS}}$ . The conversion efficiency increases with a decrease in  $d_{\text{CdS}}$  from 114 to 95 nm. In this region,  $V_{\text{OC}}$  and FF are almost unchanged, thus the improvement of conversion efficiency is caused by an increases in  $J_{\text{SC}}$  with reduction of  $d_{\text{CdS}}$ .

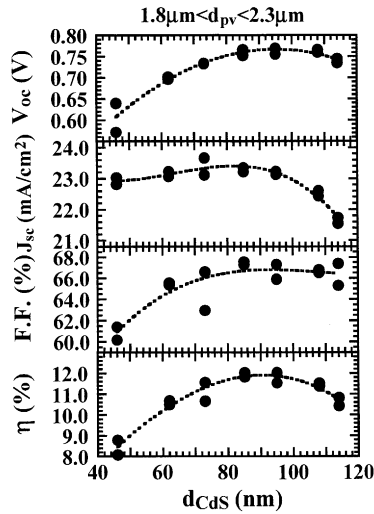


Fig. 2. PV performances as a function of CdS layer thickness,  $d_{\text{CdS}}$  (A.M. 1.5,  $100 \text{ mW/cm}^2$ ).

The increase in  $J_{\text{SC}}$  with the reduction of  $d_{\text{CdS}}$  to 95 nm, is simply explained by an increase in the spectral response at short wavelength region. The spectral response spectra of 2- $\mu\text{m}$  thick CdS/CdTe solar cells are displayed as a function of  $d_{\text{CdS}}$  in Fig. 3(a). The increase in the spectral response at short wavelength region ( $\lambda < 490 \text{ nm}$ ,  $h\nu > 2.5 \text{ eV}$ ) is clearly observed. This gives that the increase in the spectral response at the short wavelength region is due to a reduction of the optical absorption in the CdS layer.

On the other hand, with a decrease in  $d_{\text{CdS}} < 85 \text{ nm}$ , any pronounced changes are not found in  $J_{\text{SC}}$ , even though the spectral response at short wavelength region is still increased. Regarding  $V_{\text{OC}}$  and FF, with a decrease in  $d_{\text{CdS}}$ ,  $V_{\text{OC}}$  and FF are largely decreased, yielding a large reduction of conversion efficiency. Fig. 3(b) shows the external quantum efficiencies (EQE) at 1.51 eV corresponding to the band-gap energy of CdTe as a function of  $d_{\text{CdS}}$ . With a decrease in  $d_{\text{CdS}} < 85 \text{ nm}$ , the EQE at 1.51 eV is rapidly reduced. In our previous work, it has been described that the increased recombination rate of photogenerated carriers in the PV active layer is responsible for the reduction in infrared response [4]. The increase in the recombination rate is also confirmed by the dark current–voltage ( $J$ – $V$ ) measurements. As shown in Fig. 4, it is obvious that the dark current at low bias voltages rapidly increases with a reduction of  $d_{\text{CdS}}$ , and this result corresponds to the decreases in  $V_{\text{OC}}$  and FF.

It is likely that the changes of the infrared response and dark  $J$ – $V$  characteristics are caused by the change of the crystal structure of the CdS layer. Generally speaking, it is difficult for materials of different crystal systems to form a heterojunction. However, the  $c$  plane of the wurtzite structure and the (111) plane of the zincblende structure are relatively easy to form the heterojunction. Therefore, the CdTe grain grows to the  $\langle 111 \rangle$  direction onto the CdS layer which has the

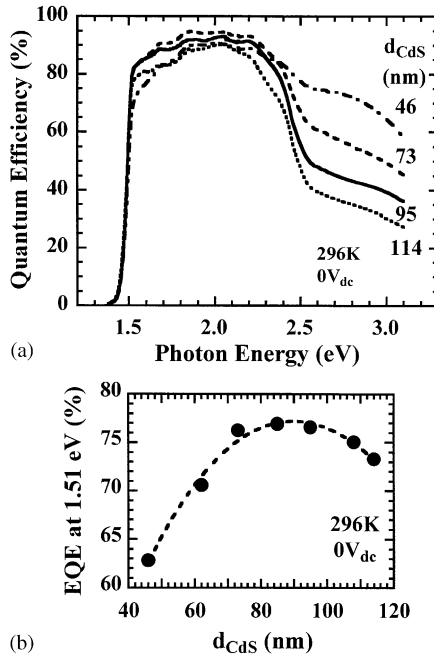


Fig. 3. Spectral responses of CdS/CdTe solar cells (a), and EQE at 1.51 eV as a function of  $d_{\text{CdS}}$  (b).

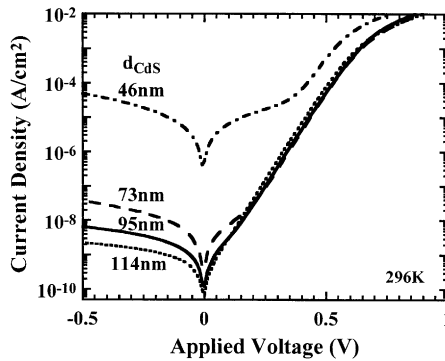


Fig. 4. Dark  $J-V$  characteristics as a function of  $d_{\text{CdS}}$ .

wurtzite structure preferentially oriented to the  $c$  plane. As the results of the XRD measurements of the CdS films prepared by our deposition process, it was confirmed that the CdS film has the wurtzite structure preferentially oriented to the (002) plane. Additionally, the results of the field emission scanning electron microscopy (FE-SEM) and the atomic force microscopy measurements showed that the CdS grain size decreases with a decrease in the thickness of the CdS film. This decrease in the CdS grain size should lead to the change of the crystallinity of the CdTe layer.

The deterioration of the crystallinity of CdTe was directly confirmed by the XRD measurements. Fig. 5(a) shows the XRD patterns of the 2- $\mu\text{m}$  thick CdTe layer deposited of different thick CdS layer. The crystal structure of CdTe is zincblende type with preferential orientation of the (1 1 1) plane parallel to the substrate. With a reduction of  $d_{\text{CdS}}$ , however, the intensity of CdTe (1 1 1) diffraction peak decreases. The change of the degree of preferred orientation of CdTe layer is clearly shown in Fig. 5(b). The degree of preferred orientation can be estimated from the peak intensities using the method of Harris for polycrystalline fiber texture analysis [5]. The degree of preferred orientation, that is, the orientation parameter of a certain crystal plane ( $hkl$ ) in a polycrystalline film can be quantified by

$$p(hkl) = N \left[ \frac{I(hkl)}{I_0(hkl)} \right] \left[ \sum_N \frac{I(hkl)}{I_0(hkl)} \right]^{-1}, \tag{1}$$

where  $N$  is the number of peaks in the region considered ( $=4$  for Fig. 5(a)),  $I(hkl)$  is the measured intensity of peak ( $hkl$ ) and  $I_0(hkl)$  is the relative intensity of the corresponding peak from a powder reference. For  $p(111) = N$ , all the grains of the CdTe layers are oriented in the (111) plane, and  $p(111) = 1$  means random orientation. As shown in Fig. 5(b), with a reduction of  $d_{\text{CdS}}$ ,  $p(111)$  decreases and

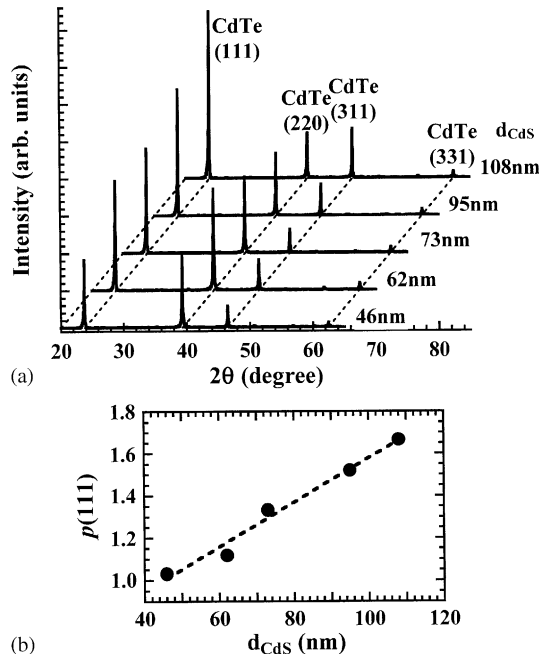


Fig. 5. XRD patterns of 2- $\mu\text{m}$  thick CdTe layers deposited on different thick CdS layers (a), and orientation parameters of CdTe (1 1 1),  $p(111)$ , as a function of  $d_{\text{CdS}}$  (b).

becomes close to 1. This result means that the thickness of the CdS layer crucially influences on the preferred orientation of CdTe.

The change of the crystallinity of CdTe with a reduction of  $d_{\text{CdS}}$  is also observed in the surface morphology of the CdTe layer. Figs. 6(a)–(c) show the FE-SEM micrographs of the surface morphologies of 2- $\mu\text{m}$  thick CdTe layers deposited on 46-, 73- and 144-nm thick CdS layers, respectively. Moreover, Fig. 6(d) shows the grain sizes of CdTe estimated from the FE-SEM micrographs. It is obviously shown that the grain size of CdTe decreases with a decrease in  $d_{\text{CdS}}$ . This result well agrees with the result of the XRD measurements. A reduction of grain size means the increase of the density of grain boundary. The grain boundary acts as the recombination center in itself. Additionally, it has been shown that the Cu diffusion increases with a decrease in grain size [6,7]. In our previous work, we also have shown that the unintentionally increased acceptor concentration makes the recombination of carriers in p-layer increase and the infrared response decrease [4]. It is reasonable to think that these increase in the recombination centers cause the changes of the dark  $J-V$  characteristics and the infrared response with the reduction of  $d_{\text{CdS}}$ .

Furthermore, it is likely that these changes of crystallinity of CdTe are concerned with the  $\text{CdTe}_{1-x}\text{S}_x$  mixed-crystal layer. The interatomic distance in the (1 1 1) plane of CdTe is over 10% larger than that in the  $c$  plane of CdS. Thus, it is necessary for

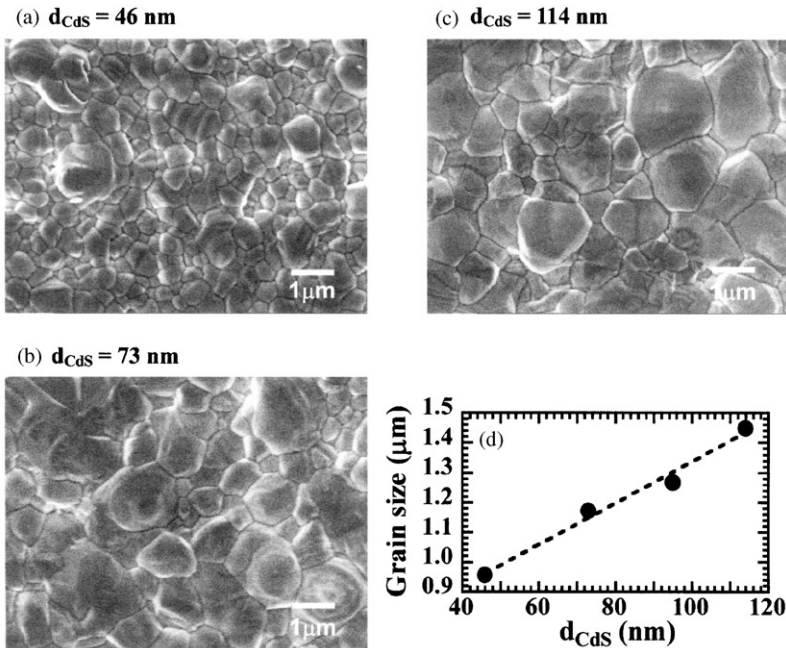


Fig. 6. Surface morphologies of CdTe deposited on (a) 46 nm-thick CdS layer, (b) 73 nm-thick CdS layer, (c) 114 nm-thick CdS layer. Also shown here are grain sizes of CdTe estimated from FE-SEM images as a function of  $d_{\text{CdS}}$  (d).

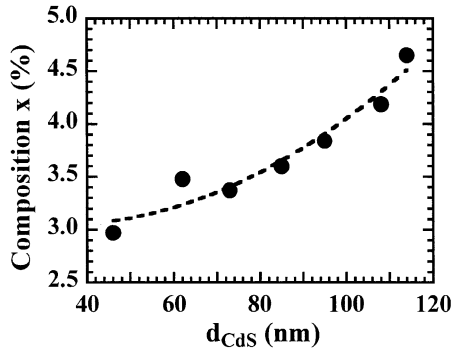


Fig. 7. Sulfur composition,  $x$  of  $\text{CdTe}_{1-x}\text{S}_x$  mixed-crystal layer plotted against  $d_{\text{CdS}}$ . They are estimated from band-gap energies of  $\text{CdTe}_{1-x}\text{S}_x$  measured by ER spectroscopy.

the formation of a heterojunction to intermix Te and S well. Sulfur has a smaller atomic radius than Te. Substituting onto Te sites in the CdTe lattice, sulfur reduces the interatomic distance and the lattice mismatch. We can estimate the degree of intermixing by the electroreflectance (ER) measurements. The detail of the ER measurement is described elsewhere [8]. We estimated the sulfur composition  $x$  of  $\text{CdTe}_{1-x}\text{S}_x$  from the band-gap energies measured by ER using the following equation [9]:

$$E_g(x) = 1.71x^2 - 1.01x + 1.51. \quad (2)$$

Fig. 7 shows the relation between the deduced sulfur composition  $x$  and  $d_{\text{CdS}}$ . It is clear that the composition  $x$  decreases with the reduction of  $d_{\text{CdS}}$ . The decrease in the composition  $x$  implies the increase in the lattice mismatch and interface states at the CdS/CdTe(S) interface. This deterioration of  $\text{CdTe}_{1-x}\text{S}_x$  mixed-crystal layer disturbs the grain growth of CdTe and reduce the grain size. These are likely to reduce the infrared response and increase the dark current at low bias voltages. Consequently, it seems appropriate that these structural deteriorations are responsible for the changes in dark  $J-V$  characteristics with a decrease in  $d_{\text{CdS}}$  below 85 nm, and finally correspond to the decreases in  $V_{\text{OC}}$  and FF.

#### 4. Conclusions

We have investigated the influences of the reduction of  $d_{\text{CdS}}$  on the PV performances of 2- $\mu\text{m}$  thick CdS/CdTe thin film solar cells. With a reduction of  $d_{\text{CdS}}$ ,  $\eta$  is increased mainly by an increase in  $J_{\text{SC}}$  in the region of  $d_{\text{CdS}} = 95\text{--}114$  nm, which is simply explained in terms of an increase in the spectral responses at short wavelength region. In contrast, at  $d_{\text{CdS}} < 85$  nm,  $\eta$  is turned to be decreased due to a decrease in  $V_{\text{OC}}$  and FF.

From results of several analyses, it is suggested that  $d_{\text{CdS}}$  crucially influences the formation of the  $\text{CdTe}_{1-x}\text{S}_x$  mixed-crystal layer and the grain growth of CdTe. The

deterioration of the crystallinity of CdTe due to a decrease in the sulfur composition  $x$  of the CdTe<sub>1-x</sub>S<sub>x</sub> mixed-crystal layer is concluded to be the most possible mechanism for the large decreases in  $V_{OC}$  and FF at  $d_{CdS} < 85$  nm. In other words, in this region, the most dominant influence of the CdS layer largely associated with the PV performances appears structural properties which result the change in the diode properties, rather than optical properties as the window layer.

### Acknowledgements

The authors would like to thank researchers in Matsushita Battery Industrial Co., Ltd. for their advice about the sample fabrication and their helpful discussion.

### References

- [1] K. Nakamura, M. Gotoh, T. Fujihara, T. Toyama, H. Okamoto, *Mater. Res. Soc. Symp. Proc.* 668 (2001) H63.
- [2] T. Aramoto, S. Kumazawa, H. Higuchi, T. Arita, S. Shibusaki, T. Nishino, J. Nakajima, M. Tsuji, A. Hanafusa, T. Hibino, K. Omura, H. Ohyama, M. Murozono, *Jpn. J. Appl. Phys.* 36 (1997) 6304–6305.
- [3] J. Britt, C. Ferekides, *Appl. Phys. Lett.* 62 (1993) 2851–2852.
- [4] T. Toyama, T. Suzuki, M. Gotoh, K. Nakamura, H. Okamoto, *Solar Energy Mater. Solar Cells* 67 (2001) 41–47.
- [5] G.B. Harris, *Philos. Mag.* 43 (1952) 113–123.
- [6] H.C. Chou, A. Rohatgi, N.M. Jokerst, S. Kamra, S.R. Stock, S.L. Lowrie, R.K. Ahrenkiel, D.H. Levi, *Mater. Chem. Phys.* 43 (1996) 178–182.
- [7] K.D. Dobson, I. Visoly Fisher, G. Hodes, D. Cahen, *Solar Energy Mater. Solar Cells* 62 (2000) 295–325.
- [8] T. Yamamoto, T. Toyama, H. Okamoto, *Jpn. J. Appl. Phys.* 37 (1998) L916–918.
- [9] K. Ohata, J. Saraie, T. Tanaka, *Jpn. J. Appl. Phys.* 12 (1973) 1641–1642.

# Photoluminescence characteristics of CdS layers deposited in a chemical bath and their correlation to CdS/CdTe solar cell performance

R. Mendoza-Pérez<sup>a,b</sup>, J. Aguilar-Hernández<sup>a</sup>, J. Sastre-Hernández<sup>a</sup>,  
N. Ximello-Quiebras<sup>a</sup>, G. Contreras-Puente<sup>a</sup>, G. Santana-Rodríguez<sup>c</sup>,  
O. Vigil-Galán<sup>a</sup>, E. Moreno-García<sup>a</sup>, A. Morales-Acevedo<sup>d,\*</sup>

<sup>a</sup> Escuela Superior de Física y Matemáticas del IPN, Edificio 9, UPALM, DF 07738, Mexico

<sup>b</sup> Universidad Autónoma de la Ciudad de México, Prolongación San Isidro, Núm. 151 Col. San Lorenzo Tezonco, Deleg. Iztapalapa, DF 09790, Mexico

<sup>c</sup> Instituto de Investigaciones en Materiales, Universidad Nacional Autónoma de México, Coyoacán 04510, DF, Mexico

<sup>d</sup> CINVESTAV-IPN, Depto. de Ingeniería Eléctrica, Avenida IPN No. 2508, DF 07360, Mexico

Received 16 June 2005; received in revised form 15 December 2005; accepted 6 January 2006

Available online 2 February 2006

Communicated by: Associate Editor T.M. Razykov

## Abstract

In this work, we study CdS films processed by chemical bath deposition (CBD) using different thiourea concentrations in the bath solution with post-thermal treatments using CdCl<sub>2</sub>. We study the effects of the thiourea concentration on the photovoltaic performance of the CdS/CdTe solar cells, by the analysis of the  $I$ - $V$  curve, for S/Cd ratios in the CBD solution from 3 to 8. In this range of S/Cd ratios the CdS/CdTe solar cells show variations of the open circuit voltage ( $V_{oc}$ ), the short circuit current ( $J_{sc}$ ) and the fill factor (FF). Other experimental data such as the optical transmittance and photoluminescence were obtained in order to correlate to the  $I$ - $V$  characteristics of the solar cells. The best performance of CdS–CdTe solar cells made with CdS films obtained with a S/Cd ratio of 6 is explained in terms of the sulfur vacancies to sulfur interstitials ratio in the CBD–CdS layers.

© 2006 Published by Elsevier Ltd.

**Keywords:** CdS; CdTe solar cells; Photoluminescence

## 1. Introduction

Chemical bath deposited (CBD) CdS thin films are regularly n-type, mainly due to sulfur vacancies. The variation of the S/Cd ratio for the chemical bath solution used for the preparation of such CdS films will presumably modify the physical

\* Corresponding author.

E-mail address: [amorales@gasparin.solar.cinvestav.mx](mailto:amorales@gasparin.solar.cinvestav.mx) (A. Morales-Acevedo).

properties of the films, such as the morphology, the optical and the electrical conductivity of these films. The S/Cd ratio will also have an influence upon the structural and electrical properties of the CdTe layer itself in CdS/CdTe solar cells, in addition to the modification of the CdS–CdTe interface. The aim of this work is to investigate the influence of the variation of the S/Cd ratio in the bath solution for CdS thin films prepared by Chemical Bath Deposition upon the characteristics of CdS/CdTe solar cells in a superstrate configuration.

It must be mentioned that CdS thin films grown by CBD has produced conversion efficiencies for CdS/CdTe solar cells as high as 16.5% (Wu et al., 2001). Hence, CdS has become an important material for this kind of solar cells. We have demonstrated that CBD–CdS films have poor crystalline quality, but they give excellent results for photovoltaic applications because of their high relative photoconductivity, in addition to their better morphological properties, like the roughness and pinhole density, in comparison with CdS films as grown by other techniques (Morales-Acevedo et al., 2002). Recently, we have studied CdS/CdTe solar cells with variable S/Cd ratio in the CdS chemical bath solution and an optimum efficiency of 12.6% was obtained with S/Cd = 5 (Mendoza-Pérez et al., 2005). In this paper we do a detailed study by varying the S/Cd ratio between 3 and 8, and try to correlate the optimum ratio for solar cells with photoluminescence and optical properties of the CdS films.

## 2. Experimental details

The CdS thin films were prepared by CBD on a commercial conducting glass (0.5  $\mu\text{m}$  thick  $\text{SnO}_2\text{:F/glass}$  with 10  $\Omega/\text{cm}$ ). For the chemical bath deposition of CdS, a beaker containing the reactants in a solution magnetically stirred was immersed in a temperature-controlled ( $\pm 1$   $^\circ\text{C}$ ) water bath. The concentrations of  $\text{NH}_3$  (2.0 mol/l),  $\text{NH}_4\text{Cl}$  (0.2 mol/l) and  $\text{CdCl}_2$  (0.1 mol/l) were kept constant in each experiment. In order to change the S to Cd atomic ratio in the solution, the  $\text{CS}(\text{NH}_2)_2$  (Thiourea) concentration was varied from 0.3 to 0.8 mol/l. The films were grown at 75  $^\circ\text{C}$  and the deposition times were also varied, accordingly to our previous knowledge of the growth kinetics, with the purpose of obtaining films with similar thickness in all cases. The solar cells were prepared by depositing CdTe thin films on  $\text{SnO}_2\text{:F/CBD–CdS}$  substrates by the hot wall close spaced vapor

transport (CSVT–HW) technique using CdTe powders (99.99% purity). The atmosphere used during the CdTe was a mixture of Ar and  $\text{O}_2$ , with an  $\text{O}_2$  partial pressure of 50%. In all cases, the total pressure was 0.1 Torr and prior to all depositions the system was pumped to  $8 \times 10^{-6}$  Torr as the base pressure. The CSVT–HW deposition of CdTe was accomplished by placing a CdTe graphite source block in close proximity (1 mm) to the substrate block. The deposition time was 3 min for all the samples deposited with substrate and source temperatures of 550  $^\circ\text{C}$  and 650  $^\circ\text{C}$ , respectively. CdTe layers of  $\approx 3.5$   $\mu\text{m}$  were obtained under these conditions. The CdTe thin films were coated with 200 nm of  $\text{CdCl}_2$  and then annealed at 400  $^\circ\text{C}$  for 30 min in air. For the back contact, Cu and Au (2.0 and 350 nm, respectively) were evaporated successively onto the CdTe layer, with an area of 0.08  $\text{cm}^2$ , and annealed at 180  $^\circ\text{C}$  in Ar ambient.

Optical transmission data were measured with a UV/Vis Shimadzu 3101 PC double beam spectrophotometer. The layer thickness was measured using a step profiler (Sloan Dektak III). For photoluminescence (PL) measurements, an  $\text{Ar}^+$  laser ( $\lambda = 457.9$  nm, 2.71 eV) was employed as the excitation source, focused on the sample through a cylindrical lens. The outgoing radiation from the sample was focused on the entrance slit of a 1403-SPEX double monochromator. The signal detection was carried out using an RCA-C31034 photomultiplier tube coupled to a photon counter thermoelectrically cooled in order to improve the signal-to-noise ratio. The PL spectrum was taken at room temperature.

## 3. Results and discussion

### 3.1. CBD–CdS thin films properties

The optical transmission spectra of the films grown for different S/Cd ratio are displayed in Fig. 1. High optical transmission and large bandgap values of the window material (CdS films) should improve the short circuit current of the solar cells. The highest average optical transmission is observed for S/Cd = 5, while for other films with smaller or higher S/Cd ratios, the optical transmission becomes lower in average. The thickness, the bandgap and the optical transmission of layers grown with different S/Cd ratios are listed in Table 1.

Fig. 2 shows the room temperature PL spectra for films with different S/Cd ratios in the solution. It is worth mentioning that the as-grown CBD–CdS films

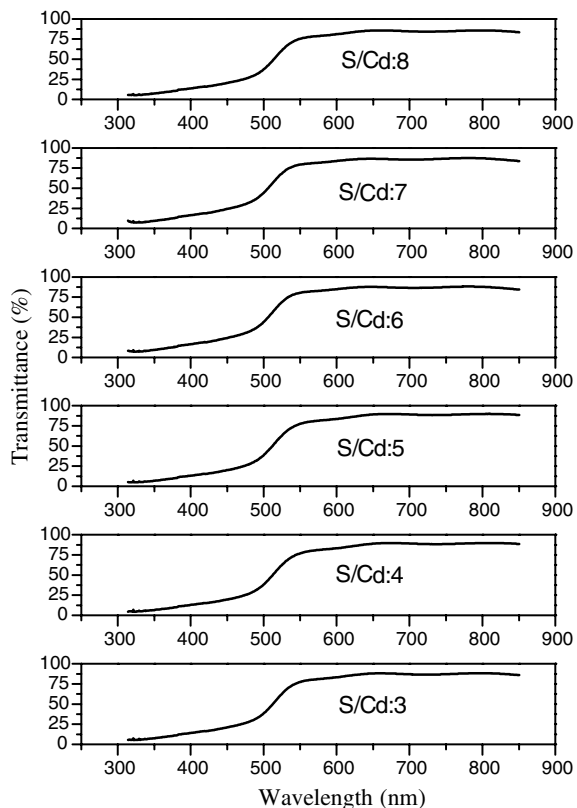


Fig. 1. Optical transmission characteristics of CBD-CdS films grown with different S/Cd ratios.

Table 1

Thickness ( $d$ ), average transmission ( $T_{av}$ ) and bandgap energy ( $E_g$ ) of the CBD-CdS samples for different S/Cd ratios

S/Cd	3/1	4/1	5/1	6/1	7/1	8/1
$d$ (nm)	145	140	130	110	111	109
$T_{av}$ (%)	83	85	88	87	86	85
$E_g$ (eV)	2.32	2.33	2.33	2.34	2.34	2.33

usually do not show any luminescence signal at room temperature possibly because of a high density of non-radiative defects with energy levels near the midgap. However, in this case, room temperature PL was detected for all the CdS samples, as can be seen in Fig. 2. All the samples showed two bands in the PL spectra, one localized at 2.30 eV and the other at 1.80 eV.

The band in the 1.60–1.85 eV range is associated to sulfur vacancies ( $V_S$ ), whereas the peak around 2.3 eV is usually related to interstitial sulfur ( $I_S$ ) (Mejía-García et al., 1999; Aguilar-Hernández et al., 2003). The enhanced PL signal is mainly due to sulfur enrichment, which gives rise to a

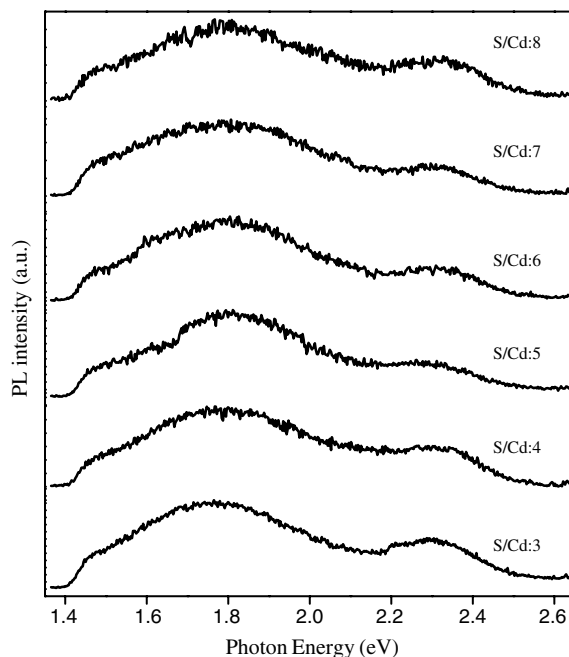


Fig. 2. Room temperature photoluminescence spectra of CBD-CdS films grown with different S/Cd ratios.

decrease of the trap density at the grain boundaries (Baccarani et al., 1978), decreasing in this way the density of non-radiative centers. In order to evaluate the effect of the sulfur enrichment we calculate the ratio of the relative intensities of  $V_S$  to  $I_S$  bands, respectively. Fig. 3, depicts the behavior as a function of the S/Cd ratio. As it can be seen, for S/Cd ratios of 3, 4 and 5 the quotient  $I_{V_S}/I_{I_S}$  increases as the S/Cd ratio increases, meaning that as more sulfur atoms are present in the bath solution more

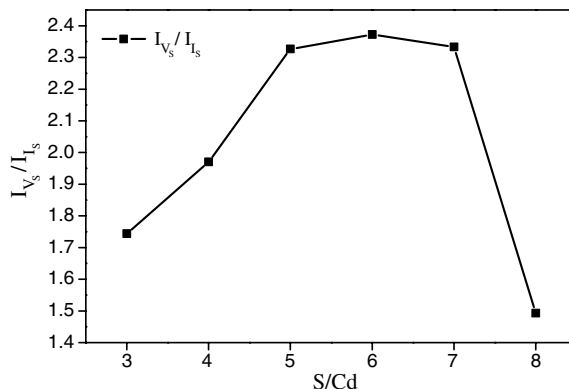


Fig. 3. Behavior of the relative sulfur vacancies ( $V_S$ ) to sulfur interstitials ( $I_S$ ) photoluminescence band intensities as a function of the S/Cd ratio.

sulfur vacancies are produced in relation to interstitial sulfur. For S/Cd ratios of 5, 6 and 7 an equilibrium between the introduction of sulfur atoms at interstitial sites and sulfur vacancies is achieved. For S/Cd ratios greater than 7, the sulfur atoms prefer to go into interstitial sites.

### 3.2. Solar cell performance

The  $I-V$  characteristics of CdS/CdTe solar cells under AM 1.5 illumination (normalized at  $100 \text{ mW/cm}^2$ ) as a function of S/Cd are shown in Fig. 4. Table 2 summarizes the values of short circuit current density ( $J_{sc}$ ), open circuit voltage ( $V_{oc}$ ), fill factor (FF) and efficiency ( $\eta$ ) of the solar cells at different S/Cd  $R_{tc}$ . As it can be observed, the values of  $J_{sc}$ ,  $V_{oc}$ , FF and  $\eta$  reach their higher values for S/Cd = 6.

From the  $I-V$  curves of the CBD–CdS based solar cells, one of the differences comes from the knee of the curves, which is partially associated to a change of the series resistance for the different samples. This feature can also be associated to a larger recombination ratio at the space-charge region

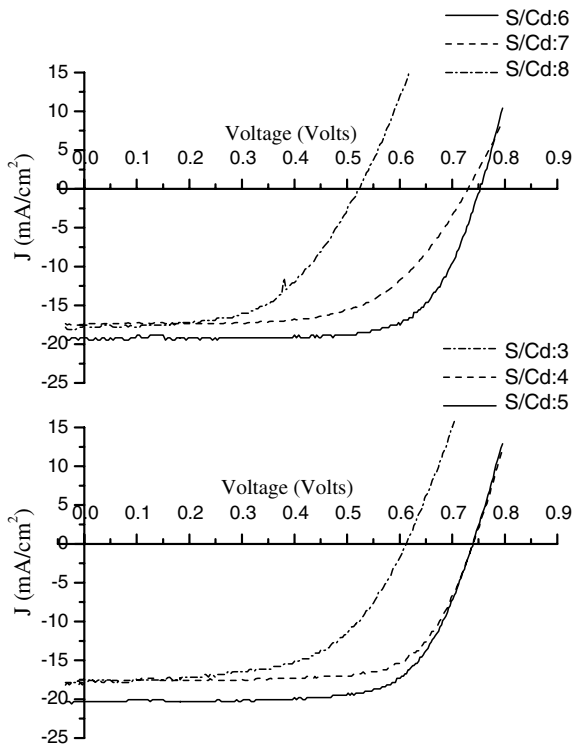


Fig. 4.  $J-V$  characteristics of the CdS/CdTe solar cells under illumination ( $100 \text{ mW/cm}^2$ ) as a function of the S/Cd ratio.

Table 2

Short circuit current density ( $J_{sc}$ ), open circuit voltage ( $V_{oc}$ ), fill factor (FF) and efficiency ( $\eta$ ) of the CdS/CdTe solar cells for different relative S/Cd concentrations

S/Cd	$R_{tc}$	$V_{oc}$ (V)	$J_{sc}$ (mA/cm <sup>2</sup> )	FF (%)	$\eta$ (%)
3/1		0.613	18.2	0.57	6.4
4/1		0.705	17.6	0.68	8.5
5/1		0.703	20.5	0.65	9.4
6/1		0.726	21.1	0.69	10.6
7/1		0.702	17.2	0.65	7.8
8/1		0.491	20.5	0.59	6.0

of the CdS/CdTe hetero-junction. It has been shown that sulfur enrichment in the CBD–CdS layers causes a decrease of carrier trap density at the grain boundaries (Baccarani et al., 1978). For samples with S/Cd ratios of 7 and 8 this enrichment could also take place, but probably at the expense of a ternary compound (CdSTe) at the CdS–CdTe interface with a larger polycrystalline disorder.

In summary, we have shown that the CBD–CdS thin films grown by varying the thiourea concentrations in the CdS bath solution cause a variation of the CdS/CdTe solar cells performance when the relative concentration of thiourea S/Cd is increased in the range from 3 to 8. We have found that the best characteristics are obtained for a S/Cd ratio of 6. This optimum value for the S/Cd ratio is related to the amount of sulfur vacancies in the films which possibly affect the amount of recombination at the CdS–CdTe hetero-junction.

### 4. Conclusions

We have found that CBD–CdS thin films grown under variable concentration of thiourea in the solution improve the CdS/CdTe solar cells performance when the relative concentration of S/Cd is increased from 3 to 8. The optimal conditions for CdS/CdTe solar cells performance are for CBD–CdS samples grown at  $75^\circ\text{C}$  with  $\text{S(thio)/Cd(CdCl}_2\text{)} = 6$  in the bath solution.

We also have found that the best performance from the  $I-V$  curves corresponds to solar cells made with CdS window layers with a large sulfur vacancy band (at 1.8 eV) in the photoluminescence measurements. More sulfur vacancies seem to contribute to a decrease of the minority carrier recombination at the CdS–CdTe interface and at the grain boundaries, allowing solar cells processed with CBD–CdS emitters to have better  $V_{oc}$ , FF and efficiency.

## Acknowledgement

This work was partially supported by CONACYT-México under Grant No. G27713A.

## References

- Aguilar-Hernández, J., Contreras-Puente, G., Morales-Acevedo, A., Vigil-Galán, O., Cruz-Gandarilla, F., Vidal-Larramendi, J., Escamilla-Esquivel, A., Hernández-Contreras, H., Hesiquio-Garduño, M., Arias-Carbajal, A., Chavarría-Castañeda, M., Arriaga-Mejía, G., 2003. Photoluminescence and structural properties of CdS thin films grown by different techniques. *Semicond. Sci. Technol.* 18, 111–115.
- Baccarani, G., Ricco, B., Spadini, G., 1978. Transport properties of polycrystalline silicon films. *J. Appl. Phys.* 49, 5565–5570.
- Mejía-García, C., Escamilla-Esquivel, A., Contreras-Puente, G., Tufiño-Velázquez, M., Albor-Aguilera, M.L., Vigil, O., Vailant, L., 1999. Photoluminescence studies of CdS films grown by close-spaced vapor transport hot walls. *J. Appl. Phys.* 86, 3171–3174.
- Mendoza-Pérez, R., Santana-Rodríguez, G., Sastre-Hernández, J., Morales-Acevedo, A., Arias-Carbajal, A., Vigil-Galan, O., Contreras-Puente, G., 2005. Effects of thiourea concentration on CdS thin films grown by chemical bath deposition for CdTe solar cells. *Thin Solid Films* 480–481, 173–176.
- Morales-Acevedo, A., Vigil-Galán, O., Contreras-Puente, G., Vidal-Larramendi, J., Arriaga-Mejía, C., Chavarría-Castañeda, M., Escamilla-Esquivel, A., Hernández-Contreras, H., Arias-Carbajal, A., Cruz-Gandarilla, F., 2002. Physical Properties of CdS Thin Films Grown by Different Techniques: A Comparative Study. In: *Proc. of the 29th IEEE Photovoltaic Specialists Conf., New Orleans (LA)*, pp. 624–627.
- Wu, X., Keane, J.C., Dhere, R.G., DeHart, C., Albin, D.S., Duda, A., Gessert, T.A., Asher, S., Levi, D.H., Sheldon, P., 2001. 16.5%-efficient CdS/CdTe polycrystalline thin-film solar cells. In: *Proc. of the 17th European PVSEC*, pp. 995–1000.



ELSEVIER

Solar Energy Materials & Solar Cells 75 (2003) 193–201

---

---

Solar Energy Materials  
& Solar Cells

---

---

www.elsevier.com/locate/solmat

# Influence of ITO surface modification on the growth of CdS and on the performance of CdS/CdTe solar cells

Jangeun Heo\*, Hokyun Ahn, Rowoon Lee, Younggun Han,  
Donghwan Kim

*Division of Materials Science and Engineering, Korea University, Anam-Dong, Sungbuk-Ku, Seoul 136-701, South Korea*

---

## Abstract

We treated the surface of indium–tin oxide (ITO) substrates in two ways, (i) coating of thin insulating ITO layer or (ii) irradiation of the surface with accelerated ions, and investigated the change in sheet resistance ( $R_{sh}$ ) and the water-contact angle (WCA).  $R_{sh}$  increased with the thickness of the insulating ITO layer or with the ion dose. WCA dropped as a result of the surface treatment to  $<15^\circ$ . The microstructure, the surface morphology, the optical transmittance, and the stoichiometry of CdS improved with the surface treatment. CdS/CdTe solar cells showed a better performance as a result of ITO surface treatment. © 2002 Published by Elsevier Science B.V.

*Keywords:* CdS/CdTe solar cell; Indium–tin oxide; Surface treatment; CBD CdS

---

## 1. Introduction

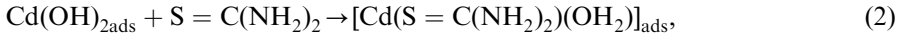
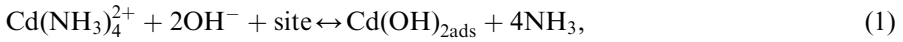
CdTe solar cells as a promising candidate for photovoltaic device are usually fabricated on transparent conducting oxides (TCO). Indium–tin oxide (ITO) is one of the most widely used TCO in optoelectronic devices including solar cells.

At present, the chemical bath deposition (CBD) method is widely used to make high quality films. The deposition process is controlled by chemical reaction kinetics in an ammonia solution of cadmium salt [1–3]. Ortega-Borges and Lincot reported

---

\*Corresponding author.

reaction steps involving cadmium acetate as follows [4]:



Cadmium complex and cadmium hydroxide species were adsorbed on the site such as ITO in Eq. (1), and then it formatted a surface complex with thiourea in Eq. (2). Then a heterogeneous nucleation and growth takes place through the atom-by-atom growth mechanism in Eq. (3).

Recently, the influence of the surface treatment of ITO has been actively investigated [5–8]. The surface energy and the polarity were changed with the surface treatments [9]. It is, therefore, not difficult to expect that the surface treatment would affect the physical properties of CdS films deposited on ITO and eventually change the performance of CdS/CdTe solar cells.

In this paper, we report the change in the characteristics of the surface-treated ITO, the morphology and the optical transmittance of CdS, and CdS/CdTe cells performance.

## 2. Experimental procedures

ITO-coated Corning 7059 glass substrates with the sheet resistance of  $5.8 \Omega/\square$  and  $7.6 \Omega/\square$  respectively were used in this study. Thin insulating ITO was deposited by the ion beam sputtering using argon ( $\text{Ar}^+$ ) and oxygen ( $\text{O}_2^+$ ) ions. Alternatively, ITO was irradiated by ions. The irradiation was carried out with 1 KeV  $\text{Ar}^+$  ions. Other types of ion beams such as nitrogen ( $\text{N}_2^+$ ),  $\text{O}_2^+$  and hydrogen ( $\text{H}_2^+$ ) plus 30%  $\text{Ar}^+$  mixture ions at doses ranging from  $5 \times 10^{15}$  to  $1 \times 10^{17} \text{ cm}^{-2}$  were used. CdS films of about 200 nm in thickness were deposited on ITO by the chemical bath deposition (CBD) using cadmium acetate (0.008 M), thiourea (0.01 M), ammonium acetate (0.08 M) and ammonia (0.05 M) in an aqueous alkaline solution. The temperature of the solution was kept at  $80^\circ\text{C}$  with the pH value in the range 10.5–11.5. CdTe films were deposited by the close-spaced sublimation (CSS). The substrate and the source temperatures were  $540^\circ\text{C}$  and  $600^\circ\text{C}$ , respectively. ITO was characterized by four-point probe method and water-contact angle (WCA) measurements. The optical transmittance was examined in the wavelength range of 400–850 nm by an UV-visible spectrophotometer. The microstructure of the CBD CdS films was studied by field emission scanning electron microscopy (FESEM).

$I$ – $V$  characteristics were measured by current–voltage measurements under global AM 1.5 condition. Structural analysis was carried out through X-ray diffraction (XRD) measurements. The chemical composition of the films was determined using Rutherford back scattering (RBS). A 2 MeV  $\text{He}^+$  ion beam incident at angle of  $10^\circ$ ,  $20 \mu\text{C}$  charge and 40 nA current was used for RBS analysis.

### 3. Results and discussions

Fig. 1 shows the change of the sheet resistance ( $R_{sh}$ ) and WCA with the thickness of the insulating ITO. While  $R_{sh}$  of non-treated ITO was  $5.7 \Omega/\square$ , higher  $R_{sh}$  was observed with the increased thickness of insulating ITO.  $R_{sh}$  seemed to saturate around the value of  $6.4 \Omega/\square$ . In a previous paper [10], we observed the resistivity of ITO changed with the type of ions used in ion beam sputtering. In case of ITO deposited by  $Ar^+$  and  $O_2^+$  mixture ions, the use of oxygen ions led to the decrease in the oxygen vacancy concentration in the films [11], and hence the increase of  $R_{sh}$ . Whereas WCA of non-treated ITO was over  $80^\circ$ , the films with the insulating ITO layer showed WCA of  $<15^\circ$ . The change in WCA indicates that the surface characteristics changed from hydrophobic to hydrophilic. In view of Ref. [12], the microstructure of CBD CdS films was dependent on the surface morphology of ITO. The change of the surface characteristics was expected to affect the growth mode of CdS in aqueous solution.

The photovoltaic performance of CdTe solar cells fabricated on ITO with a thin insulating layer is shown in Fig. 2. Insulating ITO with 10 nm in thickness showed the optimum performance of 10.5% ( $V_{oc}$ :0.70 V,  $J_{sc}$ :25.8 mA/cm<sup>2</sup>, FF:0.59).

The cell performance improved probably due to the reduced density of the adsorbed surface particles in CBD CdS similar to the case shown in Fig. 4. Moreover the shunt resistance of CdS/CdTe junction increased. For the case of 10 nm thick insulating ITO, a lower reverse saturation current ( $J_0$ ) was observed compared with the case of non-treated ITO. Whereas  $J_0$  of non-treated ITO was  $3.5 \times 10^{-5}$  A,  $J_0$  with 10 nm thick insulating ITO was in the range of  $1 \times 10^{-7}$ – $1 \times 10^{-8}$  A. This result is consistent with the higher  $V_{oc}$  obtained from the cells fabricated on the same ITO. But the increase in  $R_{sh}$  with the insulating layer beyond 15 nm in thickness resulted in a decrease of the short-circuit current ( $J_{sc}$ ) and the fill-factor (FF).

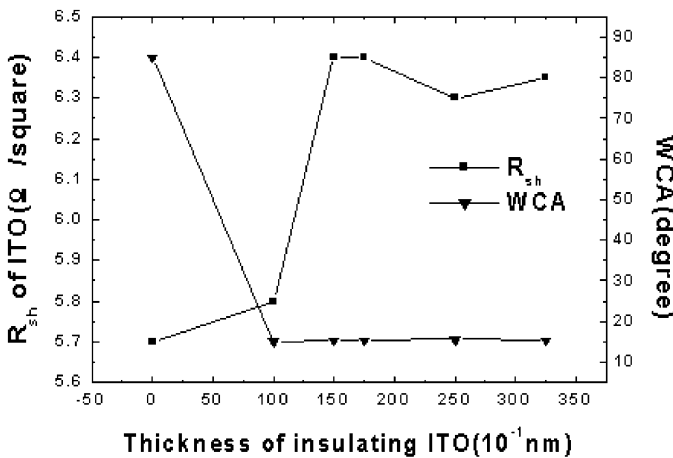


Fig. 1.  $R_{sh}$  and WCA change of ITO substrates with insulating ITO overlayers.

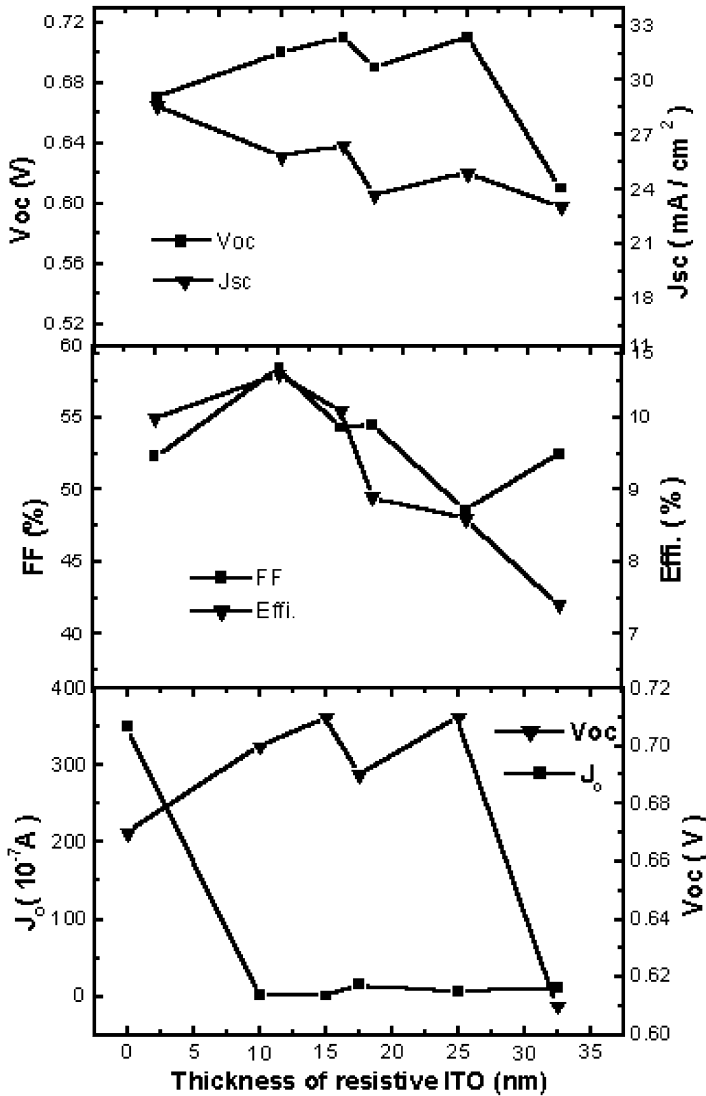


Fig. 2. Influence of insulating ITO on CdS/CdTe solar cell performance.

The dependence of  $R_{sh}$  on the ion dose and the types of ions is shown in Fig. 3. An increase in  $R_{sh}$  was observed with the irradiation doses. While  $R_{sh}$  of non-treated ITO was  $7.6 \Omega/\square$ ,  $R_{sh}$  increased up to  $8.9 \Omega/\square$  when ITO was treated with 1 KeV at  $1 \times 10^{17} \text{ cm}^{-2}$  using  $\text{H}_2^+$  plus 30%  $\text{Ar}^+$  mixture ions. ITO irradiated with  $\text{H}_2^+$  plus 30%  $\text{Ar}^+$  mixture ions showed the highest  $R_{sh}$  compared with other cases, probably due to the passivation effect of hydrogen.

The WCA values of ITO irradiated with various ions were  $< 15^\circ$ .

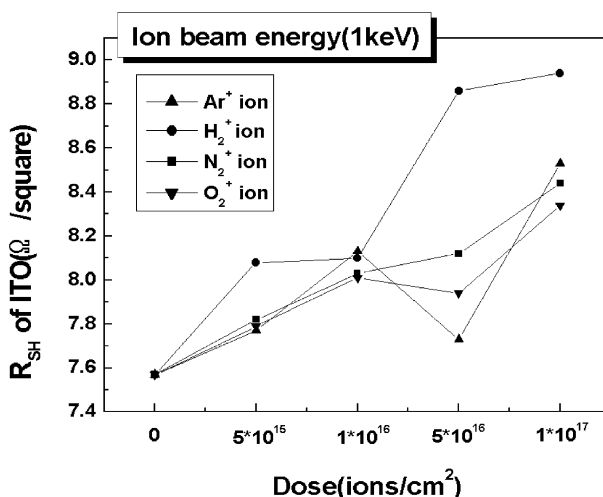


Fig. 3.  $R_{sh}$  of irradiated ITO with different ion beams at various doses.

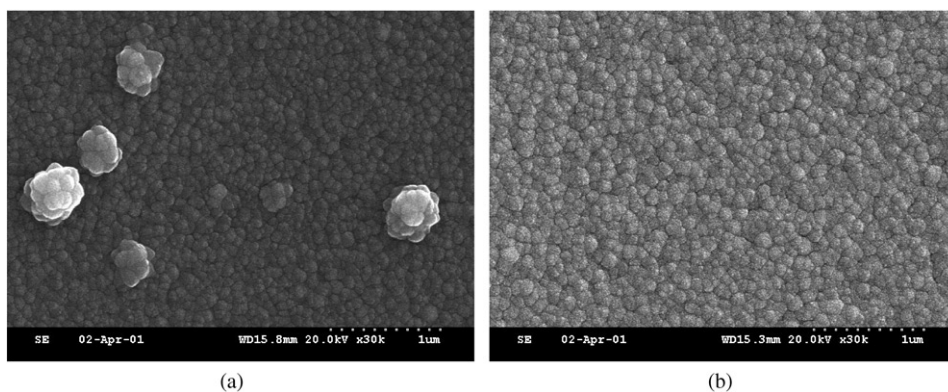


Fig. 4. Field emission scanning electron microscopy (SEM) image of CdS films ( $\times 30,000$ ): (a) CdS film of about 200 nm in thickness on non-treated ITO, (b) CdS of about 200 nm in thickness on surface-treated ITO by  $\text{H}_2^+$  plus 30%  $\text{Ar}^+$  ions at a dose of  $1 \times 10^{17} \text{cm}^{-2}$ .

Fig. 4 shows the surface morphology of CdS both on non-treated ITO and on the surface-treated ITO. The surface of CdS on the modified ITO had a smoother contour. However, the thickness of the two CdS films were the same within the measurement error. There was no difference in the grain size either. We think that the change in the surface characteristics from hydrophobic into hydrophilic promoted the heterogeneous nucleation and growth of CdS and thus resulted in the smoother surface.

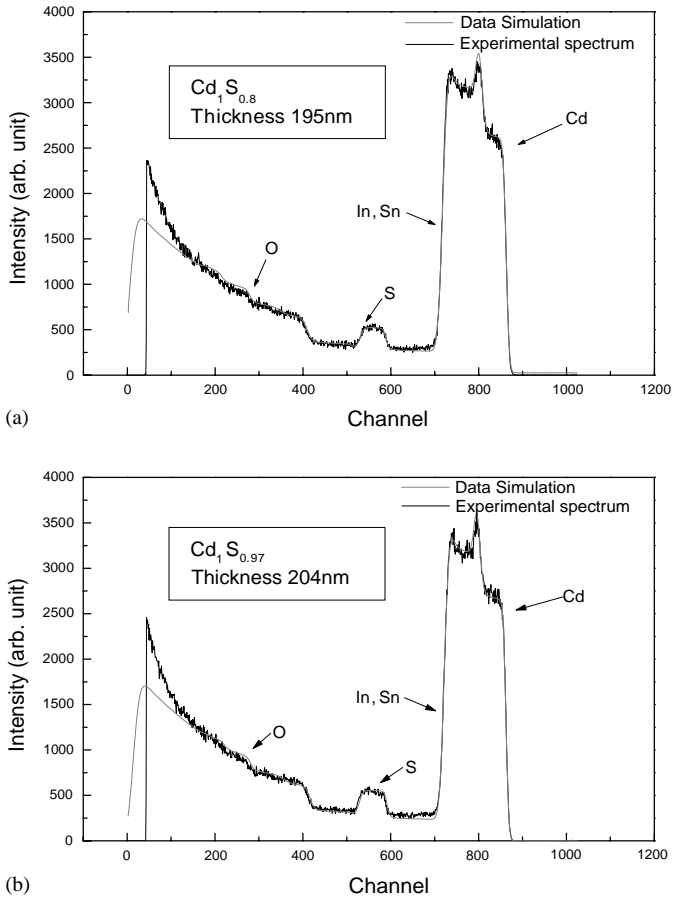


Fig. 5. Rutherford backscattering (RBS) spectra of CdS films: (a) CdS on non-treated ITO, (b) CdS on surface-treated ITO by  $H_2^+$  plus 30%  $Ar^+$  ions at  $1 \times 10^{17} \text{ cm}^{-2}$ .

Fig. 5 shows RBS spectra of the CdS films on non-treated ITO and on surface-treated ITO. Data simulation lines indicate the edges corresponding to the scattering from the respective elements at the surface.

The stoichiometry of CdS films can be calculated from the edge height  $H_{Cd}$  and  $H_S$  by using Eqs. (4) and (5)

$$H_{Cd} = \frac{\sigma_{Cd}(E_0)\Omega Q\delta E}{[\epsilon_0]_{Cd}^{CdS} \cos \theta_1}, \quad (4)$$

$$H_S = \frac{\sigma_S(E_0)\Omega Q\delta E}{[\epsilon_0]_S^{CdS} \cos \theta_1}, \quad (5)$$

where  $\sigma$ ,  $\Omega$ ,  $E_0$ ,  $Q$ ,  $\epsilon$  and  $\theta$  are the scattering cross-section ( $Z^2$  dependent), the solid angle subtended by the detector, the initial energy, the number of primary ions, the

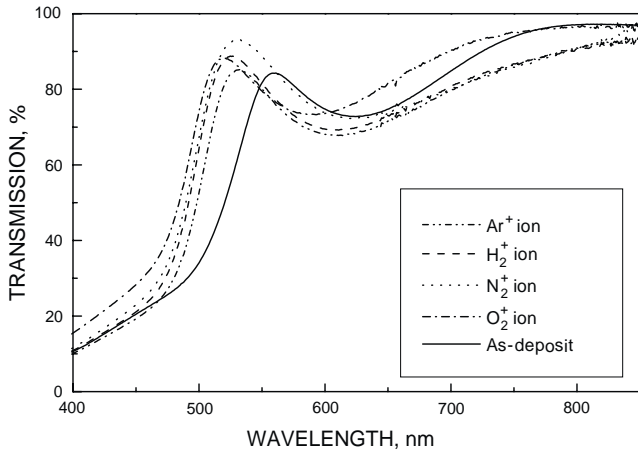


Fig. 6. Optical transmission of CdS films. The irradiation dose was  $1 \times 10^{17} \text{ cm}^{-2}$ . The thickness of CdS was 200 nm.

resultant stopping powers and the scattering angles, respectively. CdS films grown on the treated-ITO showed Cd:S ratio of 1:0.97 compared with the ratio of 1:0.8 on non-treated ITO. The stoichiometry of CdS on the treated ITO was closer to the ideal probably because the growth happened more like ion-by-ion mode due to the hydrophilic nature of the surface.

The optical transmittance spectra of CdS films, in the wavelength range of 400–850 nm are shown in Fig. 6. At shorter wavelength range, CdS films grown on surface treated ITO had a better transmission, whereas at the higher wavelengths, CdS film grown on non-treated ITO had better transmission. The enhanced transmittance was probably caused by the change in the optical index of CdS due to the different compositions as given in Fig. 5. The lower optical scattering by the adsorbed particles (Fig. 4) may have contributed to the higher optical transmittance also.

The absorption coefficient ( $\alpha$ ) of films for various wavelengths from the transmittance values was calculated by using Eq. (6) where  $t$  is the thickness of the film.

$$\alpha \propto \ln(1/T)t^{-1}. \tag{6}$$

The relation between the intensity of incident light,  $I_0$  and the detected intensity,  $I$ , is represented in Eq. (7) by the exponential form, where  $\alpha$  is the absorption coefficient and  $x$  is the penetration depth of the light.

$$I = I_0 \exp(-\alpha x). \tag{7}$$

The plot of  $\alpha^2$  versus  $h\nu_{ph}$  (photon energy) yields a straight line with an energy intercept of  $E_{Gd}$  (direct band gap energy) if a direct transition is involved as

described in Eq. (8) [13].

$$\alpha^2 \propto (\hbar\omega_{\text{pt}} - E_{\text{Gd}})^{1/2}. \quad (8)$$

Whereas the optical band gap for CdS on non-treated ITO was found to be 2.27 eV, the optical band gap of CdS on surface treated ITO was in the range 2.40–2.47. The larger  $E_{\text{Gd}}$  values of CdS on the treated ITO also suggest that the films have lower density of crystalline defects.

#### 4. Conclusions

CdS thin films were deposited on two types of surface-treated ITO: (1) an insulating ITO overcoat of 10 nm in thickness and (2) an ion-irradiated. The nature of the surface changed from hydrophobic to hydrophilic judging from the water-contact angle measurement. The sheet resistance increased slightly with the increase in the thickness of the insulating ITO. The sheet resistance also increased with the ion irradiation. The CdS films deposited on the surface-treated ITO showed a smoother surface morphology. The composition of CdS on surface-treated ITO was found to have a Cd to S ratio of 1:0.97, whereas CdS on non-treated ITO showed 1:0.8. The optical band gap for CdS on surface-treated ITO increased from 2.27 to 2.47 eV. CdS/CdTe cells with efficiencies up to about 10% were made as a result of this work.

#### Acknowledgements

The research was supported by the International Cooperation Research Program of the Ministry of Science and Technology.

#### References

- [1] I. Kaur, D.K. Pandya, K.L. Chopra, Growth kinetics and polymorphism of chemically deposition CdS films, *J. Electrochem. Soc.* 127 (1980) 943.
- [2] D. Lincot, R. Ortega, Chemical bath deposition of cadmium sulfide thin films, *J. Electrochem. Soc.* 139 (1992) 1880.
- [3] P.C. Rieke, S.B. Bentjen, Deposition of cadmium sulfide by deposition of thiourea in basic solutions, *Chem. Mater.* 5 (1993) 43–53.
- [4] R. Ortega-Bores, D. Lincot, Mechanism of chemical bath deposition of cadmium sulfide thin films in the ammonia-thiourea system, *J. Electrochem. Soc.* 140 (1993) 3464–3472.
- [5] D. Kim, Y. Han, J.-S. Cho, S.-K. Koh, Low temperature deposition of ITO thin films by ion beam sputtering, *Thin Solid Films* 377–378 (2000) 81–86.
- [6] M. Ishii, T. Mori, H. Fujikawa, S. Tokito, Y. Taga, Improvement of organic electroluminescent device performance by in situ plasma treatment of indium–tin-oxide surface, *J. Lumin.* 87–89 (2000) 1165–1167.
- [7] M.G. Mason, L.S. Hung, C.W. Tang, S.T. Lee, K.W. Wang, M. Wang, Characterization of treated indium–tin-oxide surfaces used in electroluminescent devices, *J. Appl. Phys.* 83 (3) (1999) 1688–1692.

- [8] C.-T. Lee, Q.-X. Yu, B.-T. Tang, H.-Y. Lee, Effects of plasma treatment on the electrical and optical properties of indium tin oxide films fabricated by r. f. reactive sputtering, *Thin Solid Films* 386 (2000) 105–110.
- [9] J.S. Kim, R.H. Friend, F. Cacialli, Surface wetting properties of treated indium tin oxide anodes for polymer light-emitting diodes, *Synth. Met.* 111–112 (2000) 369–372.
- [10] Y.H. Donghwan, K.J.-S. Cho, S.-K. Koh, Y.S. Song, Tin-doped indium oxide(ITO) film deposition by ion beam sputtering, *Sol. Energy Mater. Sol. Cells* 65 (2001) 211–218.
- [11] W.-F. Wu, B.-S. Chiou, Deposition of indium tin oxide films on polycarbonate substrates by radio-frequency magnetron sputtering, *Thin Solid Films* 298 (1997) 221.
- [12] R. Castro-Rodriquez, A.I. Olivia, V. Sosa, F. Caballero, J.L. Peña, Effect of indium tin oxide substrate roughness on the morphology, structural and optical properties of CdS thin films, *Appl. Surf. Sci.* 161 (2000) 340–346.
- [13] J. Choi, K.-J. Kim, J.-B. Yoo, D. Kim, Properties of cadmium sulfide thin films deposition by chemical bath deposition with ultrasonication, *Sol. Energy* 64 (1997) 41–47.

## Growth and physical properties of CdS thin films prepared by chemical bath deposition

This article has been downloaded from IOPscience. Please scroll down to see the full text article.

2009 J. Phys. D: Appl. Phys. 42 135404

(<http://iopscience.iop.org/0022-3727/42/13/135404>)

View [the table of contents for this issue](#), or go to the [journal homepage](#) for more

Download details:

IP Address: 128.235.245.73

The article was downloaded on 29/07/2010 at 23:11

Please note that [terms and conditions apply](#).

# Growth and physical properties of CdS thin films prepared by chemical bath deposition

H Moualkia<sup>1</sup>, S Hariech<sup>1</sup>, M S Aida<sup>1,3</sup>, N Attaf<sup>1</sup> and E L Laifa<sup>2</sup>

<sup>1</sup> Laboratory of Thin films and Interface, Faculty of Science, Department of Physics, University Mentouri of Constantine, 25000, Algeria

<sup>2</sup> Departement de chimie, faculté des Sciences, Université de Constantine, 25000- Constantine, Algeria

E-mail: [aida\\_salah@yahoo.fr](mailto:aida_salah@yahoo.fr)

Received 19 January 2009, in final form 15 April 2009

Published 12 June 2009

Online at [stacks.iop.org/JPhysD/42/135404](http://stacks.iop.org/JPhysD/42/135404)

## Abstract

This work deals with the preparation of cadmium sulfide (CdS) thin films by chemical bath deposition. The influence of the solution temperature is investigated in this study. We suggest that activation energy of the deposition rate measurement can be a tool for determining the nature of the deposition mechanism. We found that at low solution temperature, the growth mechanism proceeds via the ion by ion process, and found the corresponding activation energy equal to 0.06 eV. However, at higher solution temperature, the film deposition became via the cluster by cluster process, the growth rate activation energy is equal to 0.48 eV. The films' structural and optical properties were studied by x-ray diffraction analysis and UV-visible spectrophotometry. Structural analysis revealed that the deposited films have a cubic structure, and the crystallite size decreases with increasing deposition temperature. The transmission spectra of the film, in the visible range, show a high transmission coefficient (70%). The transmittance data analysis indicates that the optical band gap is closely related to the solution temperature. From this analysis, a direct band gap ranging from 2.21 to 2.34 eV was deduced. From the electrical characterization we inferred that CdS films are n-type and their dark conductivities reduced with increasing bath solution temperature. From the photoconductivity measurements we concluded that films deposited at low temperatures (less than 60 °C) or high temperatures (higher than 70 °C) have good optoelectronic properties suitable for utilization as a buffer layer in thin film solar cells.

## 1. Introduction

Due to the direct and wide band gap of CdS semiconductor, CdS thin films have attracted much interest as a potential candidate for optoelectronic devices. They are used as a window layer in CuInSe or CdTe heterojunction based solar cells [5–9], field effect transistors [10–12], photodetectors [10], gas sensors [12] and light emitting diodes [13].

The theoretical efficiency of these devices is 28%. The best efficiency recently reported is 19.8% [14], which makes these devices an interesting candidate for low cost solar energy conversion technology. CdS films act as an interface layer in the CIS solar cells; they present a lattice parameter that

matches well with that of the CIS layer (lattice mismatch around 1.2%) [15].

Several techniques have been used to fabricate CdS thin films, such as electrodeposition [16], chemical bath deposition (CBD) [17], screen printing (SP) [18] and physical vapour deposition [19]. Regardless of the deposition technique, the characterization of the post-deposited films and optimization of the deposition processes are still open subjects for research. A large number of studies have been carried out to achieve this goal in order to produce CdS thin films with good optoelectronic properties suitable for photovoltaic applications. For this purpose, the CdS thin films should have several properties: (i) relatively high transparency and not too thick to avoid absorption in the buffer layer and favour the

<sup>3</sup> Author to whom any correspondence should be addressed.

absorption in the CIS layer, (ii) not too thin to avoid short circuiting, (iii) relatively large conductivity so as not to alter the fill factor of the solar cell and higher photoconductivity so as not to alter the solar cell spectral response.

Chemical bath deposition is a favourable technique because it is a cost-effective and a large-scale method and also a nondestructive method for CdS coating on CIS thin films. It is an excellent method for producing nanomaterials [20].

The CdS deposition by CBD is based on the controlled precipitation of metallic ions in a solution containing sulfide ions of controllable concentration. This can be achieved mainly through two mechanisms: (i) ion by ion (heterogeneous reaction) or (ii) cluster by cluster (homogeneous reaction). Little attention has been paid to the determination of the mechanism involved during film formation despite the fact that the films' properties are closely related to the deposition mechanism [21]. Evidence of deposition with the ion by ion mechanism cited in the literature is that this mechanism yields a dense material and a well-adherent film with a hexagonal or mixed hexagonal and cubic structure; however, the cluster by cluster mechanism yields porous material and less adherent films with a pure cubic structure [22, 23], but these criteria are controversial [24–26]. However, it is not clear whether the deposition proceeds by the ion by ion or by the cluster by cluster mechanism. In this paper we suggest that the calculation of the deposition activation energy can be a tool for the determination of the growth process since the two mechanisms involve various chemical reactions. In this study, CdS thin film was grown by the chemical bath technique. The structural, optical and electrical properties of the CdS thin film have been investigated as a function of bath temperature in order to study their growth mechanism and optimize their optoelectronic properties.

## 2. Experimental details

The bath solution, used in this study for CdS preparation, is composed of deionized water, ammonium hydroxide  $\text{NH}_4\text{OH}$  (10M), cadmium sulfate  $\text{CdSO}_4$  (1M) as a source of cadmium and thiourea  $\text{CS}(\text{NH}_2)_2$  (1M) as a source of sulfide; the total volume of the solution is 160 ml. The solution was first homogenized by stirring in a beaker with a small magnetic bar, at room temperature. Commercial glass slides, used as substrates, were cleaned in acetone and methanol ultrasonically. The samples were kept vertically in the beaker. The solution temperatures were varied and regulated from 40 to 80 °C at a constant  $\text{pH} = 11$ . The deposition time was 25 min for each film. After deposition, the CdS films were washed with distilled water to remove the loosely adhered CdS particles on the films and finally dried in air.

The film thicknesses were determined from profilometry and ellipsometric measurements. The calculated thicknesses from both techniques were in the same order. The obtained film thicknesses range from 200 to 600 nm with increasing bath temperature. The structural characterization of the films was carried out by the x-ray diffraction (XRD) technique using an x-ray diffractometer (Philips X'Pert) with  $\text{Cu K}\alpha$  radiation. The films' grain size and strain were estimated

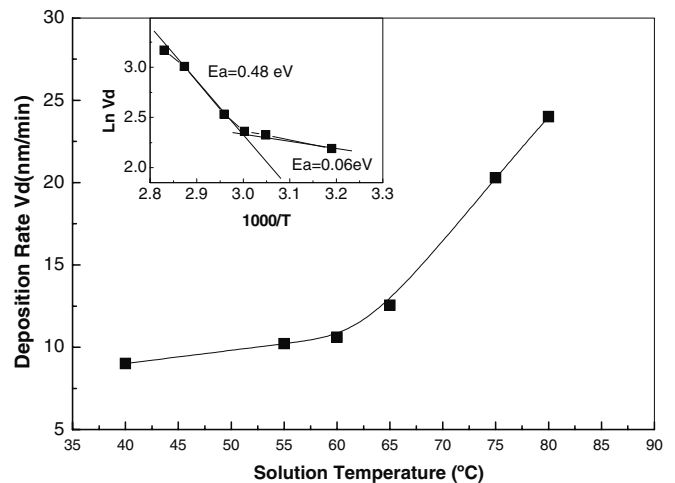


**Figure 1.** Variation of the deposition rate as a function of the bath solution temperature. Inset shows the Arrhenius plot of the deposition rate as a function of the inverse of temperature.

from the XRD patterns analysis. The optical transmittance of the films was studied using a Shimadzu 3101 PC UV–visible spectrophotometer. The optical gap and the film disorder characterized by the Urbach tail [27–29] were deduced from the recorded transmittance spectra. The electrical conductivity and the photoconductivity of the films were measured in a coplanar structure obtained by evaporation of two golden strips on the film surface. For the photoconductivity measurement, the samples were illuminated by unfiltered white light from a halogen lamp; the light intensity was 20 000 lx.

## 3. Results and discussion

### 3.1. Growth rate

In figure 1 we have reported the variation of the deposition rate of CdS thin films as a function of the bath temperature. As seen, the deposition rate is an increasing function of the bath temperature indicating a significant dependence of the growth rate on temperature. The highest growth rate, equal to 24  $\text{nm min}^{-1}$ , was obtained with films grown at 80 °C; however, at low temperature the deposition rate is around 9  $\text{nm min}^{-1}$ . Generally, the film thickness is the most reported parameter rather than the deposition rate. Thus it is hard to compare these values with the results in the literature. The increase in the deposition rate with the bath temperature is due to the kinetic enhancement of the involved reactions during film growth. In the inset of figure 1 we have reported the variation of the deposition rate in the Arrhenius plot. As seen, the deposition rate is thermally activated. In this figure two activation energies are deduced. In the low temperature range ( $T < 60$  °C) the corresponding activation energy is found to be equal to 0.06 eV and in the higher temperature range ( $T > 60$  °C) the activation energy is larger; it is equal to 0.48 eV. This means that there are two deposition processes; the first one with low activation energy is dominant at low temperatures, and the second one, with higher activation energy, is dominant at higher temperatures.

**Table 1.** Comparison of different reactions involved in the ion by ion and cluster by cluster deposition processes.

	<i>I. Reactions in the solution</i>
$\text{CdSO}_4 \rightarrow \text{Cd}^{2+} + \text{SO}_4^{2-}$	(cadmium sulfate dissociation) (1)
$\text{NH}_4\text{OH} \rightarrow \text{NH}_3 + \text{H}_2\text{O}$	(ammonia dissociation) (2)
$\text{Cd}^{2+} + 4\text{NH}_3 \rightarrow [\text{Cd}(\text{NH}_3)_4]^{2+}$	(metallic ion complexation to avoid precipitation) (3)
$\text{CS}(\text{NH}_2)_2 + 2\text{OH}^- \rightarrow \text{S}^{2-} + \text{CH}_2\text{N}_2 + 2\text{H}_2\text{O}$	(thiourea decomposition) (4)
	<i>II. Surface reactions</i>
a. Ion by ion process	b. Cluster by cluster process
$\text{Cd}^{2+} + \text{S}^{2-} \rightarrow \text{CdS}$ (5a)	Release of free $\text{Cd}^{2+}$ ions
	$[\text{Cd}(\text{NH}_3)_4]^{2+} \rightarrow \text{Cd}^{2+} + 4\text{NH}_3$ (5b)
	Cluster formation
	$n\text{Cd}^{2+} + 2n(\text{OH})^- \rightarrow [\text{Cd}(\text{OH})_2]_n$ (6b)
	$\text{Cd}(\text{OH})_2]_n + n\text{S}^{2-} \rightarrow n\text{CdS} + 2n\text{OH}^-$ (7b)

To identify these processes we turn to the CBD growth mechanism. It is well known, as mentioned in the introduction, that CdS growth by CBD occurs mainly through two processes: (i) ion by ion or (ii) cluster by cluster. These mechanisms are well explained in the review book [30]. In table 1 we have summarized the different reactions involved in each mechanism. As can be deduced from table 1, the film formation via the ion by ion process passes through a single simple reaction (reaction (5a)). However, the film formation via cluster by cluster needs to overcome many reactions (reactions (5b)–(7b)). Thereafter, we speculate that the ion by ion process is spontaneous and then less thermally activated. However, the cluster by cluster process needs higher temperature to occur. We conclude that, at low solution temperature conditions ( $T_s < 60^\circ\text{C}$ ), the deposition mechanism is achieved by the lower activation temperature process i.e. the ion by ion one. When the ion product  $[\text{Cd}^{2+}][\text{S}^{2-}]$  exceeds the solubility product  $K_{sp}$  ( $10^{-28}$ ) solid phase CdS will be formed [30]. Moreover, the deposition kinetic is governed by the mobility of the ions in the solution. Indeed, the mobility of the species is reduced at low temperature; this is the cause of the low deposition rate obtained in this temperature range.

At higher temperatures ( $T_s > 60^\circ\text{C}$ ), where the deposition rate has a larger activation energy, the cluster by cluster process is the dominant growth mechanism. An increase in the solution temperature induces higher hydroxide cluster  $\text{Cd}(\text{OH})_2$  and sulfide ion concentrations. Consequently, the deposition rate is greater in this temperature range.

### 3.2. Structural properties

The XRD patterns of the samples deposited at different temperatures are shown in figure 2. The diffraction patterns show an intense peak located at  $2\theta = 26.6^\circ$ , which is associated with the plane (1 1 1). Two small ones, located at  $44.3$  and  $52.3^\circ$ , assigned, respectively, to the (2 2 0) and (3 1 1) reflections planes, emerge when the solution temperature is equal to  $75^\circ\text{C}$ . As presented in table 2, the inter-planar spacings ( $d_{hkl}$ ) for the three diffracting planes calculated from the XRD patterns are in good agreement with the standard JCPDS card 080-0019 [31] of the CdS cubic phase values. This indicated that the obtained CdS films have a cubic structure with the preferential orientation normal to the (1 1 1) direction. The

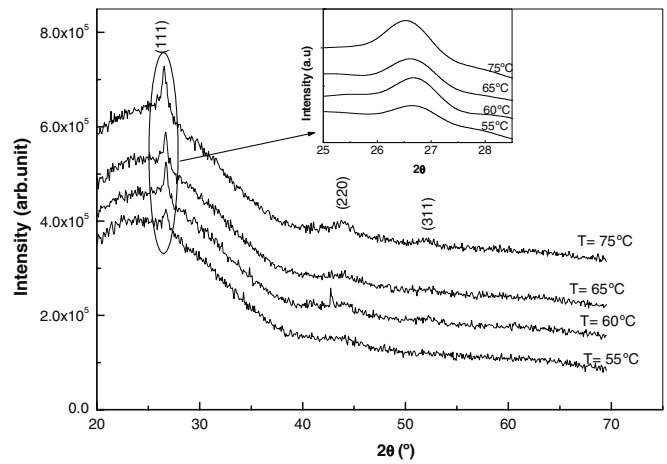


**Figure 2.** XRD patterns recorded in the CdS films prepared with different solution temperatures.

**Table 2.** Comparison of inter-planar spacings ( $d_{hkl}$ ) calculated from the XRD patterns and JCPDS data for the diffracting planes.

(hkl)	XRD (Å)	JCPDS (Å) [31]
(1 1 1)	3.35	3.354
(2 2 0)	2.05	2.054
(3 1 1)	1.74	1.752

same structure in the CdS films deposited by CBD has been reported by many authors [32, 33].

From the XRD pattern two quantities are simply calculated, the grain size  $D$  and the film strain  $\epsilon$ . The grain size can be determined using the Scherrer formula [34]:

$$D = \frac{K\lambda}{\beta \cos \theta}, \quad (1)$$

where  $\beta$  is the full width at half maximum (see inset of figure 2) of the peak,  $\theta$  is the Bragg angle,  $\lambda$  is the wavelength of the x-ray and  $K$  is the Scherrer constant, which is taken as 0.9 for the calculations [34].

It is worth noting that the XRD diffraction peak broadening can be due to the crystallite grain size and (or) to the stress in the grain. However, the size and strain broadening have different angular dependence which makes it possible to discriminate them [35]. According to this and using the Williamson–Hall method [36, 37] we concluded that the peak broadening originates mainly from the grain size.

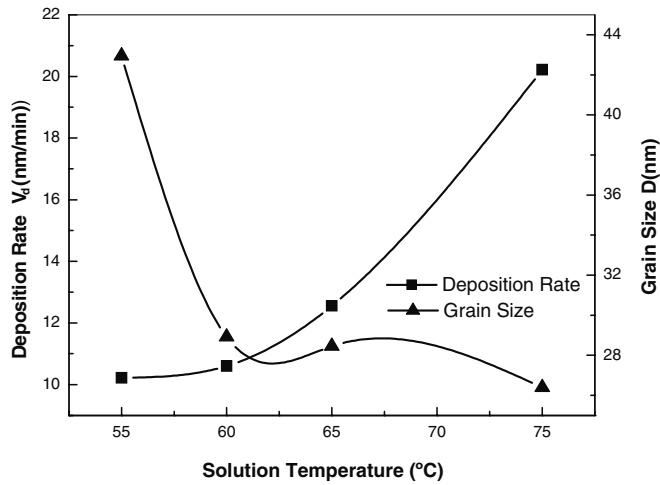


**Figure 3.** Correlation between the grain size and the deposition rate variation as a function of solution temperature.

In figure 3 the variation of the measured grain size with the bath temperature is reported. In the same figure we have reported the variation of the deposition rate. The grain size decreases with increased bath temperature. The grain size varies from 43 nm to 26.4 nm with increasing solution temperature. This trend has been reported by many authors [38, 39]. The reduction of the grain size can be explained by the variation of the growth rate. As seen in figure 3, the grain size variation is opposite to the variation of the growth rate. It is well recognized that thin film growth proceeds through three steps: (i) nucleation, (ii) subsequent coalescence and (iii) vertical growth. At high deposition rates, the nucleation step is fast; the nucleation sites concentration is then large. Thereafter, the nuclei size enlargement is limited and blocked by the surrounding nuclei. However, at low deposition rates, the low concentration of the nuclei sites enables the nuclei to grow and attain a larger size. Consequently, the grain size is larger in films deposited with low deposition rate.

### 3.3. Optical properties

The optical properties of the deposited CdS films are studied by analysing the spectroscopic optical transmittance in the visible range. In figure 4 the obtained transmittance spectra in films deposited at various solution temperatures are reported. The absorption coefficient  $\alpha$  of CdS thin films was calculated from the transmittance spectra using the Beer-Lambert approximation [40]. The variation of the coefficient of absorption with the wavelength energy was used to calculate the film optical gap  $E_g$  and the band tail width  $E_{00}$  (the so-called Urbach tail); the latter is closely related to the disorder in the film network. These quantities,  $E_g$  and  $E_{00}$ , were deduced, respectively, from the intercept of the curve  $(\alpha h\nu)^2 = f(h\nu)$  with the abscissa axis and the slope of the graph  $\text{Ln } \alpha = f(h\nu)$ .

The influence of the solution temperature on the calculated values of the optical gap and the disorder in the films' network are reported in figure 5. As can be seen, the variation of the optical gap is opposite to the disorder. This behaviour clearly indicates that the optical gap in the obtained films is

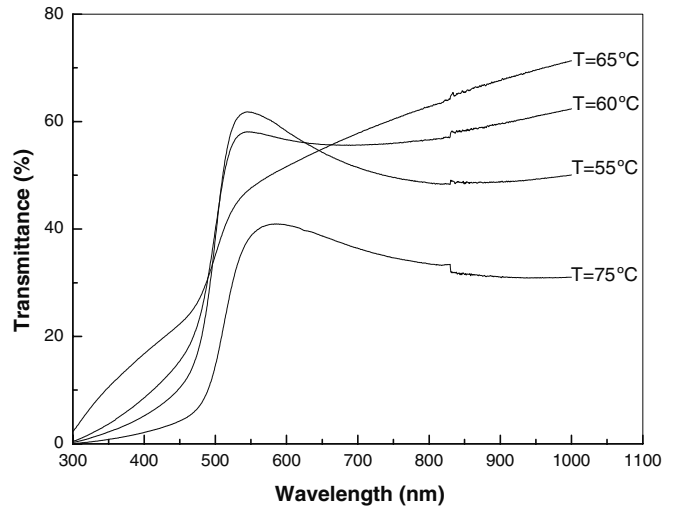


**Figure 4.** UV-visible transmittance spectra reordered in the CdS films deposited with various solution temperatures.

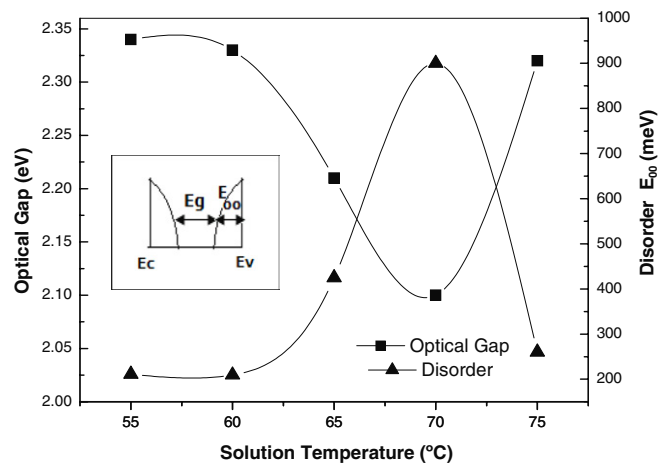


**Figure 5.** The variations of the CdS thin film optical gap and band tail width, known as the Urbach tail or disorder in the film network, as a function of the deposition temperature. Inset is a schematic drawn of the bands bending in semiconductor showing the dependence of the band tail width and the optical gap .

governed by the disorder variation. As depicted in the inset of figure 5, showing the bands bending in a semiconductor, an increase in the band tail width causes a reduction in the optical gap. The notion of disorder  $E_{00}$  associated with the tail of the sub-band-gap absorption and its correlation with the optical band gap, was first introduced in covalent semiconductors such as amorphous silicon thin films [41]. Recently, this notion was transferred to a direct band gap semiconductor such as ZnO, where a quite similar trend in the correlation between the optical band gap and the disorder variations is seen [42, 43]. However, for CdS thin film the notion of steepness is introduced, the latter describes the shape of the graph  $\alpha^2 = f(h\nu)$ . The steepness (or sharpness) value is defined as the slope of the graph at the beginning of the band to band absorption. An increase in the steepness which is associated with the reduction in the optical band gap is reported in CdS thin films deposited by CBD [44]. In this work we emphasize that the relation between the band tail width and

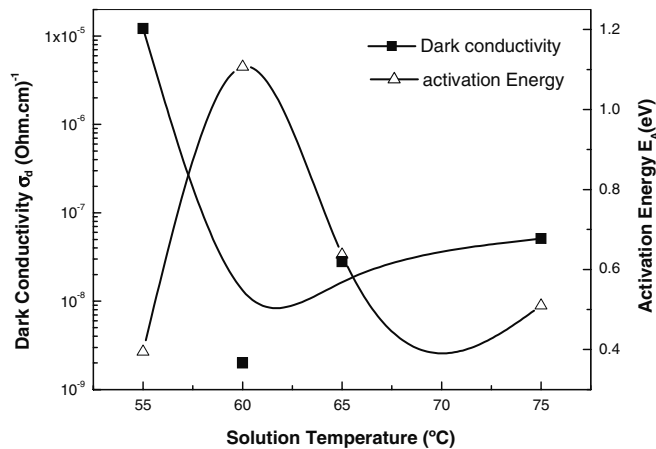


**Figure 6.** Dependence of the dark conductivity and its activation energy on the deposition temperature.

the optical band gap is quite as valid for CdS as for amorphous silicon thin films.

### 3.4. Electrical properties

The conductivity was measured in the dark at different temperatures. From the variation of the conductivity versus the measurement temperature the conductivity activation energy is deduced. We have drawn in figure 6 the variations of the dark conductivity and its activation energy as a function of the solution temperature. As can be seen, the influence of the solution temperature on the conductivity can be divided into two regions: (i) low temperature region ( $T_s < 60^\circ\text{C}$ ), where the growth mechanism is achieved via the ion by ion mechanism as mentioned above; the conductivity varies about four orders of decades, with changing solution temperature it decreases from  $10^{-5}$  to  $10^{-9}$  ( $\Omega \text{cm}$ )<sup>-1</sup>; (ii) high temperature region ( $T_s > 60^\circ\text{C}$ ), which corresponds to the deposition process through cluster by cluster, the conductivity increases slowly about one order of magnitude from  $10^{-9}$  to  $10^{-8}$  ( $\Omega \text{cm}$ )<sup>-1</sup>. The high conductivity measured in the low temperature region can be explained by the film structure. It has been argued that the ion by ion process produces a compact CdS film, whereas the cluster by cluster process gives rise to porous films [22, 23]. Moreover, the thiourea dissociation is slow at low temperatures [30]; thereafter the  $\text{S}^{2-}$  concentration is smaller than metallic  $\text{Cd}^{2+}$  one. Consequently, we speculate that CdS films deposited at low temperatures contain a large number of S vacancies. The latter act as donors in the CdS films. This explains the increase in the conduction activation energy  $E_A$  with increasing solution temperature from 55 to  $60^\circ\text{C}$  as a consequence of the reduction of these donor concentration S vacancies. The conductivity activation energy is a clear indication of the position of the Fermi level  $E_F$  regarding the minimum of the conduction band  $E_C$  ( $E_A = E_C - E_F$ ). To monitor the Fermi level position in the forbidden band, one can calculate the ratio  $2E_A/E_g$ , as shown in figure 7. When this ratio is close to unity, this means that the Fermi level is close to the mid-gap position and the semiconductor is intrinsic. However, the reduction of this ratio means that the Fermi level moves towards the minimum conduction  $E_C$  band and that the

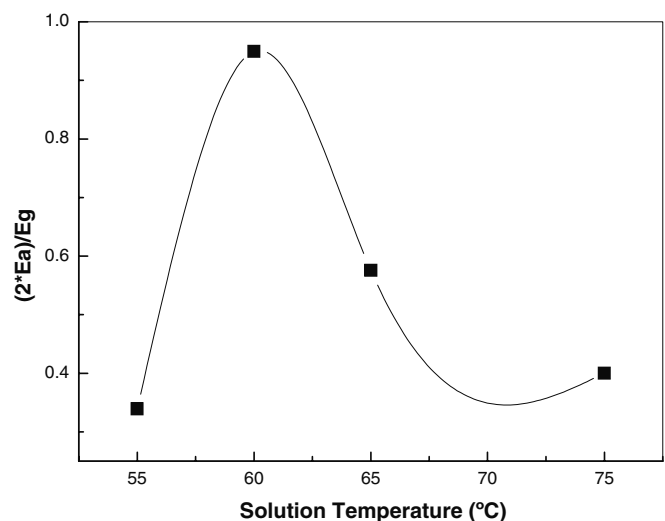


**Figure 7.** Variation of the ratio  $2E_A/E_g$  as a function of solution temperature. This ratio is used as an indication of the Fermi level position in the CdS forbidden band (see the text).

material contains a large number of donor impurities. As can be deduced from figure 7, the deposited films are n-type, which is in good agreement with the commonly reported results of CdS thin films.

The deposition temperature altered the dark conductivity and the Fermi level position in our films through its influence on the donors' impurities, namely S vacancies  $V_S$  or Cd interstices  $I_{Cd}$ . For films deposited at  $60^\circ\text{C}$  we noticed a larger value of the ratio  $2E_A/E_g$  (figure 7) equal to 0.94, which suggests that films deposited at this temperature are more stoichiometric and free of electrical defects. This temperature corresponds to the transition from the ion by ion growth to the cluster by cluster growth. It is possible that at this temperature both growth mechanisms are present; it can be considered as the transition temperature. However, films deposited at extreme temperatures i.e. low temperature ( $<60^\circ\text{C}$ ) or high temperature ( $>65^\circ\text{C}$ ) films are n-type and they contain a large number of donor defects such as S vacancies for the low temperature condition and/or Cd interstices for the higher temperature condition.

The photoconductivity measurements are carried out with an unfiltered visible light. Figure 8 represents the variation of the current in dark and under illumination recorded for a CdS sample taken as an example. As seen, the current slowly increases with illumination time; this is due to the generation process. A steady state is reached after 400 s of illumination time; this is an average time of saturation obtained in all the studied samples. However, when the light is turned off, as seen in figure 9, the current drops sharply, indicating that the generated photocarriers have a short lifetime.

In figure 9 the variation of photoconductivity on the dark conductivity ratio as a function of the bath temperature is reported. Films deposited at extreme temperatures, i.e. at a low temperature ( $55^\circ\text{C}$ ) or at a high temperature ( $75^\circ\text{C}$ ), exhibit good photoconductivity. The ratio of the photoconductivity to the dark conductivity is about  $10^3$ . However, films prepared at medium temperatures ( $60\text{--}70^\circ\text{C}$ )

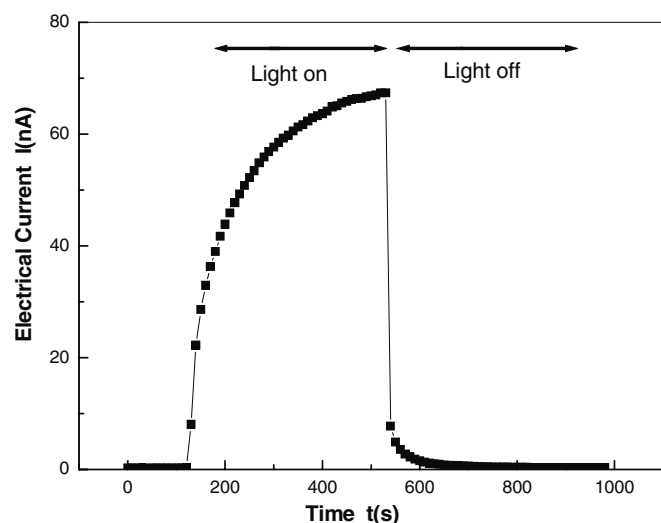


**Figure 8.** Example of variation of current flow in a CdS sample at 20 V polarization in dark and under illumination.

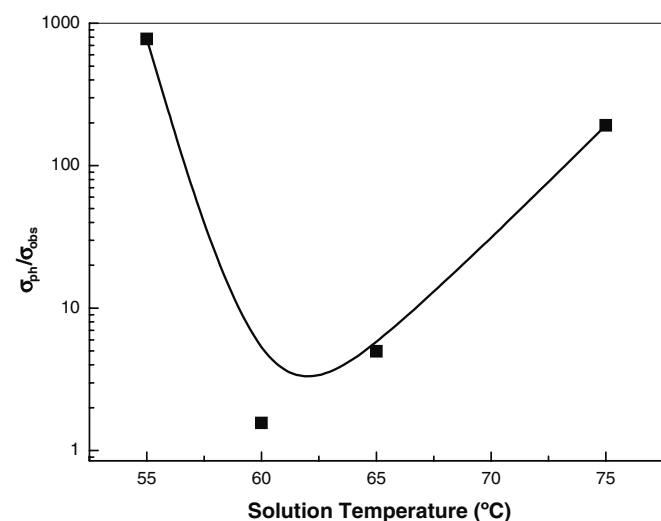


**Figure 9.** Variation of the photoconductivity and dark conductivity in CdS films as a function of the solution temperature.

have the worst photoconductivity. As mentioned above, the medium temperature corresponds to the transition of the deposition process from ion by ion to cluster by cluster. According to the value of the disorder (figure 5), films prepared at these temperatures contain more structural defects, these defects act as traps for the photogenerated carriers, and hence the reduction in their photoconductivity. This is consistent with the results of Rakhshani *et al* [27], where they claimed that strain reduces the mobility–lifetime product of photogenerated carriers and then alters the photoconductivity in CdS thin films.

#### 4. Conclusions

Cadmium sulphide thin films were deposited by the simple CBD method with varied solution temperatures from 55 to 75 °C. From the variation of the deposition rate and its activation energy we concluded that at low solution temperatures, the CdS films are grown by the ion by ion

process, and we found an activation energy of 0.06 eV for this process. However, at higher solution temperatures, the deposition mechanism is the cluster by cluster one, its activation energy being 0.48 eV. The growth rate controls the grain size and the strain in the films. An increase in the deposition rate yields films with small grain. The optical gap variation with the solution temperature is governed by the disorder in the material network. From the dark conductivity and photoconductivity measurements we inferred that films deposited at extreme temperature conditions (i.e. a low temperature of 55 °C or a high temperature of 70 °C) possess good optoelectronic properties, suggesting that these conditions are optimal for the production of CdS thin films intended for optoelectronic applications such as a buffer layer in CIS solar cells.

#### References

- [1] Zeho A and Vazquez Luna J G 2001 *Sol. Energy Mater. Sol. Cells* **68** 217
- [2] Oladeji I O, Chow L, Liu J R, Kchu W, Bustamante A N P, Fredricksen C and Schulte A F 2000 *Thin Solid Films* **359** 154
- [3] Casillo S J, Mendoza-Gahan A, Ramirez-Bon R, Espinoza-Beltran F J, Sotelo-Lerma M, Gonzalez-Hernandez J and Martinez G 2000 *Thin Solid Films* **373** 10
- [4] Savadoyo O 1998 *Sol. Energy Mater. Sol. Cells* **52** 361
- [5] Motinho H R, Albin D, Yaan Y, Dheo R G, Li X, Perkis C, Jiang C S, To B and Al Jassim M M 2003 *Thin Solid Films* **436** 175
- [6] Metin H and Esen R 2003 *Semicond. Sci. Technol.* **18** 674
- [7] Das S K and Morris G C 1993 *J. Appl. Phys.* **73** 782
- [8] Popescu V, Pica E M, Pop I and Grecu R 1999 *Thin Solid Films* **349** 67
- [9] Galau O V, Larramendi J V, Riech I, Pena Rodriguez G, Iribarren A, Aguilar-Hernandez J and Contreras-Puente G 2002 *Semicond. Sci. Technol.* **17** 1193
- [10] Pal U, Silva-Gonzalez R, Martinez-Montes G, Gracia-Jimenez M, Vidal M A and Torres S 1997 *Thin Solid Films* **305** 345
- [11] Schon J H, Schenker O and Batlogg B 2001 *Thin Solid Films* **385** 271
- [12] Levinson J, Shepherd F R, Scanlon P J, Westwood W D, Este G and Rider M 1982 *J. Appl. Phys.* **53** 1193
- [13] Calixto M E and Sebastian P J 1999 *Sol. Energy Mater. Sol. Cells* **59** 65
- [14] Kazmerski L L 2006 *J. Electron Spectrosc. Relat. Mater.* **150** 105
- [15] Kazmerski L L, White F R, Ayyagari S, Juang Y J and Patterson R P 1977 *J. Vac. Sci. Technol.* **14** 65
- [16] Sasikala G, Dhnasekaran R and Sbramanian C 1997 *Thin Solid Films* **30** 71
- [17] Martinez M A, Guillen C and Herrenro J 1999 *Appl. Surf. Sci.* **140** 182
- [18] Kuhaimi S A 1998 *Vacuum* **51** 349
- [19] Birkmire R W, Mecandless B E and Hegedus S S 1992 *Sol. Energy* **12** 45
- [20] Mondal S P, Mullick H, Lavanya T, Dhar A and Ray S K 2007 *J. Appl. Phys.* **102** 064305
- [21] Sharma S N, Sharma R K, Sood K N and Sing S 2005 *Mater. Chem. Phys.* **93** 368–75
- [22] Kaur I, Pandya D K and Chopra K L 1980 *J. Electrochem. Soc.* **127** 943

- [23] Hodes G, Albu-Yaron A, Decker F and Motisuke P 1987 *Phys. Rev. B* **36** 4215
- [24] Zhang H, Ma X and Yang D 2004 *Mater. Lett.* **58** 5–9
- [25] Sasikaka G, Thilakan P and Subramanniam C 2000 *Sol. Energy Mater. Sol. Cells* **62** 275
- [26] Martinez M A, Guillen C and Herrero G 1998 *Appl. Surf. Sci.* **136** 8
- [27] Rakhshani A E and Al Azab A S 2000 *J. Phys: Condens. Matter* **12** 8745–55
- [28] Cody G D, Tiedje T, Abeles B, Brooks B and Goldstein Y 1981 *Phys. Rev. Lett.* **47** 1480
- [29] Ates A, Yildirin M A, Kundakçi M and Yildirin M 2007 *Chinese J. Phys.* **45** 135
- [30] Hodes G 2002 *Chemical Solution Deposition of Semiconductor Film* (New York: Dekker)
- [31] 1997 *Inorganic Crystal Structure Database National Fachinformationzentrum (FIZ) Karlsruhe* file 080-0019
- [32] Mondal S P, Mullick H, Lavanya T, Dhar A and Ray S K 2007 *J. Appl. Phys.* **102** 064305
- [33] Khallaf H, Oladeji I O, Chai G and Chow L T 2008 *Thin Solid Films* **516** 7306
- [34] Nair P K, Gomez O, Daza, Arias-Carbajal Roadigos A, Campos J and Nair M T S 2001 *Semicond. Sci. Technol.* **16** 651
- [35] Cullity B D and Stock S R 2001 *Elements of X-ray Diffraction* 3rd edn (Englewood Cliffs, NJ: Prentice-Hall)
- [36] Pasquini L, Rempel A A and Würscum R 2001 *Phys. Rev. B* **63** 134114
- [37] Kozhevnik N S, Kurlov A S, Uritzkaya A A and Rempel A A J 2004 *Struct. Chem.* **45** S154
- [38] Contreras M A, Romeo M J, To B, Hasoon F, Noufi R, Ward S and Ramanathan K 2002 *Thin Solid Films* **403–404** 204–11
- [39] Wenyi L, Xan G, Qiu Long C and Bin Z 2005 *Mater. Lett.* **59** 1–5
- [40] Tauc J J 1976 *Amorphous and Liquid Semiconductor* (New York: Plenum)
- [41] Cody G D, Tiedje T, Abeles B, Brooks B and Goldstein Y 1981 *Phys. Rev. Lett.* **47** 1480
- [42] Ilican S, Caglar Y, Caglar M and Demirci B 2008 *J. Optoelectron. Adv. Mater.* **10** 2592
- [43] Paul G K, Bandyopadhyay S, Sen S K and Sen S 2003 *Mater. Chem. Phys.* **79** 71
- [44] Metin H and Esen R 2003 *J. Cryst. Growth* **258** 141



# CdS films deposited by chemical bath under rotation

A.I. Oliva-Avilés\*, R. Patiño, A.I. Oliva

Centro de Investigación y de Estudios Avanzados Unidad Mérida, Departamento de Física Aplicada. A.P. 73-Cordemex, 97310 Mérida, Yucatán, Mexico

## ARTICLE INFO

### Article history:

Received 23 February 2010  
Received in revised form 24 March 2010  
Accepted 24 March 2010  
Available online 1 April 2010

### Keywords:

Chemical bath deposition  
Rotating substrate  
CdS films  
CdS properties

## ABSTRACT

Cadmium sulfide (CdS) films were deposited on rotating substrates by the chemical bath technique. The effects of the rotation speed on the morphological, optical, and structural properties of the films were discussed. A rotating substrate-holder was fabricated such that substrates can be taken out from the bath during the deposition. CdS films were deposited at different deposition times (10, 20, 30, 40 and 50 min) onto Corning glass substrates at different rotation velocities (150, 300, 450, and 600 rpm) during chemical deposition. The chemical bath was composed by CdCl<sub>2</sub>, KOH, NH<sub>4</sub>NO<sub>3</sub> and CS(NH<sub>2</sub>)<sub>2</sub> as chemical reagents and heated at 75 °C. The results show no critical effects on the band gap energy and the surface roughness of the CdS films when the rotation speed changes. However, a linear increase on the deposition rate with the rotation energy was observed, meanwhile the stoichiometry was strongly affected by the rotation speed, resulting a better 1:1 Cd/S ratio as speed increases. Rotation effects may be of interest in industrial production of CdTe/CdS solar cells.

© 2010 Elsevier B.V. All rights reserved.

## 1. Introduction

Chemical bath deposition (CBD) is a low cost and scaleable technique for growing polycrystalline and epitaxial CdS films. It is an adequate method to produce industrially the promising CdTe/CdS solar cells with conversion efficiency of 15.8% [1]. By using the CBD technique it is possible to obtain thinner and thicker films by using the process on the same substrate with a single, multiple and/or continuous dip [2]. This CBD process normally uses a magnetic stirrer for chemical bath agitation in order to homogenize the temperature and the chemical components, such that hard, transparent, adherent and stoichiometric CdS films can be obtained [3,4]. However, different techniques to agitate the chemical bath and/or the substrate, such as ultrasonication [5], oscillation [6], and microwaves [7] have been reported. The agitation effects have been reported to produce a strong influence on the films quality. For example, longer reaction times to achieve thicker films using different agitation techniques produce an initial adherent layer and further porous overlayers caused by the limited source growing process of the CBD technique [8]. Thus, the deposition rate can be modified not only by changing the bath temperature [9] and the chemical reagents concentrations, but also with the type of bath agitation used during deposition. The importance of the bath and/or substrate agitation can be directly related with the physical properties of the CdS films. In a preliminary work [6], clean and transparent CdS films were obtained without col-

loids formation just oscillating the substrate into the bath during deposition. However, scarce information has been found in the literature pointing the effects of the relative bath/substrate motion on the CdS films properties. Some efforts on the CdS films preparation by CBD technique, affirm that stirring rate in the traditional magnetic agitation of the bath does not affect the deposition rate because the process is not controlled by diffusion [10]. However, recent methods proposed for CdS preparation have demonstrated that the substrate-ion interaction can influence on several aspects of the films properties [11,12].

In this work, CdS thin films were prepared by the CBD technique by using a new modality of bath agitation: rotating the substrates into the chemical bath at different and controlled speeds. The morphology, band gap energy, stoichiometry and crystalline structure of the CdS films were analyzed as a function of the rotation speed.

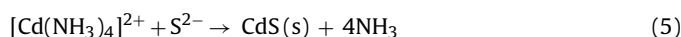
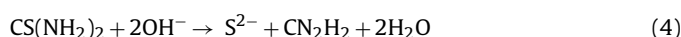
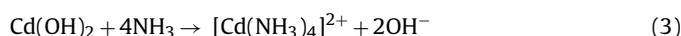
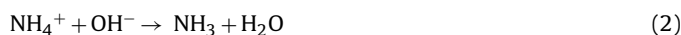
## 2. Materials and methods

### 2.1. Chemical reaction

The growth of CdS by CBD is given by the decomposition of the thiourea (CS(NH<sub>2</sub>)<sub>2</sub>) in presence of a cadmium salt in a basic solution with ammonia as complexing agent. Heating the chemical bath improves the chemical reaction. The importance of the formation of the tetra-amino-cadmium complex ions, [Cd(NH<sub>3</sub>)<sub>4</sub>]<sup>2+</sup>, is determinant for the liberation of the Cd<sup>2+</sup> ions and a further recombination with S<sup>2-</sup> ions to produce CdS. The chemical process can be described through the following chemical reactions:



\* Corresponding author. Tel.: +52 9999429436; fax: +52 9999812917.  
E-mail address: [aoliva@mda.cinvestav.mx](mailto:aoliva@mda.cinvestav.mx) (A.I. Oliva-Avilés).



The CdS deposition in the chemical bath takes place both on the surface of the glass substrate and the inner reactor walls (heterogeneous reaction) or in the chemical bath (homogeneous reaction). The homogeneous reaction is not desirable given the formation of colloids, which precipitate, yielding powdery and nonadherent films [13].

## 2.2. Substrates

Corning glass substrates were mainly used for CdS deposition. In addition, an experiment was performed on indium tin oxide (ITO) substrates for comparison. ITO is a deposited-on-glass conductor material commonly used as transparent electrical contact in solar cells. Substrates were cut in 1 cm × 1 cm pieces and cleaned following a protocol which includes washing steps with aqueous soap, trichloroethylene, acetone, and isopropyl alcohol, using distilled water for rinsing in an ultrasonic bath and air-drying in every step. Cleaning was performed just before deposition experiments.

## 2.3. Chemical solutions

Four aqueous solutions were prepared for every chemical bath: 200 ml of 0.50 M potassium hydroxide (KOH), 80 ml of 1.50 M ammonium nitrate ( $\text{NH}_4\text{NO}_3$ ), 80 ml of 0.20 M thiourea ( $\text{CS}(\text{NH}_2)_2$ ) and 80 ml of 0.025 M cadmium chloride ( $\text{CdCl}_2$ ). Distilled water was used with all the reactants from Aldrich without further purification and fresh solutions were used for every experiment. The final solution was prepared mixing the four previous solutions,

leading to a total volume of 440 ml, with the following concentrations: 4.5 mM  $\text{CdCl}_2$ , 36 mM  $\text{CS}(\text{NH}_2)_2$ , 227 mM KOH and 273 mM  $\text{NH}_4\text{NO}_3$ .

## 2.4. Design and fabrication of the rotatory system

A substrate-holder made of polymeric material was implemented in order to apply a rotation effect to the substrates (and bath) during films deposition (Fig. 1a). The substrate-holder system consists of five PVC holder discs mounted on a common acrylic cylindrical rod used as rotation axis. The materials for the discs and rod were chosen to be chemically inert. The discs (50 mm diameter, 5 mm thickness) are parallel mounted along the cylindrical rod (190 mm length, 10 mm diameter) with similar separation between them (see Fig. 1b). Each disc can hold various substrates and it has a small and elevated border on the external edge to maintain fixed the substrates during rotation. Substrates are horizontally located on the surface of each disc, such that their upper faces are directly in contact with the aqueous solution. Before deposition, the formed rod-discs system is submerged into the chemical bath (Fig. 1c). A step-motor holds the cylindrical rod on the upper extreme. Rotation and vertical displacement are the basic movements of the substrate-holder during deposition. Thus, the substrate-holder is also used to agitate the chemical bath during rotation; meanwhile the films are being deposited. Before deposition, the rotatory system was calibrated at different conditions in order to determine the maximum rotation speed (600 rpm), such that below this speed, the formation of vortices on the bath surface is avoided. The selected range of rotation speeds was found to be between 150 and 600 rpm (2.5–10 Hz) for our experimental system. This range of speed is minor than the magnetic stirring (tenths of Hz) and the ultrasonic agitation (30–40 kHz) values reported in others works. The rotation speed of the step-motor was selected and maintained through a manual controller (Master Servodyne) and verified with a

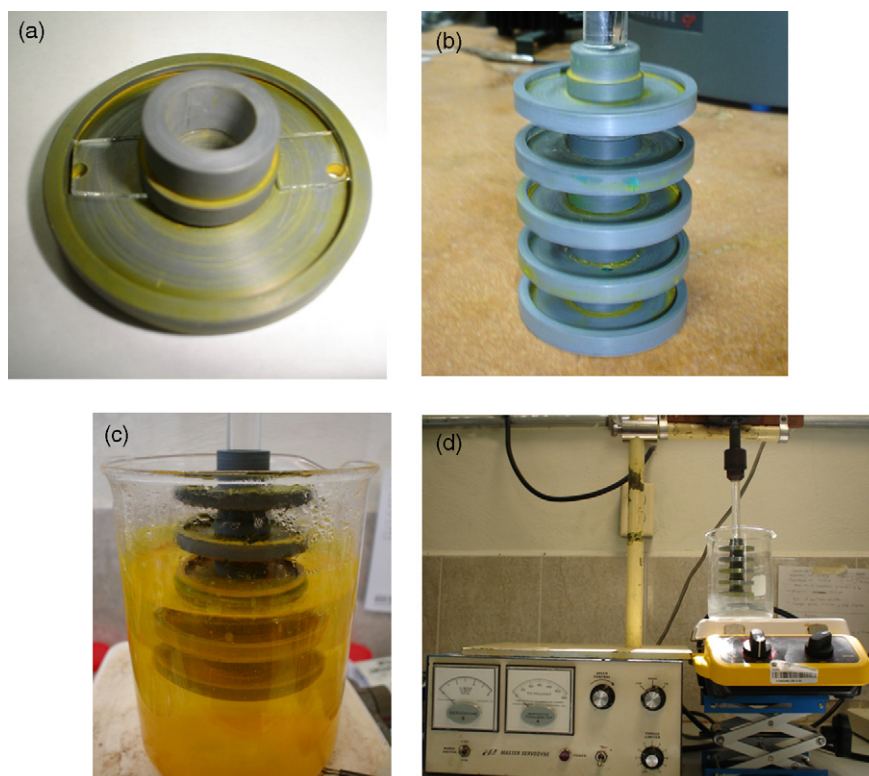


**Fig. 1.** a) PVC disc designed as substrate-holder; b) discs-rod system; c) rotation of the substrates into the bath during CdS films deposition by CBD technique; d) general view of the implemented deposition system with rotatory substrates.

stroboscope light (Strobotac 1531). During deposition process, the rod-disk system is raised, each time, by means of a “jiffy-jack”, such that the corresponding disc is got out from the aqueous solution. Thus, a continuous deposition process is produced by the remaining submerged disks. A general view of the system can be seen in Fig. 1d.

### 2.5. Chemical bath deposition

CdS films were deposited by the CBD technique on glass and ITO substrates under rotation. Two substrates were attached to each one of the five discs assembled to the rod, which was rotated at a specific speed. The discs are immersed into a 500-ml glass-beaker which is located on a heater plate. The beaker-heater plate system is moved by a jiffy-jack to extract the selected disc with samples from the chemical bath (Fig. 1d). At the beginning of every experiment, the five discs are submerged into a mixture with the solutions of CdCl<sub>2</sub>, KOH and NH<sub>4</sub>NO<sub>3</sub>. The rod is started to rotate and the plate is heating on until the mixture reaches 75 °C, as measured with a mercury thermometer. Following, the thiourea solution is added to the mixture and the CdS formation is performed. With time, the color of the chemical bath changes from pale to intense yellow, while the temperature is maintained at 75 °C. In order to obtain films with different thickness, the jiffy-jack is moved down every 5 or 10 min to get one disc out of the bath. The experiment finishes when the five discs are out of the bath. Finally, the chemical bath shows a deep-yellow color, as a result of the exhausted solution.

### 2.6. Rotation experiments

The CBD technique was performed at four rotation speeds: 150, 300, 450 and 600 rpm. Three experiments at 600 rpm were performed. Rotations over 600 rpm produce turbulent mixing with bubbles, which are not desirable to obtain homogeneous films. Five pairs of samples were obtained at different times for every rotation speed. For all rotation speeds, deposition times were 10, 20, 30, 40 and 50 min. Particularly, experiments at 600 rpm were repeated by using 5, 10, 15, 20 and 25 min as deposition time due to the high deposition rate. Just after the experiment, the deposited films were rinsed with distilled water in an ultrasonic bath and dried with air. The CdS material deposited on the back-side of the substrate was carefully eliminated with cotton using a 10% HCl aqueous solution. Homogeneous, transparent and brilliant yellow CdS films were obtained.

### 2.7. Samples characterization

The deposited films were analyzed using different techniques. The analysis by atomic force microscopy AFM (Autoprobe CP, Park Scientific) was performed on samples in order to obtain morphological images of the deposited films and the root mean square (rms) roughness value. UV–vis analysis was performed with a spectrophotometer (StellarNet EPP2000) in the wavelength range from 200 to 850 nm. The absorbance spectrum was used to obtain the band gap energy of the films. A profilometer (Dektak 8) was used to measure the thickness of the films through a formed step on the corner of the substrate where the material was removed with a 10% HCl aqueous solution. Stoichiometry of the films was determined with the energy dispersive spectroscopy (EDS) technique included into a scanning electron microscope (Philips XL-30). Finally, the X-ray diffractometer (Siemens D5000) was used in the grazing incident mode to characterize the crystalline structure of the films.

## 3. Results and discussion

Uniform, transparent, and adherent CdS films were obtained with substrate rotation technique. The growth of films at different

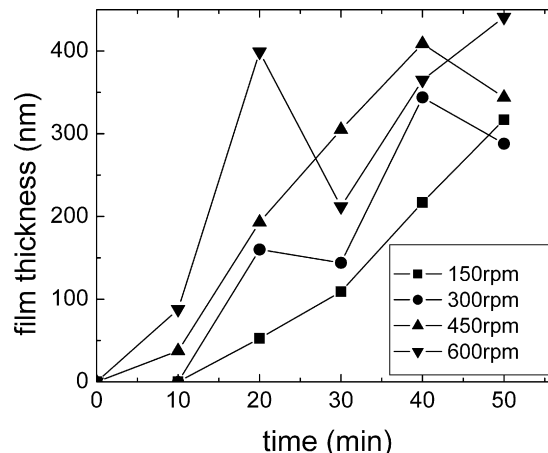


Fig. 2. Growth of CdS film thickness with time at four different rotation rates.

rotation speeds is shown in Fig. 2 where the film thickness is plotted as a function of deposition time. An increase of thickness with the increase of rotation speed can be observed. The initial slope of these curves was taken as the deposition rate of the CdS material. The initial slope was observed to increase with the rotation speed. From Fig. 2 for CdS films grown at 150, 300, and 450 rpm speed, a near linear increase with time of the thickness is observed. However, for 600 rpm, the growth process is interrupted diminishing the thickness at certain time, and increasing again, this effect can be clearly seen for the film deposited at 20 min. We assumed that this effect is due to the detachment of CdS material because of the high rotation speed. The new increase of film thickness after 30 min, explains the active chemical reaction of the bath at this time. Thus, high rotation speeds increase the rate deposition of CdS films.

Rotation energy  $E_r$  may be calculated from rotation speed  $\Omega$  (rpm) using the equation:

$$E_r = \frac{1}{2}I\omega^2 = B \left( \frac{2\pi\Omega}{60} \right)^2 \quad (6)$$

where  $B = I/2$ , with  $I$  being the moment of inertia of the discs, a constant during the experiments, and  $\omega$  is the angular velocity ( $s^{-1}$ ). The deposition rate ( $r$ ) of CdS films was estimated from the initial slope estimated through a linear fitting from Fig. 2. A plot of the deposition rate as a function of  $\omega^2$  is represented in Fig. 3, where the value at 600 rpm ( $\omega = 63 s^{-1}$ ) was taken as an average from three experiments. The  $r$  value was found to be almost linear with the rotation energy. The intercept of the fitted line ( $R = 0.992$ ) at  $\omega = 0$

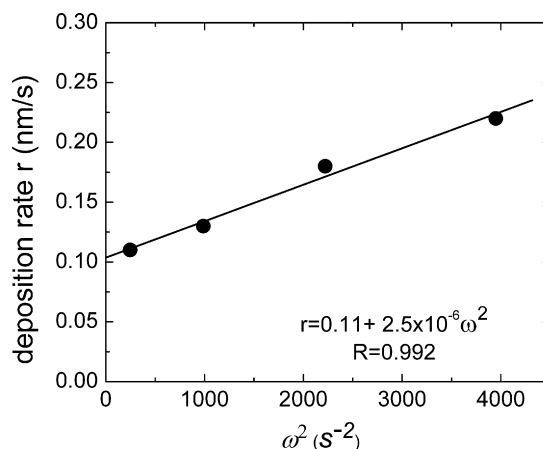


Fig. 3. CdS deposition rate as a function of substrate rotation energy.

**Table 1**

Band gap energy  $E_g$  (eV) values of CdS films for different rotation speeds and deposition times. The bolded values were used to calculate the mean value.

Time (min)	Rotation speed					
	150 rpm	300 rpm	450 rpm	600 rpm	600 rpm	600 rpm
10	n.a.	n.a.	2.00	2.25	n.a.	n.a.
15					2.49	2.57
20	2.26	<b>2.39</b>	<b>2.38</b>	<b>2.41</b>	<b>2.40</b>	<b>2.45</b>
25					<b>2.45</b>	<b>2.44</b>
30	<b>2.42</b>	<b>2.35</b>	<b>2.42</b>	<b>2.45</b>		
40	<b>2.44</b>	<b>2.36</b>	<b>2.33</b>	<b>2.37</b>		
50	<b>2.35</b>	<b>2.32</b>	<b>2.40</b>	<b>2.42</b>		

$E_g = (2.40 \pm 0.04)$  eV (mean value)

n.a. = not available.

can be interpreted as the  $r$  value without rotation. From Fig. 3, a value of  $r = 0.11$  nm/s was estimated, and is interpreted as the deposition rate in which only the thermal energy (i.e. temperature) is responsible of the collision of chemical reactants to form the CdS film. Higher rotation speed means minor deposition time to achieve certain thickness, because of the higher deposition rate. This effect can be explained by the formation of the metastable complex in the heterogeneous chemical reaction (Eqs. (3) and (4)) when the energy activation is increased by the high rotation speed as was recently proved by Kim et al. [14]. CdS films with similar characteristics with rotation speed between 70–80 rpm were recently reported [15].

The band gap energy  $E_g$  was computed for every CdS film into the UV–vis region, given that CdS is a semiconductor with a direct band gap at room temperature. This optical property was calculated from the absorption spectra through the relation.

$$\alpha^2(h\nu) = A^2(h\nu - E_g) \quad (7)$$

where  $\alpha$  is the optical absorption coefficient,  $h\nu$  is the energy of the incident light,  $h$  is the Planck's constant and  $\nu$  the light frequency. Plotting  $\alpha^2$  vs  $h\nu$ , the band gap energy of the films is estimated from the initial absorption edge line when  $\alpha = 0$ .

The band gap energy values are shown in Table 1 for different deposition times and rotation speeds. As can be seen, during the first 10 min and low rotation speeds, it was not possible to compute a band gap energy because of the scarce material deposited on the substrates. But for longer times, the band gap energy values obtained on films did not show important changes with the rotation speed and deposition time. The values reported in Table 1 represent an average of the band gap energy after several measurements on different parts of each film. The estimated mean value for all bolded values and its standard deviation was  $E_g = (2.40 \pm 0.04)$  eV, a good agreement value with the typical values (2.42 eV) reported by different authors [16–18].

AFM images of  $1 \mu\text{m} \times 1 \mu\text{m}$  were obtained for every deposited film. Fig. 4 shows the group of images for CdS films deposited from 10 to 40 min at 150 rpm. No film deposition can be observed after 10 min, but small grains (about 100 nm of diameter) were deposited on substrates after 20 min. With deposition time, the grains grow forming clusters, as shown for films at 30 and 40 min. A similar behaviour was observed when the rotation speed is increased. Fig. 5 includes the AFM images for CdS films deposited after 50 min and 150, 300, 450 and 600 rpm as rotation speed. In general, the grain size at the end of the experiment does not show important dependence with the rotation speed. These results are quantitatively verified by comparing the rms-roughness values calculated from the AFM images. Table 2 shows these values as a function of deposition time and rotation speed. The bolded values are only considered to obtain a mean rms-roughness of all films, which was estimated as  $R_{\text{rms}} = (18 \pm 5)$  nm.

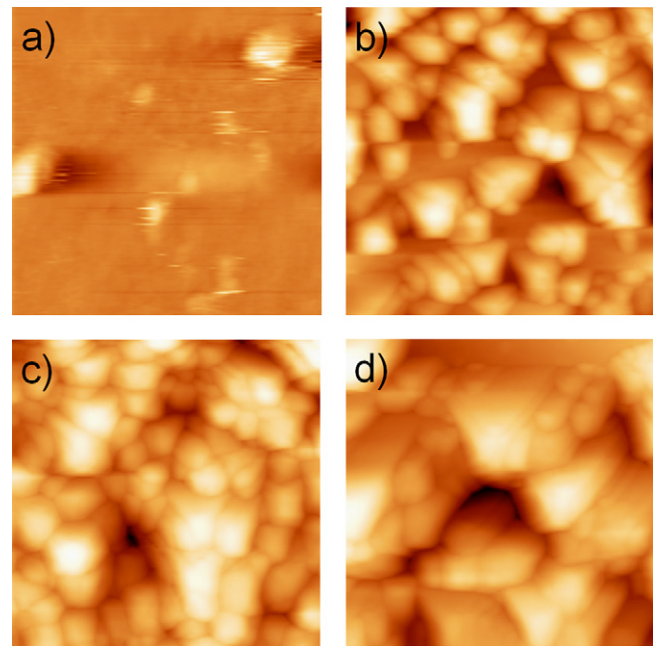


**Fig. 4.** AFM images for films deposited with 150 rpm at: a) 10 min, b) 20 min, c) 30 min, and d) 40 min as deposition time.

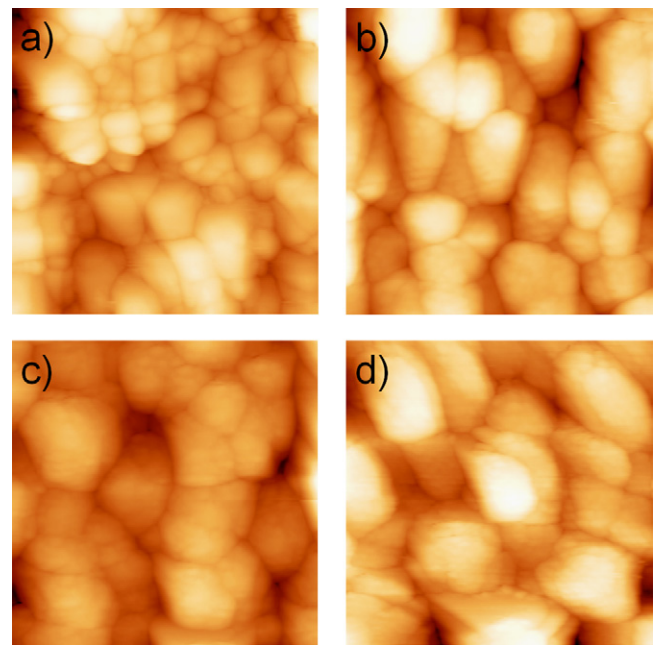


**Fig. 5.** AFM images for films deposited at 50 min with: a) 150 rpm, b) 300 rpm, c) 450 rpm, and d) 600 rpm as rotation speed.

**Table 2**

Rms-roughness values (nm) from AFM data for different rotation speed and deposition times. The bolded values were used to calculate the mean value.

Time (min)	Rotation speed					
	150 rpm	300 rpm	450 rpm	600 rpm	600 rpm	600 rpm
10	4.5	5.8	<b>25.5</b>	<b>14.0</b>	n.a.	n.a.
15					<b>17.0</b>	<b>10.8</b>
20	<b>22.0</b>	<b>25.1</b>	17.1	<b>20.2</b>	<b>17.0</b>	<b>9.6</b>
25					<b>19.0</b>	<b>9.3</b>
30	<b>25.6</b>	<b>24.3</b>	<b>19.0</b>	<b>17.2</b>		
40	<b>19.4</b>	<b>16.8</b>	<b>19.0</b>	<b>18.4</b>		
50	<b>20.9</b>	<b>14.3</b>	<b>19.1</b>	<b>22.3</b>		

$R_{\text{rms}} = (18 \pm 5)$  nm (mean value)

n.a. = not available.

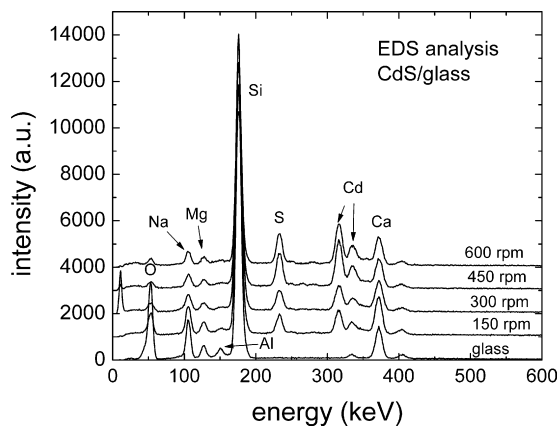


**Fig. 6.** EDS spectra of CdS films deposited at different rotation speeds. The Si peak corresponds to the Corning glass substrate. Deposition time: 50 min.

The EDS analysis allows to quantify the stoichiometric composition of the CdS films. Fig. 6 shows the measured spectra for films deposited at 50 min with different rotation speeds. Once considering the Si, Ca, O, Mg and Na signals coming from the substrate (Corning glass) it is possible to verify that only CdS is deposited. The intensity of every peak is not only associated with a particular chemical element but also with its relative abundance in the samples. Cd and S peaks, increase in intensity when the rotation speed is increased. Following this elemental quantification, it is possible to observe a clear correlation between the rotation speed and the chemical stoichiometry of the CdS films. This relation is observed in Fig. 7, where again, the reported value at 600 rpm is an average from three experiments. The 1:1 Cd/S stoichiometry is favored when the rotation speed is increased. However, as was shown in Tables 1 and 2, the  $E_g$  and  $R_{rms}$  values of the CdS films, were not affected for this change in stoichiometry.

Also for samples deposited at 50 min, X-ray diffractograms were obtained in order to analyze the crystalline structure of the CdS films. Fig. 8 shows these diffractograms for films deposited at different rotation speeds. According to the JCPDS [19] reference, the deposited CdS films grow with face centered cubic (fcc) structure and this crystalline structure improves when the rotation speed increases given the high intensity of the diffraction signal. The fcc structure is confirmed with the main (1 1 1) peak and the weak signals of the secondary (2 2 0) and (3 1 1) peaks of diffraction.

Finally, CdS was simultaneously deposited both on ITO and glass substrates into a chemical bath with similar conditions with 600 rpm as rotation speed and 25 min as maximum deposition time

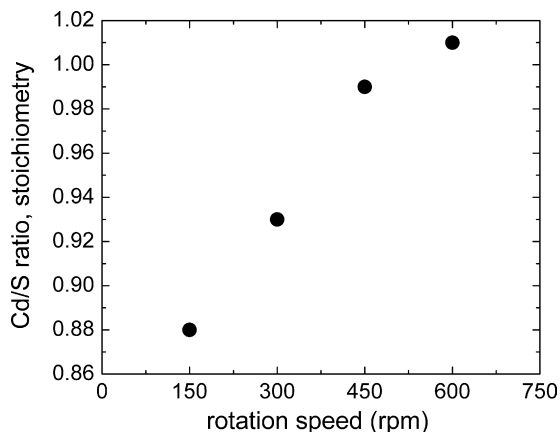


**Fig. 7.** Cd/S ratio measured as a function of the rotation rate.

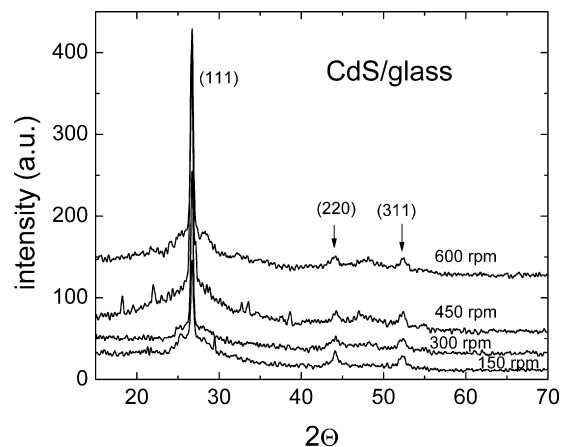


**Fig. 8.** CdS films diffractograms at different rotation rates. The fcc structure is confirmed with the (1 1 1), (2 2 0) and (3 1 1) peaks.

**Table 3**

Comparison of CBD-CdS films deposited onto glass and ITO substrates. Rotation speed: 600 rpm. Deposition time: 25 min.

Measured parameters	Glass substrate	ITO substrate
Deposition rate (nm/s)	0.12	0.17
$E_g$ (eV)	2.45	2.48
$R_{rms}$ (nm)	9.9	10.0
Cd/S ratio	1.02	0.96

in order to compare properties between deposited films. Table 3 gives the obtained results and their comparison. From these results, it is possible to affirm that deposition rate increases when CdS is deposited on ITO substrate due to a major thickness achieved (266 nm) after 25 min substrates as compared with CdS thickness obtained (213 nm) on glass substrates. CdS films deposited on glass presents a slightly smaller band gap energy value and similar  $R_{rms}$  values as compared with ITO substrates, and a slightly bigger value [20–22] as compared with the typical value reported of 2.42 eV. On the other hand, the 1:1 Cd/S ratio is slightly favored when glass substrate is used instead of ITO.

#### 4. Conclusions

CdS films were prepared by chemical bath deposition under substrates rotation. Rotation speeds from 150 to 600 rpm were performed to the substrates through a sample holder composed by a rotatory rod and a series of parallel disks in order to study changes on the physical properties of films. The obtained band gap energy and rms-roughness of CdS films do not show important variations with rotation speed as compared with previously reported values. However, films stoichiometry, tends to increase toward the 1:1 Cd/S ratio with the increase of the rotation speed. CdS films deposited both on glass and on ITO substrates under rotation show main differences on the deposition rate. CdS films deposited on ITO substrates, give major thickness and deposition rate, but nearly values of band gap energy and rms-roughness under similar conditions. Thus, the relative movement between the chemical bath and the substrates needs to be considered when some physical properties are required for the CBD-CdS films.

#### Acknowledgements

Work supported by Conacyt-México through project F1-54173. Authors thank to Emilio Corona Hernández for his technical help.

## References

- [1] C. Ferekides, J. Britt, Y. Ma, L. Killian. Proceedings of the 23rd IEEE Photovoltaic Specialists Conference, Louisville, KY, 10–14 May 1993, p. 389.
- [2] I.O. Oladeji, L. Chow, J.R. Liu, W.K. Chu, A.N.P. Bustamante, C. Fredricksen, A.F. Schulte, *Thin Solid Films* 359 (2000) 154–159.
- [3] I. Kaur, D.K. Pandya, K.L. Chopra, *J. Electrochem. Soc.* 127 (1980) 943.
- [4] J.M. Doña, J. Herrero, *J. Electrochem. Soc.* 144 (1997) 4091.
- [5] A.I. Oliva, R. Castro-Rodríguez, O. Solís-Canto, Víctor Sosa, P. Quintana, J.L. Peña, *Appl. Surf. Sci.* 205 (2003) 56–64.
- [6] Y.A. Salazar, R. Patiño, J.L. Peña, W. Cauch, A.I. Oliva, *Braz. J. Phys.* 36 (2006) 1058–1061.
- [7] J.Y. Choi, K.J. Kim, J.B. Yum, D. Kim, *Solar Energy* 64 (1998) 41.
- [8] D. Lincot, R. Ortega-Borges, *J. Electrochem. Soc.* 139 (1992) 1880.
- [9] H. Moualkia, S. Hariech, M.S. Aida, *Thin Solid Films* 518 (2009) 1259.
- [10] J.M. Doña, J. Herrero, *J. Electrochem. Soc.* 144 (1997) 4081.
- [11] J. Hiie, T. Dedova, V. Valdna, K. Muska, *Thin Solid Films* 511–512 (2006) 443.
- [12] H.H. Abu-Safe, M. Hossain, H. Naseem, W. Brown, A. Al-Dhafiri, *J. Electron. Mater.* 33 (2004) 128.
- [13] R. Ortega-Borges, D. Lincot, *J. Electrochem. Soc.* 140 (1993) 3464.
- [14] M. Kim, B.K. Min, Ch.D. Kim, S. Lee, H.T. Kim, S.K. Jung, S. Sohn, *Curr. Appl. Phys.*, in press.
- [15] V.B. Sanap, B.H. Pawar, *Chalcogenide Lett.* 6 (2009) 415.
- [16] M. Ichimura, F. Goto, E. Arai, *J. Appl. Phys.* 85 (1999) 7411.
- [17] V. Popescu, E.M. Pica, I. Pop, R. Grecu, *Thin Solid Films* 349 (1999) 67.
- [18] O. Zelaya-Angel, R. Lozada-Morales, *Phys. Rev. B* 62 (2000) 13064.
- [19] JCDPS International Centre for diffraction data, 2000.
- [20] L. Brus, *J. Chem. Phys.* 90 (1986) 2555.
- [21] Y. Wang, A. Suna, W. Mahler, R. Kasowski, *J. Chem. Phys.* 87 (1987) 7315.
- [22] K.K. Nanda, S.N. Sarangi, S. Mohanty, S.N. Sahu, *Thin Solid Films* 322 (1998) 21.

# Effects of thiourea concentration on CdS thin films grown by chemical bath deposition for CdTe solar cells

R. Mendoza-Pérez<sup>a,b,1</sup>, G. Santana-Rodríguez<sup>c,2</sup>, J. Sastre-Hernández<sup>a</sup>, A. Morales-Acevedo<sup>d</sup>,  
A. Arias-Carbajal<sup>2</sup>, O. Vigil-Galan<sup>2</sup>, J.C. Alonso<sup>c</sup>, G. Contreras-Puente<sup>a,\*</sup>

<sup>a</sup>Escuela Superior de Física y Matemáticas del IPN, Edificio 9, U.P.A.L.M., 07738 México, D.F. Mexico

<sup>b</sup>UPIBI-IPN, Av. Acueducto s/n Col. Barrio la Laguna Ticomán, 07340 México, D.F. Mexico

<sup>c</sup>Instituto de Investigación en Materiales, UNAM, AP 70-360, Coyoacán 04510, D.F. México

<sup>d</sup>CINVESTAV-IPN, Depto. de Ingeniería Eléctrica, Ave. IPN No. 2508, 07360 México, D.F. Mexico

Available online 2 December 2004

## Abstract

We study the effects of thiourea concentration on CdS thin films deposited by chemical bath deposition (CBD), submitted to post-thermal treatments of CdCl<sub>2</sub>, and its effect on the characteristics of CdS/CdTe solar cells. We compare these cells with similar ones fabricated with CdS-films grown by Close Space Vapor Transport (CSVT). The CBD-CdS cells shows higher open circuit voltage ( $V_{oc}$ ) and fill factor (FF), while the short circuit current remains with little change, as the ratio of S to Cd in the CBD solution goes from 1 to 5. This dependence changes when there is a variation of the CBD-CdS layer thickness. We have obtained cells with more than 12% efficiency when the CdS layers are deposited by the best CBD condition (S/Cd=5) as compared to the best cells with CdS layers prepared by CSVT that had 11% efficiencies. Other measurements such as spectral response were performed and their results were correlated to the I–V characteristics of the solar cells so that the best performances of CBD-CdS solar cells are explained in terms of the chemical composition of this layer.

© 2004 Elsevier B.V. All rights reserved.

**Keywords:** CdS/CdTe solar cells; Thiourea; Cell efficiency

## 1. Introduction

Among the II–VI semiconductor compounds, CdS is a representative material with many applications such as large area electronic devices and solar cells. We are particularly interested in the latter because it is a good window layer for CdTe and chalcopyrite-based solar cells. In fact, the best efficiency (16.5%) for a CdTe solar cell has been achieved [1] with a CdS window layer grown by chemical bath deposition (CBD), although CBD gives poor crystalline quality for CdS layers in comparison with other

deposition techniques. As we have already shown in a previous paper [2], CBD gives the best photoconductivity and morphological properties such as roughness and pinhole density when compared to films processed by other techniques.

A good window layer must fulfill several characteristics: low carrier recombination, low resistivity, and being a good match to CdTe. It is the purpose of this work to study CdS films processed by CBD using different thiourea concentrations in the bath solution with post-thermal treatments using CdCl<sub>2</sub>. These films were used to make CdS/CdTe solar cells and compare these devices with those with CdS layers grown CSVT with similar characteristics (film thickness, post thermal treatments, etc.). The results show that those devices with CdS grown by CBD are better possibly due to a higher photo-

\* Corresponding author. Tel.: +52 57296139; fax: +52 55862957.

E-mail address: [gerardo@esfm.ipn.mx](mailto:gerardo@esfm.ipn.mx) (Contreras-Puente).

<sup>1</sup> Tel.: +52 57296000x55188.

<sup>2</sup> Permanent address: IMRE, Universidad de la Habana, Cuba.

Table 1

Thiourea to CdCl<sub>2</sub> ratio and bath time used to process the several CBD samples

S/Cd	C (Thiourea) in the bath (mol/l)	Growth time (min)
1.0	$2.4 \times 10^{-3}$	120
2.5	$6.0 \times 10^{-3}$	100
5.0	$1.2 \times 10^{-2}$	120

conductivity that causes a smaller series resistance in the cells.

## 2. Experimental details

For the deposition of the CdS films by chemical bath, a 150-ml beaker containing the reactants in a solution magnetically stirred was immersed in a temperature controlled ( $\pm 1$  °C) water bath. The concentrations of NH<sub>3</sub> (2.3 mol/l), NH<sub>4</sub>Cl ( $2 \times 10^{-2}$  mol/l) and CdCl<sub>2</sub> ( $2.4 \times 10^{-3}$  mol/l) were kept constant in every experiment. In order to change the S to Cd ratio in the solution, the CS(NH<sub>2</sub>)<sub>2</sub> (thiourea) concentration was varied. All the films were grown on SnO<sub>2</sub>/F conducting glasses (10 Ω cm) at 75 °C, which is assumed as the substrate temperature. The deposition time was also varied, according to our previous knowledge of the growth kinetics [3], with the purpose of having films with similar thickness. The thiourea concentration and deposition time for each S/Cd relation are listed in Table 1.

The CdS films grown by CSVT have been already described elsewhere [4], and had similar thickness to those grown by CBD. Deposition times of 100, 120 and 140 s were used obtaining thickness of the order of 130 to 150 nm. The chamber pressure was kept at 13.33 Pa in Ar ambient, using source and substrates temperatures of 725 and 450 °C. Thermal treatment of CdCl<sub>2</sub> was provided after the deposition by CBD and CSVT during 30 min at 400 °C in air.

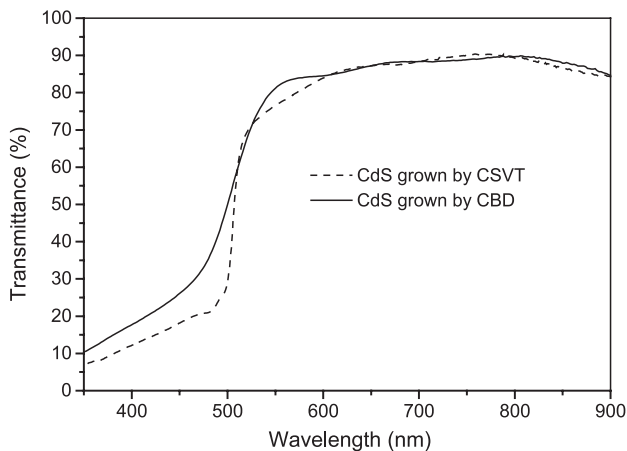


Fig. 1. Optical transmission of CBD and CSVT-CdS samples processed in this work.

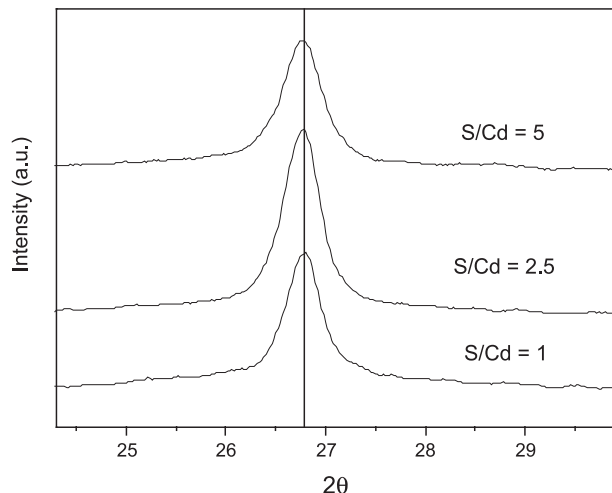


Fig. 2. X-ray diffraction spectra of the CBD-CdS film samples. They show preferential orientation in the (002) direction of the hexagonal structure.

We have not performed electrical measurements of the CdS films grown in this work by the CBD and CSVT techniques, but from our previous results [2] typical dark resistivity values are in the order of  $1 \times 10^6$  and  $1 \times 10^7$  Ω cm, respectively.

The solar cells for the CBD and CSVT-CdS films were made in the supersaturate configuration by depositing the CdTe thin films by CSVT on the CdS films, using 99.999% grade powders. The atmosphere used during the CdTe deposition was a mixture of Ar and O<sub>2</sub>, with an O<sub>2</sub> partial pressure of 50%. Prior to all the depositions, the system was pumped to  $1 \times 10^{-9}$  Pa as the base pressure. The CSVT deposition of CdTe was accomplished by placing a CdTe source block in close proximity (1 mm) to the substrate. The deposition time was 3 min with substrate and source temperatures of 550 and 650 °C, respectively. Under these conditions, CdTe layers of approximately 3.5 μm were obtained. The CdTe thin films were coated with 200 nm of CdCl<sub>2</sub> and then annealed at 400 °C for 30 min in air. The metallic back contacts were Cu (2 nm) and Au (350 nm) evaporated with an area of 0.08 cm<sup>2</sup> onto the CdTe and annealed at 180 °C in Ar.

## 3. Results and discussion

### 3.1. Films characteristics

The optical transmission, in the visible region, for the best CdS layers grown by CBD (grown with a solution ratio

Table 2

Physical properties (optical and morphological) of the CdS film with S/Cd=5 processed by CBD and the best CdS film processed by CSVT

Film	Thickness <i>d</i> (nm)	Grain size (nm)	FWHM (°)	<i>T</i> <sub>av</sub> above 500 nm (%)	BGE (eV)
CSVT	150	68.5	0.25	84.2	2.51
CBD	138	47.2	0.40	85.0	2.52

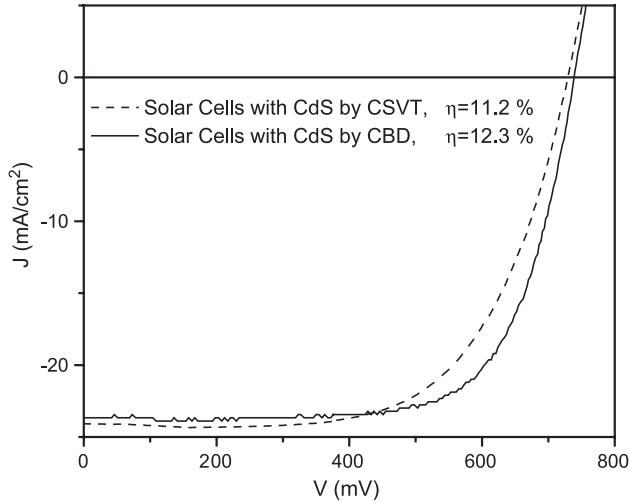


Fig. 3. I–V characteristics for the best solar cells with CBD and CSVT-CdS layers.

of S/Cd=5 and CdCl<sub>2</sub> annealing) and the best CdS layers grown by CSVT (grown for 140 s and CdCl<sub>2</sub> annealing) are shown in Fig. 1. We observe that for both samples the transmission is near 90% for wavelengths above 550 nm for films that had thickness between 138 and 150 nm. The band gap (BGE) was near 2.52 eV.

From X-ray diffraction measurements for the CBD-CdS layers as shown in Fig. 2, the lattice parameter of the sample with S/Cd=5 is larger than for the other two samples, possibly associated to a reduction of sulfur vacancies. The FWHM of the XRD peaks also increases as a consequence of smaller crystallites for this film. It has been shown in a previous paper [2] that the photoconductivity to dark conductivity ratios are higher for samples grown by CBD, in comparison with samples grown by other techniques like CSVT.

Table 2 summarizes the growth parameters, the morphological characteristics and other properties for the best CBD-CdS sample with S/Cd=5 in the solution. In addition, in this table the parameters for the best CSVT-CdS sample are shown.

### 3.2. Solar cells devices characteristics

The CBD-CdS and CSVT-CdS solar cell I–V performances were measured under AM1.5 (100 mW/cm<sup>2</sup>) illumination, and the results are graphed in Fig. 3. Table 3 shows the results obtained for the set of CBD-CdS solar cells, where we can notice that the best results are obtained for the

Table 3  
Comparison of solar cell performances for CBD-CdS window layer

S/Cd R <sub>ic</sub>	R <sub>s</sub> (Ω cm <sup>2</sup> )	R <sub>p</sub> (Ω cm <sup>2</sup> )	V <sub>oc</sub> (mV)	J <sub>sc</sub> (mA/cm <sup>2</sup> )	FF	η (%)
1/1	6.8	318	617	20.8	0.55	7.1
2.5/1	4.4	800	690	21.8	0.56	8.3
5/1	2.9	757	740	23.8	0.70	12.3

Table 4  
Comparison of solar cell performances for CSVT-CdS window layer

Samples (growth time in second)	R <sub>s</sub> (Ω cm <sup>2</sup> )	R <sub>p</sub> (Ω cm <sup>2</sup> )	V <sub>oc</sub> (mV)	J <sub>sc</sub> (mA/cm <sup>2</sup> )	FF	η (%)
100	3.6	350	701	24	0.56	9.4
120	5.6	813	727	23.9	0.60	10.5
140	5.7	750	714	24	0.65	11.2

S/Cd=5 with an efficiency of 12.3%. In a similar form, Table 4 shows the results obtained for the set of CSVT solar cells. In Table 4, we can observe that the best results are obtained for solar cells made with CdS grown during 140 s.

From Tables 3 and 4, we can see the results for the best devices, i.e. those made with CdS grown by CBD and CSVT, whereas Fig. 4 displays the spectral response of these devices. From these tables, we can notice that the fill factor is better for the best CBD-CdS solar cell, while J<sub>sc</sub> and V<sub>oc</sub> are almost the same as for the CSVT-CdS solar cell with a difference of less than 3%, which is within the possible measurement error. Notice from these I–V curves of the CBD and CSVT solar cells that the main difference comes from the fill factor of the curves, a fact that can be associated to the larger series resistance (almost the double) for CSVT solar cells as compared to CBD cells. It has been shown that sulfur enrichment in CBD-CdS layers causes a decrease of carrier trap density at the grain boundaries. Hence, the difference in the FF values may arise from the larger photoconductivity for the CBD-CdS layers. The small difference shown in Fig. 4 for the spectral response of these cells in the short wavelength range indicates a better interface between the CBD-CdS and CdTe than for CSVT and the CdTe layers in this case, although the total short circuit current density is almost the same for both kinds of solar cells.

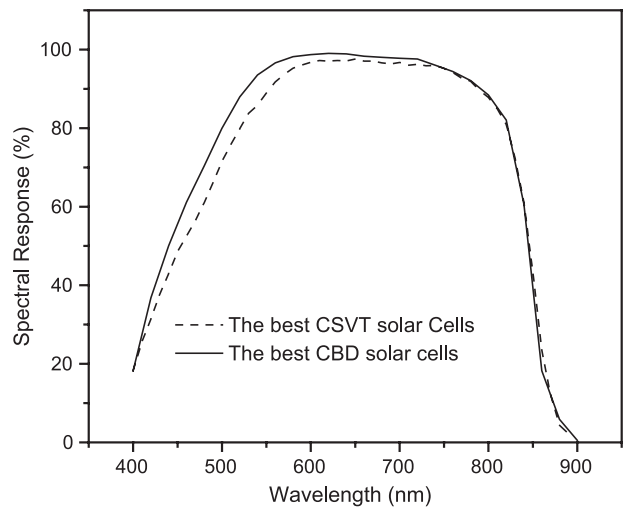


Fig. 4. Spectral response comparison for the best CBD and CSVT cells in the 400–900-nm wavelength region.

In summary, the main difference for CBD and CSVT-CdS layers for solar cells in this study is due to the higher resistivity (and smaller photoconductivity) associated to the CSVT-CdS layers. This fact gives a higher series resistance for cells done with CSVT-CdS layer than for CBD solar cells.

#### 4. Conclusions

A set of CdS samples grown by chemical bath with different concentrations of thiourea in the solution were used as window layers for CdTe solar cells. It was found that varying the thiourea to CdCl<sub>2</sub> concentration solar cells present better performances for a larger S/Cd ratio in the CBD solution. On the other hand, we have found that the best performance as determined from the I–V curves corresponds to solar cells made with CdS window layers processed by CBD as compared to CdS grown by CSVT. This fact can be attributed to the best photoconductivity of the CdS layer. It has been observed that similar results have been obtained for the  $V_{oc}$  and  $J_{sc}$  values of solar cells with CBD and CSVT-CdS layers. The main difference for these

cells is due to the higher series resistance of the latter, a difference that affects the fill factor and therefore the efficiency of the cells. Hence, it seems that CBD-CdS layers are slightly better than CSVT-CdS ones when used in solar cells, although both kind of materials can be used on CdTe for attaining high efficiency solar cells (above 11%), as shown in this paper.

#### References

- [1] X. Wu, J.C. Keane, R.G. Dhere, C. DeHart, A. Duda, T.A. Gessert, S. Asher, D.H. Levi, P. Sheldon, Proc. 17th European Photovoltaic Solar Energy Conf. (Munich, Germany 22–26 October 2001), 2001, p. 995.
- [2] A. Morales-Acevedo, O. Vigil-Galán, G. Contreras-Puente, J. Vidal-Larramendi, G. Arriaga-Mejía, M. Chavarria-Castañeda, A. Escamilla-Esquivel, H. Hernández-Contreras, A. Arias-Carbajal, F. Cruz-Gandarilla, Proceedings of the 29th IEEE Photovoltaic Specialists Conference, 2002, p. 624.
- [3] A. Arias-Carbajal Reádigos, L. Vaillant, O. Vigil-Galán, G. Contreras-Puente, Mod. Phys. Lett. B 15 (2001) 659.
- [4] C. Mejía-García, A. Escamilla-Esquivel, G. Contreras-Puente, M. Tufiño-Velázquez, M.L. Albor-Aguilera, O. Vigil, L. Vaillant, J. Appl. Phys. 86 (1999) 3171.

## Recent progress on CdTe/CdS thin film solar cells

N. Romeo<sup>a,\*</sup>, A. Bosio<sup>a</sup>, V. Canevari<sup>b</sup>, A. Podestà<sup>a</sup>

<sup>a</sup> *Department of Physics, University of Parma, Parco Area delle Scienze 7/a, Parma 43100, Italy*

<sup>b</sup> *IMEM-CNR Institute, Parma, Italy*

Received 12 December 2003; received in revised form 12 May 2004; accepted 15 July 2004

Available online 21 September 2004

Communicated by: Associate Editor T.M. Razykov

### Abstract

The CdTe/CdS thin film solar cell is the most suitable to be fabricated on the form of thin films. The processes used to make all the films, which compose the cell, are quite simple and fast. An efficiency of 16.5% has been reached on laboratory scale and modules of  $0.6 \times 1.2 \text{ m}^2$  with efficiency larger than 8% are now fabricated and commercialized. A strong contribution to the development of this type of solar cells has been given by the Parma University group with the discovery of a new ohmic back contact for CdTe which is very stable in respect to any other ohmic contact used for CdTe, and by the development of a new all dry process to make the cell. An efficiency of 15.8% has been recently obtained on a  $10^{-4} \text{ m}^2$  soda-lime glass without using any copper or any other metal of the first group of the periodic table of the elements at the back contact.

© 2004 Elsevier Ltd. All rights reserved.

*Keywords:* Thin film; CdTe; CdS; Solar cells

### 1. Introduction

Bonnet and Rabenhorst (1972) published an interesting paper on CdTe/CdS thin film solar cells in 1972 reporting an efficiency of 6%. The 10% efficiency value was overcome by Tyan and Perez-Albuerné (1982) and finally an efficiency of 15.8% has been reached by Ferekides et al. (1993). Very recently the group of NREL reported a record efficiency of 16.5% (Wu et al., 2001). However, all these groups used as a back contact for CdTe a material containing Cu, which is known to be a fast diffusor in CdTe. The diffusion of Cu could be

beneficial for the solar cell since it can dope CdTe p+ giving a momentary increase in the efficiency but, in any case, at long run the efficiency is doomed to decrease since Cu can segregate at grain boundaries (Dobson et al., 2000; Baetzner et al., 2001). In order to avoid Cu, a new contact, namely  $\text{Sb}_2\text{Te}_3$ , was developed at the University of Parma (Romeo et al., 2000a).

$\text{Sb}_2\text{Te}_3$  is a p-type material and exhibits a resistivity of  $2 \times 10^{-2} \Omega\text{m}$ . We verified that  $\text{Sb}_2\text{Te}_3$  makes an ohmic contact with CdTe. However, since this contact does not diffuse into CdTe (giving a high stability to the solar cell), it does not dope CdTe and so the efficiency that can be obtained is lower than the 16.5% NREL record.

In any case, with  $\text{Sb}_2\text{Te}_3$  contact, made directly on a non-etched CdTe surface, we were able to obtain a stable efficiency of 15.8%.

\* Corresponding author. Tel.: +39 0521 905257; fax: +39 0521 905223.

E-mail address: [romeo@fis.unipr.it](mailto:romeo@fis.unipr.it) (N. Romeo).

## 2. The structure of CdTe/CdS solar cell

The CdTe/CdS solar cell is composed of 4 layers that are:

1. a transparent and conducting oxide (TCO) which acts as a front contact;
2. a CdS film which is the so called window layer;
3. A CdTe film which is the absorber layer made on top of CdS;
4. the back contact on top of CdTe (Fig. 1).

## 3. The transparent conducting oxide (TCO)

The characteristics that are required in order for a TCO to be used as a front contact for CdTe/CdS thin film solar cells are:

1. a high transparency, better than 85% in the wavelength region of interest (400–860 nm);
2. a low resistivity on the order of  $2 \times 10^{-2} \Omega\text{m}$  or a sheet resistance less than  $10 \Omega_{\text{square}}$ ; <sup>1</sup>
3. a good stability at the maximum temperature (500 °C) at which one of the layer, namely CdTe, is prepared. This means that no diffusion from the TCO into the layers deposited subsequently must happen.

Several types of TCOs have been used and tested for the CdTe/CdS solar cell. Among these:

1. Fluorine doped SnO<sub>2</sub>, which is a quite stable material but it exhibits a sheet resistance of about  $10 \Omega_{\text{square}}$  or more that could be not low enough for this kind of solar cells.
2. Tin doped In<sub>2</sub>O<sub>3</sub> (ITO), which exhibits a low resistivity ( $2.5 \times 10^{-2} \Omega\text{m}$ ) but we found out that some In can diffuse into CdS and/or CdTe when this material is used as a front contact. In this case a SnO<sub>2</sub> buffer layer can be used as a diffusion barrier (Visoly-Fisher et al., 2003).
3. Cadmium stannate (Cd<sub>2</sub>SnO<sub>4</sub>) which exhibits both the characteristics of high transparency and low resistivity but it is difficult to be handled since, as we found out, it is quite hygroscopic.
4. Finally we developed a new TCO that is fluorine doped In<sub>2</sub>O<sub>3</sub> which exhibits all the characteristics which are needed. This material is prepared by sputtering using a target of pure In<sub>2</sub>O<sub>3</sub> supplied by Cerac. The doping with fluorine is done by introducing in the sputtering chamber Ar containing  $\approx 5\%$  of

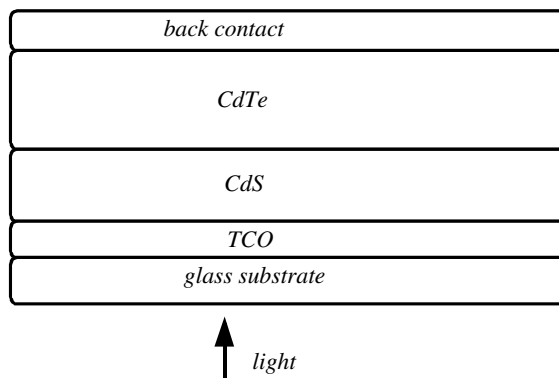


Fig. 1. Sequence of the layers constituting the solar cell. The structure of CdTe/CdS solar cells is of the superstrate arrangement, which means that the solar light enters the cell through the substrate glass.

CHF<sub>3</sub> (trifluoromethane). This gas is decomposed and ionized in the sputtering discharge freeing F which, being strongly electronegative, is directed to the substrate which is the positive electrode and dopes In<sub>2</sub>O<sub>3</sub> during the growth. This material exhibits a resistivity of  $2 \times 10^{-2} \Omega\text{m}$ , a transparency better than 90% between 400 and 800 nm and is quite stable at a temperature of 500 °C as it has been verified by the good stability of CdTe/CdS solar cells grown on it (Romeo et al., 2003).

## 4. The CdS layer

CdS is prepared by several methods that are evaporation from a single crucible, sputtering, chemical bath deposition (CBD) and closed space sublimation (CSS).

All these methods are suitable to prepare a CdS layer that, when used in the CdTe/CdS solar cell, can give efficiency larger than 10% even though the highest efficiency (Ferekides et al., 1993; Wu et al., 2001) was obtained by using a CdS prepared by CBD. The choice of the CBD method was probably due to the fact that CBD makes a very compact film that covers perfectly the TCO layer. However it must be considered that CBD is not suitable for large-scale production since it is not fast and gives a waste that needs to be recycled. In our case we prepared CdS by sputtering or by closed space sublimation (CSS). CdS by sputtering was grown in presence of fluorine by introducing in the sputtering chamber Ar containing 3% of CHF<sub>3</sub>. Despite fluorine is a donor for CdS, we did not see any lowering of the CdS resistivity when it was grown in presence of fluorine.

CdS by CSS was prepared at a pressure of  $10^3$  Pa in an atmosphere composed of 50% of Ar and 50% of O<sub>2</sub>.

<sup>1</sup>  $\Omega_{\text{square}}$  is the sheet resistance of a 1-cm<sup>2</sup> film.

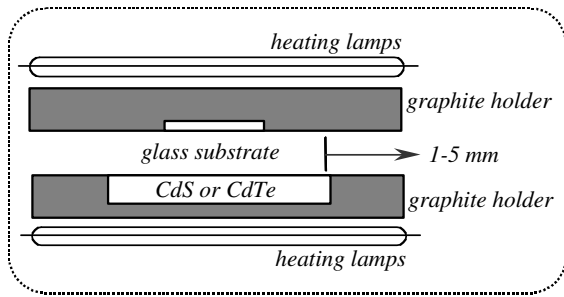


Fig. 2. Outline of the close-spaced sublimation system.

The CSS method (Fig. 2) consists in putting the sublimation source (in this case CdS) very close to the substrate ( $2\text{--}4 \times 10^{-3}$  m) and doing the evaporation in an atmosphere that could be inert (Ar) or reactive (Ar + O<sub>2</sub>). The CSS has the characteristic of allowing the deposition of materials at a substrate temperature much higher than that used in vacuum evaporation. As an example, when CdS is deposited by evaporation in high vacuum, the substrate temperature must be not much higher than 150 °C because, at temperatures higher than 150 °C, S has a very high evaporation rate and it is re-evaporated before combining with Cd.

When CdS is made by CSS, a substrate temperature as high as 500 °C can be used since the sticking of CdS is assured by the gas pressure that is maintained in the chamber and by the fact that the substrate is very close to the source. Furthermore, the deposition of materials at a high substrate temperature guarantees high crystalline quality, due to the high adatoms superficial diffusion coefficient.

We found out that both CdS(F) by sputtering or CdS(O) by CSS are suitable to make high efficiency cells if they are treated for 20 min. in an atmosphere of Ar containing 20% of H<sub>2</sub> at 400 °C substrate temperature (Romeo et al., 2003, in press). We explained this fact by considering that CdS(F) contains CdF<sub>2</sub> segregated in the grain boundaries and in the surface. While the CdF<sub>2</sub> segregated in the grain boundaries is useful to passivate the grain boundaries, the CdF<sub>2</sub> segregated in the surface has to be removed in order to allow CdS to interact with CdTe thus forming a good CdTe/CdS junction.

The same happens when CdS is made in presence of O<sub>2</sub> but in this case CdO and/or CdSO<sub>3</sub> is formed in the grain boundaries and in the CdS surface. CdO and/or CdSO<sub>3</sub> formed in the surface is removed by the H<sub>2</sub> treatment.

The thickness of the CdS layer is, in both cases, 80 nm.

## 5. The CdTe layer

CdTe is a material that exhibits a forbidden gap of 1.45 eV very close to the maximum of solar energy con-

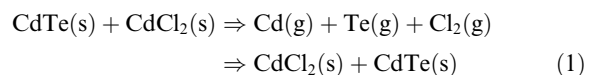
version. Besides, its gap is direct and as a consequence its absorption coefficient is higher than  $10^7$  m<sup>-1</sup> for energy larger than the forbidden gap. This means that only a few microns of material are enough to absorb all the light. A practical efficiency of 18.5% could be expected for this material with an open-circuit voltage of 0.880 V and a short-circuit current density of 270 A/m<sup>2</sup> (with a negligible thin CdS) (Sites and Liu, 1985).

Several methods have been used to deposit CdTe, namely vacuum evaporation, (Romeo et al., 2000b) electrodeposition (Johnson, 2000) and closed space sublimation (CSS). All these techniques are able to produce cells with efficiency larger than 10%. However, the highest efficiency solar cells have been prepared by closed space sublimation (CSS) (Ferekides et al., 1993; Wu et al., 2001; Romeo et al., 2000). This last technique has been also used in our laboratory but with a substantial modification, which consists in the use of a compact block of CdTe, previously melted and resolidified, instead of CdTe granules. The use of a compact block of CdTe is effective in getting a uniform heating of the material thus avoiding any spitting of microparticles from the source to the substrate.

The higher efficiency obtained by using CSS seems to be due to the fact that a high substrate temperature, namely 500–600 °C, is used. At these temperatures part of the CdS mixes with CdTe forming a mixed CdS<sub>x</sub>Te<sub>1-x</sub> (with  $x \approx 0.07$ ), since only 7% of CdS can enter in the matrix of CdTe (Lane et al., 2000). If CdTe is deposited on top of CdS at low substrate temperature, as in the case of vacuum evaporation or electrodeposition, than the mixing process only happens when CdTe is treated with CdCl<sub>2</sub> at 400 °C substrate temperature. The CdS–CdTe mixing seems to be very important in order to get solar cells with efficiencies larger than 10%.

## 6. The CdCl<sub>2</sub> treatment

This treatment is necessary independent of the technique used to deposit CdTe. If the CdCl<sub>2</sub> treatment is not performed, the short circuit current of the solar cell is very low and also the efficiency is very low. The treatment consists in depositing 300–400 nm of CdCl<sub>2</sub> on top of CdTe with a subsequent annealing at 400 °C for 15–20 min in air or in an inert gas like Ar. During this process the small CdTe grains are put in vapour phase and recrystallize giving a better-organized CdTe matrix following possibly the reaction shown in Eq. (1):



The presence of  $\text{Cl}_2$  could favour the crystalline growth of CdTe by means of a local vapour phase transport. In this way the small grains disappear and the CdS/CdTe interface is reorganized. If this process is carried out in air, some oxides are formed on the CdTe surface. These oxides need to be removed before making the back contact and an acid etching or a cleaning in a solution of Br-methanol is necessary (Romeo et al., 2000b). In an in-line production any use of acids or liquid solutions should be avoided in order to not interrupt the process and also for safety considerations.

For this reason we developed a new method for  $\text{CdCl}_2$  treatment that consists simply in exposing the CdTe surface to a  $\text{CdCl}_2$  vapour in an inert atmosphere such as Ar.

The process works like a closed space sublimation (CSS) in which the source is  $\text{CdCl}_2$  and the substrate is CdTe. In order to remove any residual of  $\text{CdCl}_2$  which could be present on the CdTe surface, after the treatment, the  $\text{CdCl}_2$  source temperature is lowered and a high vacuum is maintained in the chamber keeping the substrate at 400 °C. At this temperature in vacuum, the residual  $\text{CdCl}_2$  re-evaporates from the CdTe surface leaving a surface that is ready for the subsequent back-contact deposition. In this way no etching or cleaning process of the CdTe surface is necessary.

## 7. The back contact

Most researchers make a back contact on CdTe with a material containing Cu such as Cu–Au alloy,  $\text{Cu}_2\text{Te}$ ,  $\text{ZnTe:Cu}$  (Gessert et al., in press) and  $\text{Cu}_2\text{S}$  (Kim et al., in press). It is believed that Cu is necessary to make an ohmic contact on CdTe since CdS/CdTe solar cells made with contacts not containing Cu have a high series resistance.

In our opinion the series resistance does not come from the contact but from CdTe which possibly is more conducting at the interface than in the bulk. The higher conductivity, close to the interface could come from the fact that CdTe mixes with CdS and its gap lowers down. In any case, in useful cells Cu must not be used since in the long run it segregates at grain boundaries and the solar cell degrades. It must be considered that the highest efficiency solar cell so far reported has been made with some copper at the back contact. Copper, by diffusing into CdTe lowers its resistivity and for a while it gives a higher efficiency.

We developed a new contact, namely  $\text{Sb}_2\text{Te}_3$ , which has a low gap ( $\approx 0.3$  eV), is p-type and exhibits a very low resistivity ( $2 \times 10^{-2} \Omega\text{m}$ ) when it is deposited at a substrate temperature of 300 °C.  $\text{Sb}_2\text{Te}_3$

can be deposited easily by sputtering, but it can also be deposited by vacuum evaporation (Romeo et al., 2000a).

We verified that  $\text{Sb}_2\text{Te}_3$  makes an ohmic contact with CdTe thin films. We also found out that  $\text{Sb}_2\text{Te}_3$  makes an ohmic contact on a p-type CdTe single crystal whose resistivity is on the order of  $10^7 \Omega\text{m}$ . With  $\text{Sb}_2\text{Te}_3$  as a back contact we obtained CdS/CdTe thin film solar cells with a maximum efficiency of 15.8%. These cells are heated up to 200 °C under 20 suns without degrading. Instead, they generally exhibit a higher efficiency after the 200 °C treatment.

## 8. Recent results

Recently, a further improvement in the efficiency of CdTe/CdS solar cell has been obtained in our laboratory. We found out that, by depositing CdTe on top of CdS by CSS in presence of  $\text{O}_2$ , the fill factor of the CdTe/CdS solar cell increases from around 0.65–0.66 to 0.71–0.74. In this way we were able to obtain on a  $10^{-4} \text{m}^2$  solar cell, prepared on soda lime glass, an efficiency of 15.8% with an open circuit voltage of 0.862 V, a short circuit current density of 255  $\text{A/m}^2$  and a fill factor of 0.72. On average, the efficiency of our cells made in similar conditions is in the range of 15.2–15.8%. This efficiency has been measured with an Oriol™ solar simulator under  $10^3 \text{W/m}^2$  AM 1.5 solar light. The measurement system has been calibrated with a 14% efficient CdTe/CdS thin film solar cell previously certified at the Renewable Energies Unit of the Joint Research Center, Ispra, Italy. An important remark is that no copper or any other element of group I of the periodic table of the elements has been used to make the back contact. Instead, we used 300 nm of  $\text{Sb}_2\text{Te}_3$  followed by 300 nm of Mo deposited by sputtering. It is generally believed that copper is necessary to make a good contact on CdTe since it is generally observed that both fill factor and efficiency increase very much with a contact containing copper. We believe that Cu is not necessary to make a good contact and that the momentary improvement of the efficiency is due only to the doping of CdTe by copper since this last element is a strong diffusor. However, the cells made with some copper at the back contact are doomed to degrade since copper, at long run, segregates at the grain boundaries.

In order to obtain high efficiency solar cells with a high fill factor, as said before, one has to deposit CdTe by CSS in presence of  $\text{O}_2$ . In our case, CdTe is deposited with a gas pressure of  $10^4$  Pa of Ar containing 2–10% of  $\text{O}_2$  with a distance between crucible and substrate of about  $4 \times 10^{-3}$  m. The substrate temperature is varied between 480 and 520 °C. CdTe is

covered by 100–500 nm of CdCl<sub>2</sub> and annealed in air or Ar at a temperature varying between 380 and 420 °C for 20 min. The efficiency of the solar cell depends on the amount of O<sub>2</sub> in the CSS chamber, on the substrate temperature during the deposition and the CdCl<sub>2</sub> annealing temperature. A high amount of O<sub>2</sub> or a high CdCl<sub>2</sub> annealing temperature tend to give a higher fill factor and a lower open circuit voltage.

The short circuit current is generally not affected but in the case in which a very large amount of O<sub>2</sub> and/or a high CdCl<sub>2</sub> annealing temperature is used. In extreme cases the short circuit current density could be much lower than 255 A/m<sup>2</sup>. A high substrate temperature, namely 520 °C, during the CdTe deposition tends to decrease the fill factor since, at this temperature, less O<sub>2</sub> is incorporated in the film. In order to interpret these results, we made the hypothesis that O<sub>2</sub>, mixing with CdS and CdTe, forms at the interface a mixed compound containing Cd, S, Te and O with a forbidden gap close to that of CdTe which is n-type. In this way a pseudo-homojunction is formed between this compound and p-type CdTe and this can explain the strong increase in the fill factor.

This hypothesis is corroborated by several facts:

1. The  $I$ - $V$  characteristic in the dark exhibits an  $A$  factor close to 1 where  $A$  is given in the diode formula  $J = J_0 \exp[(eV/AkT) - 1]$ . An  $A$  factor close to 1 is typical of a homojunction.
2. When a high amount of O<sub>2</sub>, namely more than 10%, and/or a high CdCl<sub>2</sub> annealed temperature, namely more than 420 °C, are used, the short circuit current density is much lower than 250 A/m<sup>2</sup> despite a high open circuit voltage and principally a high fill factor (0.74–0.75) are obtained. In our vision, this means that a thick n-type layer larger than the absorption length is formed and a good part of the carriers created by the light do not reach the junction region. As a consequence, we deduce that the amount of O<sub>2</sub> used during the CdTe deposition is very important in order to control the formation and the thickness of this presumed n-type layer. The formation of an n-type thick layer has been confirmed by measurements of the photocurrent as a function of wavelength: when the solar cell exhibits a  $J_{sc}$  much lower than 250 A/m<sup>2</sup> the photocurrent response drops very quickly for wavelengths shorter than that corresponding to the gap of CdTe. The difference between the characteristics of two cells, one prepared using O<sub>2</sub> and the other prepared without O<sub>2</sub> is put in evidence in Fig. 3.
3. It has been reported (Hernández-Fenollosa, 2003) that O<sub>2</sub> in presence of Chlorine enhances the concen-

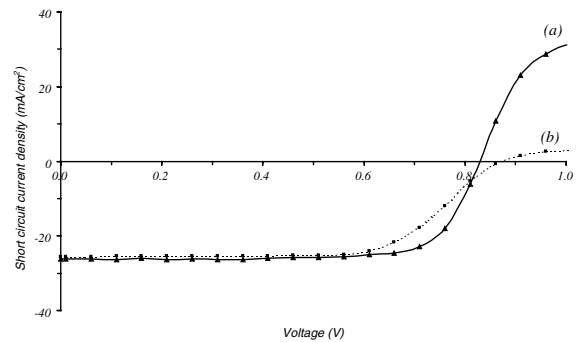


Fig. 3. Comparison between the  $J$ - $V$  characteristics of two CdTe/CdS solar cells taken under  $10^3$  W/m<sup>2</sup> AM 1.5 simulated solar light: (a)  $J$ - $V$  characteristic of a CdTe/CdS solar cell in which CdTe has been prepared by CSS in an atmosphere of Ar containing 2% of O<sub>2</sub>. Fill factor and efficiency are respectively: 0.73% and 15.45%. (b)  $J$ - $V$  characteristic of a CdTe/CdS solar cell in which CdTe has been prepared by CSS in an atmosphere of pure Ar. Fill factor and efficiency are respectively: 0.63% and 13.67%. All the other layers that compose the cells, namely TCO, CdS and back contact have been prepared in the same way.

tration of Cl<sub>Te</sub><sup>2</sup> which is a donor for CdTe and can form an n-type CdTe(S,O) layer at the interface.

## 9. A possible in-line dry process

The techniques, which we use to make CdTe/CdS solar cells, are CSS and sputtering both fast and easily scalable. A possible in-line process is shown in Fig. 4. Modules of  $0.6 \times 1.2$  m<sup>2</sup> can be covered with a process time of a few minutes.

The glass, moved on a rail, first enters in a washing machine and then is heated up to 400 °C and goes into a sputtering chamber where 500 nm of TCO are deposited. A laser scribing eliminates the TCO along parallel lines  $10^{-2}$  m distant one from each other. The temperature is raised up to 500 °C and 80 nm of CdS and 4000–5000 nm of CdTe are deposited in sequence both by CSS.

A CdCl<sub>2</sub> treatment is done in another chamber at 400 °C substrate temperature, in an Ar atmosphere as described before. Then, a second laser scribing is done in order to remove CdS and CdTe in parallel lines close to the ones made before. Afterwards, the glass enters in a sputtering machine where 300 nm of Sb<sub>2</sub>Te<sub>3</sub> are deposited at a substrate temperature of 300 °C. In sequence 300 nm of Mo are sputtered on top of Sb<sub>2</sub>Te<sub>3</sub> in order to increase the conductivity of the back contact. Finally a third laser scribing is done in parallel lines close to those made by the second laser scribing in order to have a module made up of solar cells  $10^{-2}$

<sup>2</sup> Cl which substitutes Te.

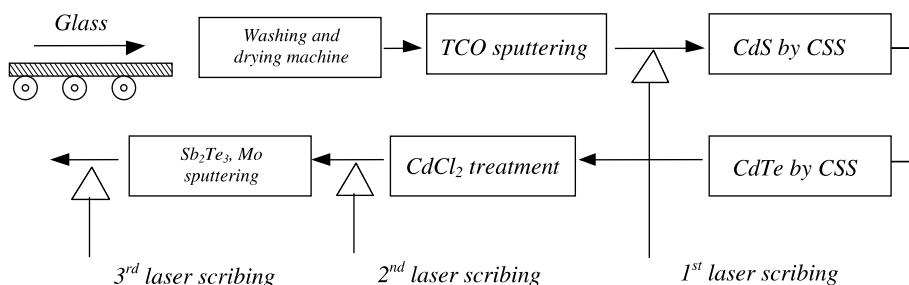


Fig. 4. Schematic of a possible in-line dry process for the production of CdTe/CdS solar cells modules.

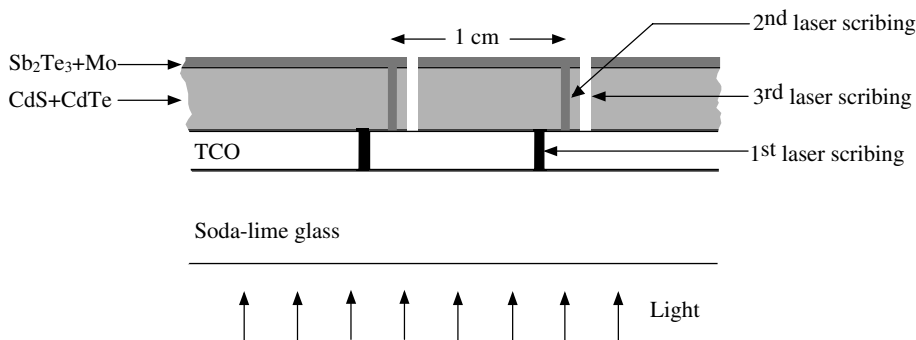


Fig. 5. Typical interconnect scheme for a CdTe/CdS solar cell module.

m large and as long as the length of the glass all put in series (Fig. 5).

## 10. Conclusion

The technology to fabricate CdTe/CdS thin film solar cells can be considered mature for the large-scale production of CdTe/CdS modules. The stable efficiency of single laboratory  $10^{-4} \text{ m}^2$  cells is around 15.8% and it is expected that a  $0.6 \times 1 \text{ m}^2$  module can exhibit an efficiency of 12% or more. Due to the simple and fast techniques that are used for the preparation of the cells, a production cost less than 1 Euro/Watt is foreseen.

The contribution of Parma University group to the development of such type of solar cells has been substantial. Three parts of the preparation process have been implemented:

1. A new stable TCO has been realized, namely fluorine doped  $\text{In}_2\text{O}_3$ .
2. A dry process, which excludes any use of acid or liquid solutions, was shown to be effective in treating CdTe with  $\text{CdCl}_2$ .
3. A new stable and ohmic back contact for CdTe, namely  $\text{Sb}_2\text{Te}_3$ , has been invented.

A stable efficiency of 15.8% has been obtained by depositing CdTe by CSS in presence of  $\text{O}_2$ .

## References

- Baetzner, D.L., Romeo, A., Zogg, H., Wendt, R., Tiwari, A.N., 2001. Development of efficient and stable back contacts on CdTe/CdS solar cells. *Thin Solid Films* 387, 151–154.
- Bonnet D., Rabenhorst H., 1972. New results on the development of a thin film p-CdTe–n-CdS heterojunction solar cell. In: *Proceedings of the 9th Photovoltaic Specialists Conference*, pp. 129–131.
- Dobson, K.D., Visoly-Fisher, I., Hodes, G., Cahen, D., 2000. Stability of CdTe/CdS thin-film solar cells. *Solar Energy Mater. Solar Cells* 62, 295–325.
- Ferekides, C., Britt, J., Ma, Y., Killian, L., 1993. High efficiency CdTe solar cells by close spaced sublimation. In: *Proceedings of Twenty-Third-Photovoltaic-Specialists-Conference IEEE*, New York, USA, p. 389.
- Gessert, T.A., Romero, M.J., Dhere, R.G., Johnston, S., Duda, A., 2003. Cross-sectional, spectroscopic cathodoluminescence studies of ZnTe:Cu contact process for CdS/CdTe solar cells. In: *Proceedings of 3rd World Conference on Photovoltaic Energy Conversion*, Osaka, Japan.
- Hernández-Fenollosa, M.A., Halliday, D.P., Durose, K., Campo, M.D., Beier, J., 2003. Photoluminescence studies of CdS/CdTe solar cells treated with oxygen. *Thin Solid Films* 431, 176–180.

- Johnson, D.R., 2000. Microstructure of electrodeposited CdS/CdTe cells. *Thin Solid Films* 361–362, 321–326.
- Kim, D., McCandless, B.E., Hegedus, S.S., Birkmire, R.W., 2003. Cu<sub>2</sub>S back contact for CdTe solar cells. In: *Proceedings of 3rd World Conference on Photovoltaic Energy Conversion*, Osaka, Japan.
- Lane, D.W., Rogers, K.D., Painter, J.D., Wood, D.A., Özsan, M.E., 2000. Sulfur diffusion in cadmium telluride thin films: Part 1: the grain boundary diffusion coefficient. *Thin Solid Films* 1, 361–362.
- Romeo, A., Baetzner, D.L., Zogg, H., Tiwari, A.N., 2000. Recrystallization in CdTe/CdS. *Thin Solid Films* 361–362, 420–425.
- Romeo, N., Bosio, A., Tedeschi, R., Canevari, V., 2000a. Back contacts to CSS CdS/CdTe solar cells and stability of performances. *Thin Solid Films* 361, 327.
- Romeo, N., Bosio, A., Tedeschi, R., Canevari, V., 2000b. Growth of polycrystalline CdS and CdTe thin layers for high efficiency thin films solar cells. *Mater. Chem. Phys.* 66, 201–206.
- Romeo, N., Bosio, A., Canevari, V., Terheggen, M., Vaillant-Roca, L., 2003. Comparison of different conducting oxides as substrates for CdS/CdTe. *Thin Solid Films* 431–432, 364–368.
- Romeo, N., Bosio, A., Canevari, V., 2003. The role of CdS preparation method in the performance of CdTe/CdS thin film solar cells. In: *Proceedings of 3rd World Conference on Photovoltaic Energy Conversion*, Osaka, Japan.
- Sites, J.R., Liu, X., 1985. Performance comparison between polycrystalline thin-film and single crystal solar cells. *Progr. Photovoltaics* 3, 307.
- Tyan, Y.S., Perez-Albuerno, E.A., 1982. Efficient thin film CdS/CdTe solar cells. In: *Proceedings of 16th IEEE Photovoltaic Specialists Conference*. IEEE Publishing, New York, p. 794.
- Visoly-Fisher, I., Cohen, S.R., Cahen, D., Ferekides, C.S., 2003. Electronically active layers and interfaces in polycrystalline devices: cross section mapping of CdS/CdTe solar cells. *Appl. Phys. Lett.* 83, 4924–4926.
- Wu, X., Keane, J.C., Dhere, R.G., DeHart, C., Albin, D.S., Duda, A., Gessert, T.A., Asher, S., Levi, D.H., Sheldon, P., 2001. 16.5%-Efficient CdS/CdTe polycrystalline thin-film solar cell. In: *Proceedings of the 17th European Photov. Solar Energy Conf.*, Munich, Germany, II, p. 995.



ELSEVIER

Available online at [www.sciencedirect.com](http://www.sciencedirect.com)

SCIENCE @ DIRECT®

Solar Energy Materials  
& Solar Cells

Solar Energy Materials & Solar Cells 82 (2004) 315–330

[www.elsevier.com/locate/solmat](http://www.elsevier.com/locate/solmat)

# Nano-structured CdTe, CdS and TiO<sub>2</sub> for thin film solar cell applications

R.S. Singh<sup>a</sup>, V.K. Rangari<sup>b</sup>, S. Sanagapalli<sup>a</sup>, V. Jayaraman<sup>a</sup>,  
S. Mahendra<sup>a</sup>, V.P. Singh<sup>a,\*</sup>

<sup>a</sup> Center for Micro-Magnetic and Electronic Devices, Department of Electrical and Computer Engineering, University of Kentucky, 453 F. Paul Anderson Tower, Lexington, KY 40506-0046, USA

<sup>b</sup> Center for Advanced Materials, Tuskegee University, Tuskegee, AL, USA

## Abstract

Nano-crystalline CdTe and nano-structured CdS films in crystalline, porous and fiber forms were deposited on ITO-coated glass substrates. CdTe films exhibited a typical particle size of 10 nm and a blue shift in the absorption with an effective band gap of 2.8 eV. CdS films exhibited a typical particle size of 15 nm and an effective band gap of 2.98 eV. Also, porous CdS and porous TiO<sub>2</sub> films were deposited on plastic substrates by a self-assembly method. Typical pore sizes were 80 and 70 nm, respectively. These can be used in nano-structured solar cell configuration where the pores are filled with a suitable absorber material. Additionally, CdS fibers and nano-crystalline films of TiO<sub>2</sub> on plastic substrates were fabricated. Typical particle size in TiO<sub>2</sub> was 10 nm and CdS fibers were about 80 nm wide and 1.5 μm long.

© 2004 Elsevier B.V. All rights reserved.

*Keywords:* CdS/CdTe solar cell; Nano-crystalline; Nano-porous; Thin film; TiO<sub>2</sub>

## 1. Introduction

Many nano-structured materials are now being investigated for their potential applications in photovoltaic, electro-optical, micromechanical and sensor devices [1–3]. Our interest lies in taking advantage of the benefits offered by nanotechnology to make inexpensive and efficient solar cells on a large scale. To this end, nano-structured layers in thin film solar cells offer three important advantages. First, due to multiple reflections, the effective optical path for absorption is much larger than the actual film thickness. Second, light generated electrons and holes need to travel

\*Corresponding author. Tel.: +1-859-257-3092; fax: +1-859-257-3092.

E-mail address: [vsingh@engr.uky.edu](mailto:vsingh@engr.uky.edu) (V.P. Singh).

over a much shorter path and thus recombination losses are greatly reduced. As a result, the absorber layer thickness in nano-structured solar cells can be as thin as 150 nm instead of several micrometers in the traditional thin film solar cells [4]. Third, the energy band gap of various layers can be tailored to the desired design value by varying the size of nano-particles. This allows for more design flexibility in the absorber and window layers in the solar cell. In particular nano-structured CdS, CdTe and TiO<sub>2</sub> are of interest as window and absorber layers in thin film solar cells [5–10]. Fabrication and characterization of these films constitute the focus of this work.

Production of large-area solar cells would also require a process for inexpensive fabrication of large periodic arrays of semiconductor nanostructures that will allow for (a) controlled variations in the size and composition of the nanostructures, (b) encapsulation of the semiconductor nanostructures in a rugged host material, (c) flexibility to use a variety of substrate materials, and, preferably, (d) compatibility with standard silicon fabrication techniques. Self-assembly is such a process. We have used the self-assembly process to fabricate a variety of nano-structured films including CdTe and CdS on ITO-coated glass substrates. In addition nano-porous CdS and TiO<sub>2</sub> films were fabricated on a plastic substrate with a view to making devices on a lightweight, flexible substrate. Fabrication techniques and material characteristics of these films and their applications to solar cells are described below. Results on CdTe, CdS and TiO<sub>2</sub> are presented in Sections 2, 3 and 4, respectively.

## 2. Nano-crystalline CdTe films

Nano-crystalline CdTe films are of interest because of their potential applications as n-type window layers in a p–n homojunction thin film CdTe solar cell (Fig. 1) and in electroluminescent displays devices [11–13]. CdTe nanocrystals were prepared by microwave-assisted synthesis and films were cast from colloidal solutions containing

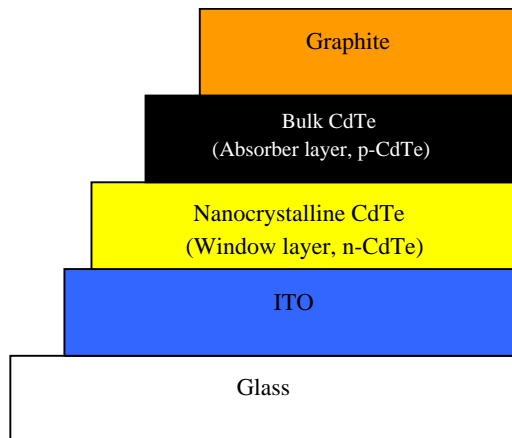


Fig. 1. Device configuration of a Glass/ITO/n-Nano-CdTe/p-bulk CdTe/graphite solar cell.

nano-CdTe. These films were characterized by optical absorption, photoluminescence spectroscopy, profilometer and scanning electron microscopy on glass and plastic substrates for various conditions. The microwave-assisted synthesis was carried out in a custom made 1000 W/2.45 GHz Sharp-R21-HT-microwave oven supplied by Microwave Specialties Inc., USA. The oven's cavity was modified to include a complete refluxing system. In the present experiment, a 250 ml long neck flask with a refluxing condenser assembly was used. All the reactions were carried out with continuous heating at 50% power of the 1000 W, under flow of argon gas. A coolant liquid ( $\sim 5^{\circ}\text{C}$ ) was circulated through the refluxing condenser throughout the experiment. A few glass capillary tubes (3–5) were also added to the reaction mixture to avoid the sudden liquid bumps.

1 g of cadmium (II) acetate dihydrate was dissolved in 100 ml of ethylene glycol and then stoichiometric quantity (0.40 g) of tellurium powder was added. The system was purged for 10 min with argon and the reaction vessel was exposed to microwave radiation continuously for 30 min. At this stage, the reaction mixture turned to grayish color then the reaction mixture was diluted with ethanol to precipitate and centrifuged at 5000 rpm. The precipitate was further washed with ethanol several times and dried overnight under vacuum.

The nano-crystalline CdTe powder thus obtained by microwave assisted synthesis was dispersed in methanol and coated on to ITO-coated glass. The resulting films were examined with a FE-SEM and the electron micrograph shows a particle size of about 10 nm (Fig. 2). The UV–VIS spectra recorded on this film shows a blue shift in

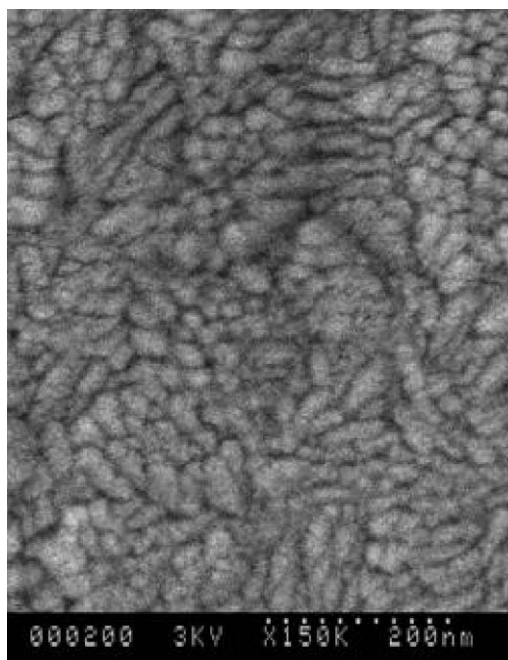


Fig. 2. FE-SEM image of a nanocrystalline CdTe film on ITO-coated glass substrate.

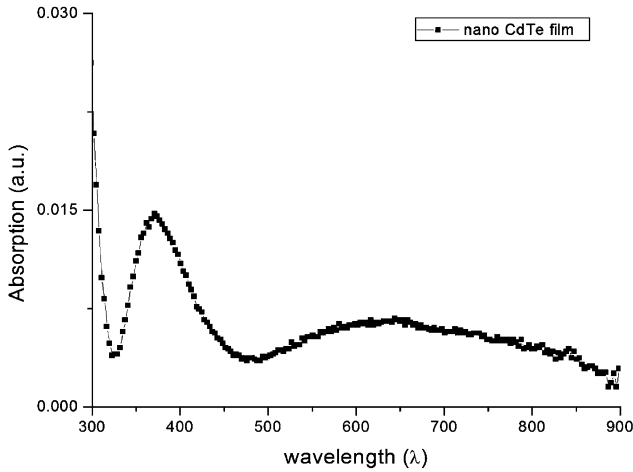


Fig. 3. Absorption spectrum of a nanocrystalline CdTe film on ITO-coated glass substrate.

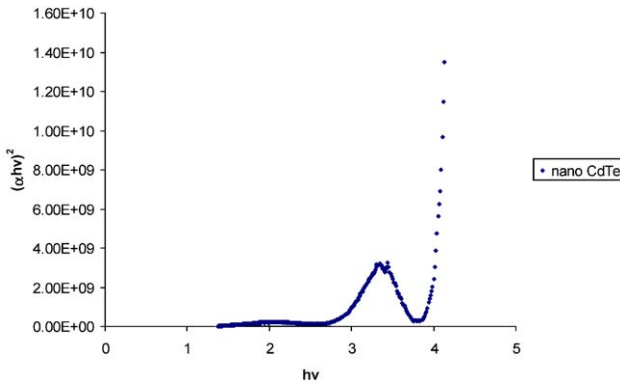


Fig. 4. Tauc's law calculation for a nanocrystalline CdTe film on ITO-coated glass substrate.

absorption due to smaller particle size (Fig. 3). Tauc's relation was used to determine the effective band gap ( $E_{\text{eff}}$ ) for the films.  $(\alpha hv)^2$  was plotted against  $hv$  (Fig. 4) and  $E_{\text{eff}}$  was obtained by extrapolation to zero value of  $(\alpha hv)^2$ . Band gap estimate using Tauc's law indicates a value of about 2.8 eV as compared to a bulk CdTe band gap of 1.5 eV. This increased band gap makes CdTe a good candidate for electroluminescent display devices [11–13] and for window layers in n-CdTe/p-CdTe homojunction solar cells (Fig. 1).

### 3. Nano-structured CdS films

Nano-structured CdS was fabricated in crystalline, porous and fiber forms. The fabrication and characterization of these films are described below.

### 3.1. Nano-crystalline CdS

CdS films were fabricated by three different techniques namely, solution growth (type A), sonochemical (type B) and microwave-assisted synthesis (type C).

For types B and C, nano-crystalline CdS was first prepared in powder form by sonochemical and microwave methods. SEM micrographs of the CdS powder obtained by sonochemical and microwave synthesis methods showed spherical particles, 15 nm in size. The X-ray diffraction pattern of the nano-crystalline CdS powder shows peaks at  $2\theta$  positions of  $27^\circ$ ,  $44^\circ$  and  $52^\circ$  corresponding to the (1 1 1), (2 2 0) and (3 1 1) planes of the cubic CdS phase, respectively. The XRD patterns obtained match with the JCPDS data (10-0454 Hawleyite). Sonochemical method involves ultrasound irradiation of the sample during synthesis while microwave method involves microwave irradiation. Sonochemistry is driven by acoustic cavitation, formation, growth, and implosive collapse of bubbles in liquids irradiated with high-intensity ultrasound. Sonochemical synthesis takes place when a strong acoustic field is applied to an aqueous solution leading to cavity filled microbubbles. Energy is transferred upon the growth and collapse of these microbubbles from the macroscale acoustic wave to the microscale vapor inside the bubbles. Extremely high pressures (hundreds of atmospheres) and temperatures (thousands of degree Kelvin) result from the high localization [14–16].

Next, types B and C CdS films were deposited on ITO-coated glass by dip coating in a suspension of the CdS powder. Type A films were deposited on ITO-coated glass by the solution growth method. Further details on the synthesis of these films can be found in our previous publication [5]. Particle size and the morphology of the films were studied with SEM. Figs. 5(a)–(c) show the electron micrographs of CdS films deposited by three different techniques. The solution growth films (Fig. 5(a)) have a smooth morphology with a particle size of 110 nm and the film thickness is equal to the particle size indicating a monolayer. Particle sizes in types B and C films, with a typical value of 15 nm, are an order of magnitude smaller than in type A. A hyperbolic band model [17] was used to estimate the energy gap as a function of particle size.

$$E = [E_g^2 + 2(\hbar)^2 E_g (\pi/r)^2 / m^*]^{1/2}, \quad (1)$$

where  $E_g$  is the bulk band gap,  $r$  is the particle radius, and  $m^*$  is the electron effective mass. The particle size corresponds to an energy gap of 2.98 eV for sonochemically prepared CdS and shows a blue shift from the band gap of bulk CdS (2.4 eV).

X-ray diffraction measurements on the films indicated a cubic CdS phase. Optical absorption plots of CdS films on ITO-coated glass were recorded using a UV–VIS spectrophotometer. A comparison of optical absorption of CdS prepared by sonochemical, microwave and solution growth methods is shown in Fig. 6. The onset of absorption is at nearly 500 nm and a peak can be seen at close to 350 nm for type B, while a peak at nearly 375 nm was observed for microwave (type C). Brus describes this peak as 1S–1S transitions in CdS nanocrystals [18]. Thicker CdS films show a second peak that can be attributed to a second excitation level [19]. Compared to bulk CdS deposited by solution growth, the optical absorption spectra

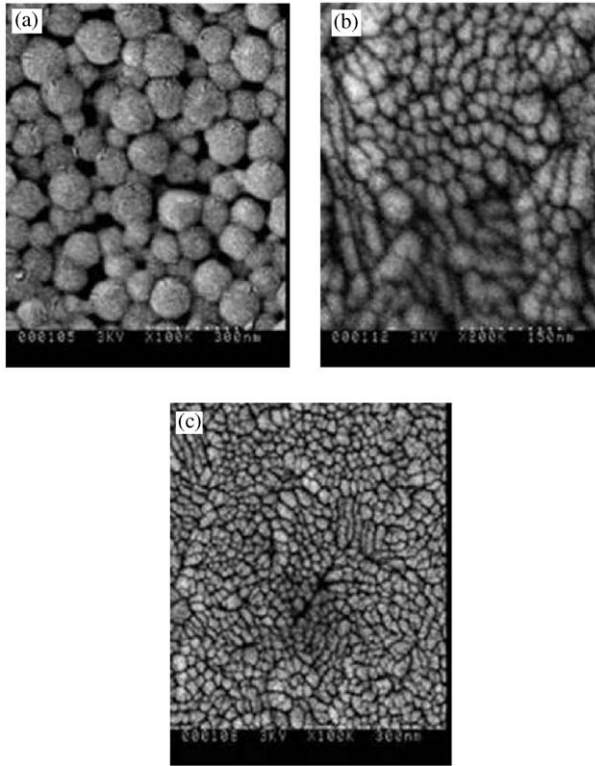


Fig. 5. (a) FE-SEM image of CdS film prepared by solution growth method on ITO-coated glass substrate. (b) FE-SEM image of CdS film prepared by sonochemical method on ITO-coated glass substrate. (c) FE-SEM image of CdS film prepared by microwave method on ITO-coated glass substrate.

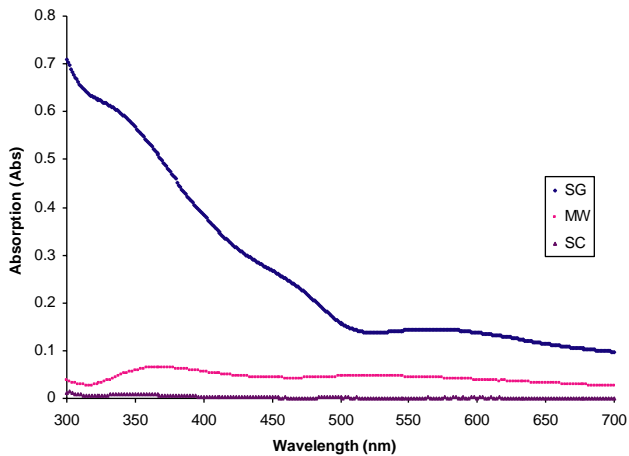


Fig. 6. Comparison of UV-vis absorption spectra of CdS films fabricated by sonochemical, microwave and solution growth methods on ITO-coated glass substrates.

show a blue shift as a result of quantum confinement effects. Solution growth CdS (type A) shows an optical absorption plot without a peak because of its larger crystallite size.

### 3.2. CdS–Ag Schottky diodes

Schottky diodes were formed by depositing polycrystalline (bulk) CdS and nano CdS on to ITO/glass substrates and subsequently depositing an Ag top contact. The representative  $I$ – $V$  curve of bulk CdS Schottky diode is shown (Fig. 7). The characteristics of Schottky diodes on nano-CdS were substantially different from those on bulk CdS (Fig. 8). In theory, nano-CdS/Ag Schottky diodes should have a higher turn on voltage because of the larger band gap of nano-CdS, leading to a higher barrier height. Yet the Schottky diodes fabricated on bulk CdS showed a higher turn on voltage. We attribute this unexpected behavior to the fact that the nanoCdS films are just 20 nm thick and the depletion layer may therefore extend into ITO in this case. Since ITO is a degenerate semiconductor the effective depletion layer width would be the thickness of nano-CdS film. Thus, in parts of the Schottky barrier junction, the electrons would be able to “punch through”, leading to a reduction in the effective turn-on voltage. In comparison, the CdS thickness in polycrystalline CdS layer is 110 nm.

Also, the  $I$ – $V$  characteristics of the nano-CdS–Ag devices show some steps in the plot. This can be understood as follows. As the nano-CdS is expected to be completely depleted in this device the structure ITO/nano-CdS/Ag can be assumed to behave like a metal/insulator/metal. The step behavior could be due to coulomb blockade which is usually seen in such structures.

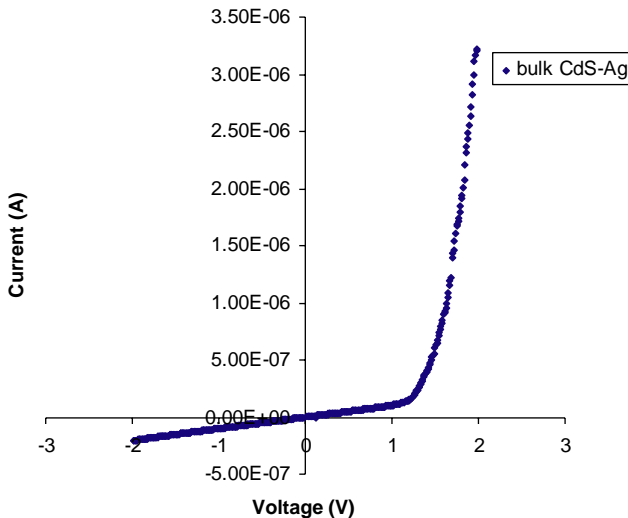


Fig. 7. Device configuration of a glass/ITO/n-nano-CdS/p-bulk CdTe/nano-CdTe/Au solar cell.

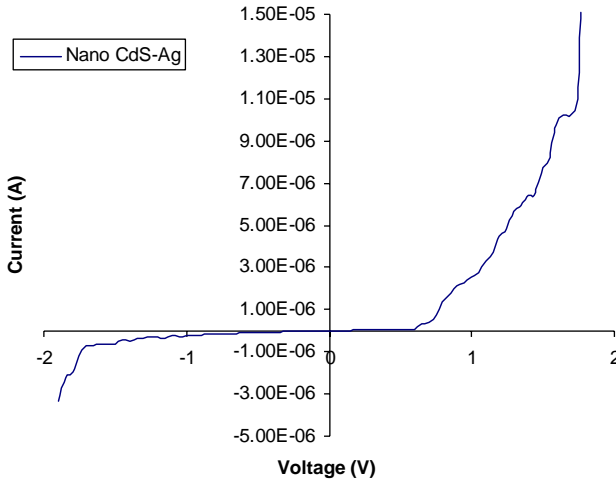


Fig. 8.  $I$ – $V$  curve of a glass/ITO-bulk CdS–Ag Schottky diode.

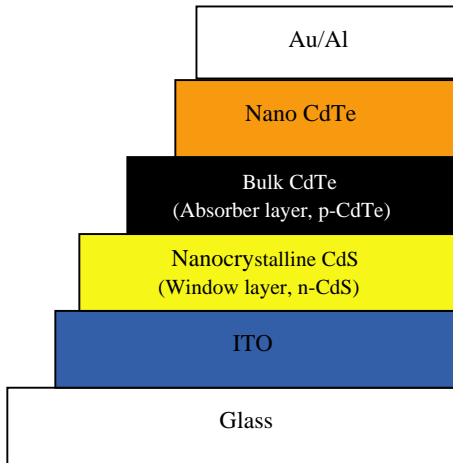


Fig. 9.  $I$ – $V$  curve of a glass/ITO-nano CdS–Ag Schottky diode.

An application of nano-structured CdS to solar cells is illustrated in Fig. 9. Wider band gap makes it a more effective window layer. We are now in the process of using these larger band gap CdS films as window layers in the fabrication of experimental CdS–CdTe thin film solar cells.

### 3.3. Porous CdS films

Our objective is to make porous structure of CdS, deposit an absorber material like, copper indium diselenide, copper sulfide or cadmium telluride into the pores

and study the nano-structured, CdS-based heterojunction solar cells. This structure will allow for a device design involving an n-type material as a porous film and an extremely thin p-type absorber material filling the pores. The advantages are that the transport path for excited charge carriers in the absorber is reduced and at the same time, the optical path for photon absorption is increased. Due to the nano-porous structure of the cell, the distance that photoexcited electrons must travel within their lifetime can be reduced to less than 100 nm [20–22]. This design is also of critical importance in case of organic solar cells and hybrid junctions between inorganic and organic layers, where the traditional non-nano-structured designs are not beneficial for electron/hole transport. This is due to the fact that organic films tend to have short diffusion lengths and because of anisotropy, the conducting axis in the organic layer is not always along the film thickness.

Nano-porous CdS films were fabricated on a plastic substrate by using ultrasound irradiation during dip-coating. We term this process as ultrasound-assisted synthesis (UAS). Ultrasound irradiation was used as a tool to fabricate porous semiconductor films; it is known to cause significant effect on processes that occur at the surface of the solids immersed in liquids. Ultrasonic irradiation generates acoustic cavitation in the liquid, resulting in the formation of microbubbles. These microbubbles collapse on colliding with the solid surface causing erosion [23]. We believe that this process is responsible for the formation of a porous structure in our CdS films. In our method, the plastic substrate is dipped in CdS solution and exposed to ultrasound irradiation; it is thought that the microbubbles collapse at the surface of substrate and cause erosion of the CdS particles stuck to the substrate. Furthermore, since ultrasonicator generates acoustic cavitation uniformly throughout the liquid, the pores formed are uniform throughout the film.

SEM results showed uniform pore structure with a pore size of about 80 nm (Fig. 10). In contrast, the films deposited on ITO/glass substrates with UAS showed a crystalline film with voids. The optical absorption results of all these films showed a blue shift and an increase in the effective band gap (Figs. 11 and 12).

The method reported above is applicable to other materials and constitutes a practical route to prepare inexpensively, large area, flexible, lightweight, porous metal sulfide semiconductor films with an ordered nano-porous array structure. These films can serve as the underlying layers not only for the advantageous inorganic and organic solar cells designs as explained above, but also for sensors and other optoelectronic devices. This is because the large surface area in the nano-porous films can provide a highly active reaction interface and enhanced mass transfer properties.

### 3.4. CdS fibers

We fabricated nano-fibers of CdS by a combination of solution chemistry and ultrasound. High-intensity, high-frequency ultrasound irradiation was found to play a critical role in the crystallization and the preferential one-dimensional growth of the nano-wires of CdS in the solution. During ultrasound irradiation of liquid-powder slurries, cavitations and shock waves it creates can accelerate solid particles

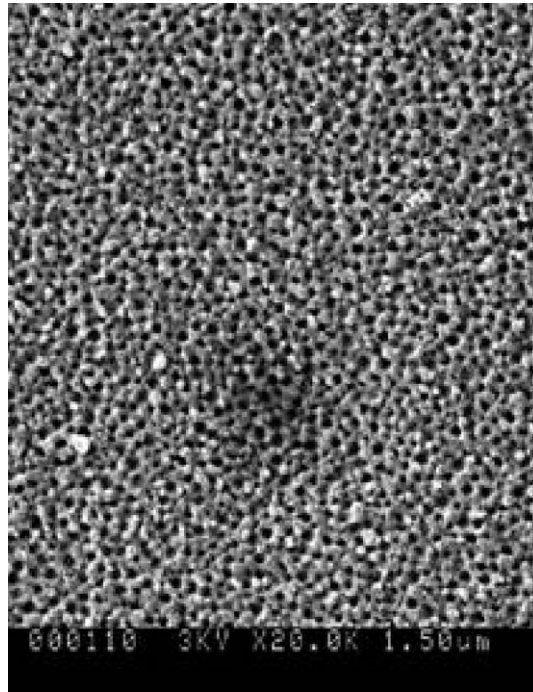


Fig. 10. FE-SEM image of porous CdS film on plastic substrate.

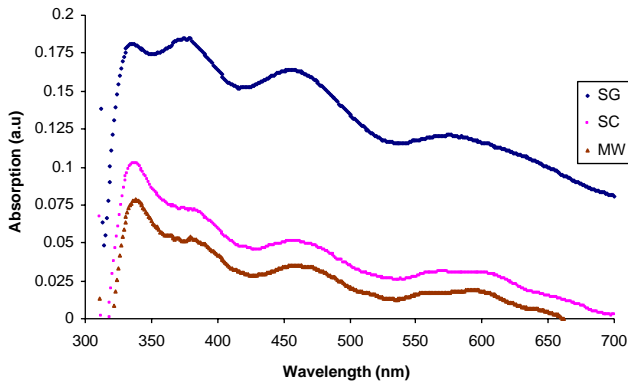


Fig. 11. Comparison of UV-vis absorption spectra of porous CdS films fabricated by sonochemical, microwave and solution growth methods on plastic substrates.

to high velocities. The inter-particle collisions that result are capable of inducing striking changes in morphology, composition, and reactivity of the solids. During the inter-particle collisions, the particles can be driven together at sufficiently high speeds to induce effective melting at the point of collision. It is thought that the energy generated during collision induced the crystallization and 1-D growth of CdS

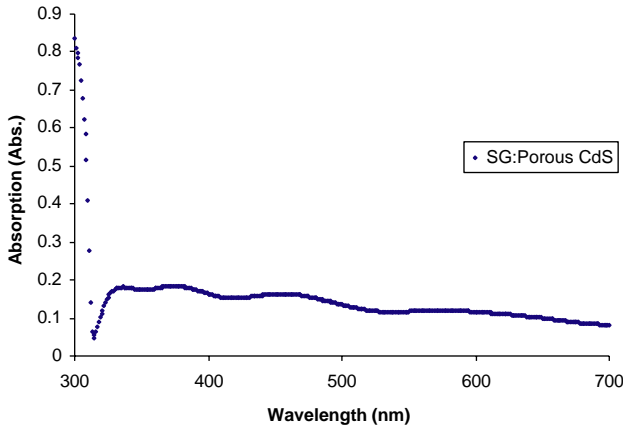


Fig. 12. Optical absorption of porous CdS films by solution growth method.

nanowires. It was observed that temperature, pressure, and reaction time played important roles in the solvothermal fabrication of nano-scale-sized CdS fibers. Only when the reaction was carried out in sealed systems, in the presence of high intensity and high frequency ultrasound, the CdS nano-fibers were formed. The physical effects of ultrasound cavitations in liquid–solid systems are primarily responsible for the enhancement of the generation of surface damage at the liquid–solid interface by shock waves or microjets and fragmentation of friable solids to increase the surface area. The impingement of microjets or shock waves on the solid surface creates the localized erosion, which is responsible for the ultrasound cleaning and many other sonochemical effects on heterogeneous reactions [24]. This phenomenon was also observed in the case of porous CdS films fabricated using an ultrasound-assisted synthesis, as described in the previous section.

The typical length of the fibers was about 1.5  $\mu\text{m}$  and the diameter was about 80 nm. The fiber length was found to be a function of reaction time. The typical scanning electron micrograph of CdS nano-fiber is shown in Fig. 13. The optical absorption measurements of CdS fibers dispersed on an ITO/glass substrate indicate a broad hump around 475 nm and a peak at 330 nm (Fig. 14). These fibers are potential candidates for channels in thin film transistors and have applications in flexible, wearable and disposable electronics.

#### 4. Nano-structured $\text{TiO}_2$ films

$\text{TiO}_2$  films were deposited on plastic substrates by the sol–gel method. The  $\text{TiO}_2$  sol was prepared using the standard procedure starting with high-purity reagents, titanium tetra isopropoxide, isopropanol and nitric acid (70% redistilled). This method is based on the hydrolysis of metal alkoxides or ethoxides in alcoholic solutions in the presence of acid catalysts. The procedure for the preparation involved the dissolution of TTIP as precursor in isopropanol as a solvent, followed

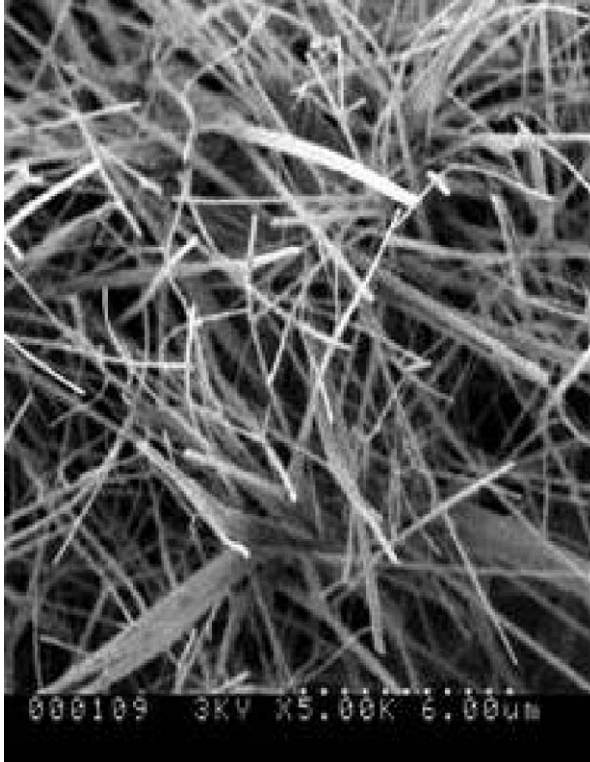


Fig. 13. FE-SEM image of CdS fibers on ITO-coated glass substrate.

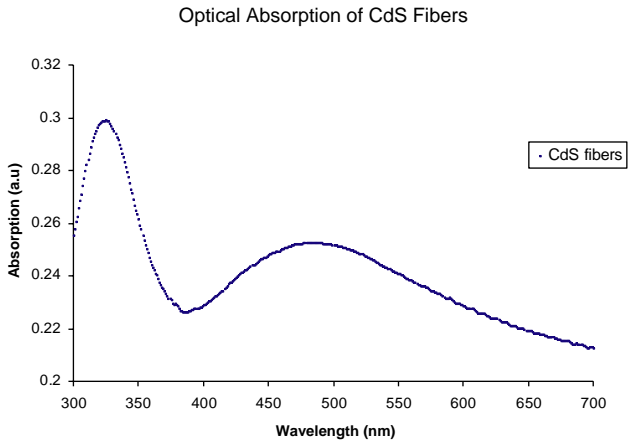


Fig. 14. Optical absorption of CdS fibers on ITO-coated glass substrate.

by adding deionized water and nitric acid (70%). The reaction was carried out with nitrogen gas flowing into the hood. TTIP was added to isopropanol and to this solution, deionized water was added dropwise while stirring. Nitric acid was added dropwise slowly to TTIP, isopropanol and deionized water while still stirring under the hood. The stirring was continued for 2 h and then the solution was covered with a parafilm and placed under the hood. In a typical preparation of 0.1 M  $\text{TiO}_2$  sol, 1 ml of TTIP, 0.05 ml of  $\text{HNO}_3$  (70% distilled), 0.1 ml of deionized water and 32.7 ml of isopropanol were used. The films were deposited by means of spin or dip coating (withdrawal rate 0.5 mm/s) on a clean substrate. Before coating, the substrates were cleaned with a flow of acetone and deionized water with intermediate drying in flowing nitrogen. After cleaning, substrates were either spin or dip coated. For obtaining the nano-porous films, subsequent to the coating process, the substrates were dried under hot water vapor; nitrogen was passed through a hot bubbler, with the humidity controlled by the flow rate of the nitrogen gas ( $\approx 1.3$  cm/s through the chamber). The humidity and temperature of the chamber were monitored with a digital hygrometer. The nano-crystalline  $\text{TiO}_2$  films, on the other hand, were spin or dip coated from a  $\text{TiO}_2$  sol (0.01 M) on to the plastic substrates and dried in ambient.

The material characterization of the films was performed using a Hitachi S-900 FE-SEM for studying morphology and pore structure. A Shimadzu UV-2501 UV–Vis spectrometer was used for optical absorption studies. The thickness of the films was measured using an Alpha step profilometer. The scanning electron micrographs (Figs. 15(a) and (b)) show a porous structure over large areas. The pore size was estimated to be 70 nm. The walls of the pores were found to be thicker than in case of films made via Benard-marangoni convection [25]. The scanning electron micrograph of a typical nano-crystalline  $\text{TiO}_2$  film fabricated by drying the films in ambient is shown in Fig. 16. These films are smooth and have a particle size of about 10 nm. The optical absorption of the films was measured in the near UV and visible

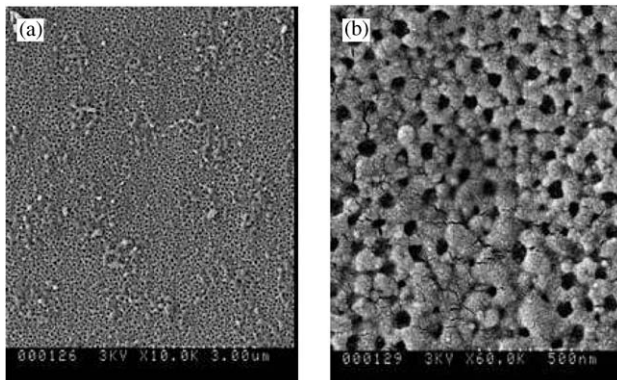


Fig. 15. (a) FE-SEM image of porous  $\text{TiO}_2$  on plastic substrate, at low magnification. (b) FE-SEM image of porous  $\text{TiO}_2$  on plastic substrate, at high magnification.

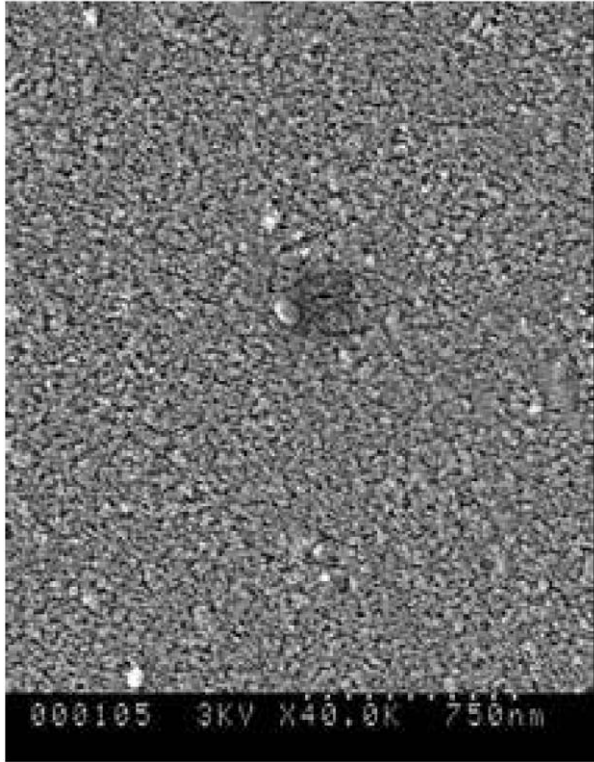


Fig. 16. FE-SEM image of Crystalline TiO<sub>2</sub> on plastic substrate.

range using a Shimadzu spectrometer. The spectral dependence, in general, shows one region of fundamental absorption edge ( $E_g$ ) and the other region characterized by interference peaks at higher wavelengths. All of the three nano-porous films of different thicknesses showed a peak at 334 nm in the optical absorption spectra, but, as expected, the magnitude of absorption is higher in thicker films (Fig. 17).

Just as in case of porous CdS films, porous TiO<sub>2</sub> films can serve as the underlying layers for efficient solar cell designs. Absorber materials like copper indium diselenide, copper sulfide or cadmium telluride can be deposited into the pores of TiO<sub>2</sub> and nano-structured, heterojunction solar cells obtained. Also, the large surface area in the nano-porous films can provide a highly active reaction interface and enhanced mass transfer properties.

## 5. Conclusions

Nano-crystalline CdTe films were deposited on ITO coated glass substrates and characterized. The results indicated particle sizes of 10 nm and a blue shift in the

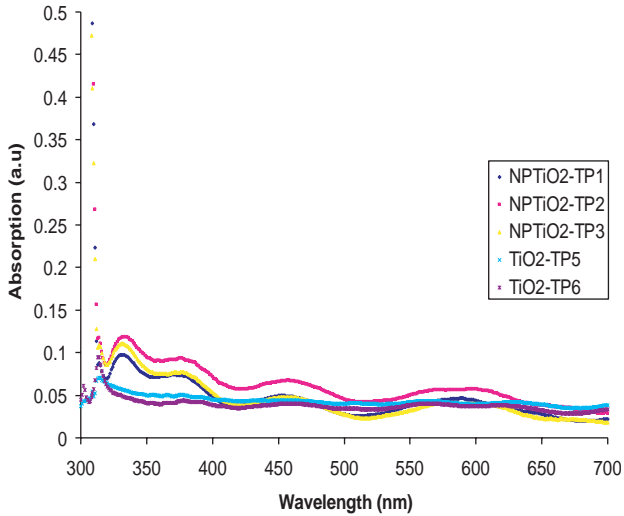


Fig. 17. Comparative UV-vis absorption spectra of porous and crystalline  $\text{TiO}_2$  films on plastic substrates.

absorption with an effective band gap of 2.8 eV. This opens the possibility of using nano-crystalline n-type CdTe as a window layer in an n-CdTe/p-CdTe homojunction solar cell. Nano-crystalline CdS films on ITO-coated glass substrates exhibited particle sizes of 15 nm and an effective band gap of 2.98 eV as compared to the 2.4 eV value for the band gap of bulk CdS. This makes nano-crystalline CdS a better window material in an n-CdS/p-CdTe heterojunction solar cell. We are now in the process of evaluating these advantages by fabricating test structures of n-CdS/p-CdTe and n-CdTe/p-CdTe solar cells.

Porous CdS and porous  $\text{TiO}_2$  films were deposited on plastic substrates by a self-assembly method. Typical pore sizes were 80 and 70 nm, respectively. These can be used in nano-structured solar cell configuration where the pores are filled with a p-type absorber material. Due to the nano-structured character of the absorber, the transport path for the light generated electrons in the absorber is reduced. At the same time, the optical path for photon absorption is increased due to multiple reflections.

Also, CdS fibers and nano-crystalline films of  $\text{TiO}_2$  on plastic substrates were fabricated. Typical particle size in nano-crystalline  $\text{TiO}_2$  was 10 nm and CdS fibers were about 80 nm wide and 1.5  $\mu\text{m}$  long.

## Acknowledgements

The authors thank the Kentucky Science and Engineering foundation for support through Grants KSEF-148-502-02-27 and KSEF-148-502-03-68. One of the authors

(VKR) thanks Dr. Shaik Jeelani, Director, T-CAM, Tuskegee University for support and encouragement.

## References

- [1] G.M. Whitesides, Bartosz Grzybowski, *Science* 295 (2002) 2418–2421.
- [2] Xiangfeng Duan, Chunming Niu, Vijendra Sahi, Jian Chen, J.W. Parce, S. Emedocles, J. Goldman, *Nature* 425 (2003) 274–278.
- [3] M.C. McAlpine, R.S. Friedman, Song Jin, Keng-hui Lin, Wayne U. Wang, C.M. Lieber, *Nano Lett.* 3 (2003) 1531–1535.
- [4] K. Ernst, A. Belaidi, R. Konenkamp, *Semicond. Sci. Technol.* 18 (2003) 475.
- [5] V.P. Singh, R.S. Singh, G.W. Thompson, V. Jayaraman, S. Sanagapalli, V.K. Rangari, *Sol. Energy Mater. Sol. Cells* 81 (2004) 293–303.
- [6] V.P. Singh, J.C. McClure, *Sol. Energy Mater. Sol. Cells* 76 (2003) 369–385.
- [7] V.P. Singh, O.M. Erickson, J.N. Chao, *J. Appl. Phys.* 78 (7) (1995) 4538–4542.
- [8] D.L. Linam, V.P. Singh, J.C. McClure, G.B. Lush, X. Mathew, P.J. Sebastian, *Sol. Energy Mater. Sol. Cells* 70 (2001) 335–344.
- [9] M.E. Calixto, J.C. McClure, V.P. Singh, P.J. Sebastian, *Sol. Energy Mater. Sol. Cells* 63 (4) (2000) 325–334.
- [10] X. Mathew, J.P. Enriquez, P.J. Sebastian, J.C. McClure, V.P. Singh, *Sol. Energy Mater. Sol. Cells* 63 (4) (2000) 355–365.
- [11] Wei Chen, D. Grouquist, J. Roark, *J. Nanosci. Nanotechnol.* 2 (2002) 47.
- [12] V.P. Singh, A. Aguilera, A. Garcia, D.C. Morton, *IEEE Trans. Electron Dev.* 48 (10) (2001) 2242–2248.
- [13] Mingyuan Gao, C. Lesser, S. Kirstein, H. Mohwald, A.L. Rogach, H. Weller, *J. Appl. Phys.* 87 (2000) 2297.
- [14] Cuiling Gong, D.P. Hart, *J. Acoust. Soc. Am.* 104 (1998) 2675–2682.
- [15] K.S. Suslick, *Sonochemistry: a physical perspective*, AIP Conference Proceedings, Nonlinear Acoustics at the Turn of the Millennium, Vol. 524, 2000, pp. 95–104.
- [16] K.S. Suslick, *Sonochemistry*, *Science* 247 (1990) 1439–1445.
- [17] J.A. Akintunde, *Phys. Status Solidi. A* 179 (2000) 363.
- [18] L. Brus, *J. Chem. Phys.* 90 (1986) 2555.
- [19] Y. Wada, H. Kuramoto, J. Anand, T. Kitamura, T. Sakata, H. Mori, S. Yanagida, *J. Mater. Chem.* 11 (2001) 1936.
- [20] Yu, T. Isobe, M. Senna, *Mater. Res. Bull.* 30 (1995) 975.
- [21] D.J. Lockwood, A. Wang, B. Bryskiewicz, *Solid State Commun.* 89 (1994) 587.
- [22] K. Ernst, A. Belaidi, R. Konenkamp, *Semicond. Sci. Technol.* 18 (2003) 475.
- [23] A. Vogel, W. Lauterborn, R. Timm, *J. Fluid Mech.* 206 (1989) 299.
- [24] K.S. Suslick (Ed.), *Ultrasound: Its Chemical, Physical and Biological Effects*, VCH, Weinheim, 1988.
- [25] R.S. Singh, C.A. Grimes, E.C. Dickey, *Mater. Res. Innov.* 5 (2002) 178.

# Ordered CdTe/CdS Arrays for High-Performance Solar Cells

DAVID ZUBÍA,<sup>1,3</sup> CESAR LÓPEZ,<sup>1</sup> MARIO RODRÍGUEZ,<sup>1</sup>  
AREV ESCOBEDO,<sup>1</sup> SANDRA OYER,<sup>1</sup> LUIS ROMO,<sup>1</sup> SCOTT ROGERS,<sup>1</sup>  
STELLA QUIÑÓNEZ,<sup>1</sup> and JOHN McCLURE<sup>2</sup>

1.—Department of Electrical and Computer Engineering, University of Texas at El Paso, El Paso, TX 79968, USA. 2.—Department of Materials and Metallurgical Engineering, University of Texas at El Paso, El Paso, TX 79968, USA. 3.—e-mail: dzubia@utep.edu

The deposition of uniform arrays of CdTe/CdS heterostructures suitable for solar cells via close-spaced sublimation is presented. The approach used to create the arrays consists of two basic steps: the deposition of a patterned growth mask on CdS, and the selective-area deposition of CdTe. CdTe grains grow selectively on the CdS but not on the SiO<sub>2</sub> due to the differential surface mobility between the two surfaces. Furthermore, the CdTe mesas mimic the size and shape of the window opening in the SiO<sub>2</sub>. Measurements of the current density in the CdTe were high at 28 mA/cm<sup>2</sup>. To our knowledge, this is the highest reported current density for these devices. This implies that either the quantum efficiency is very high or the electrons generated throughout the CdTe are being concentrated by the patterned structure analogous to solar concentration. The enhancement in crystal uniformity and the relatively unexplored current concentration phenomenon could lead to significant performance improvements.

**Key words:** Solar cells, cadmium telluride, epitaxy, lithography

## INTRODUCTION

Cadmium telluride (CdTe) is a good absorber layer for solar cells with a predicted efficiency of 29% due to its near-optimal direct bandgap of 1.5 eV and large optical absorption ( $>10^4$  cm<sup>-1</sup>) above the bandgap.<sup>1,2</sup> This promise has generated much research interest in thin-film CdTe/CdS photovoltaic modules. Encouraging early work in the late 1970s on cells prepared by epitaxial growth of CdS on *p*-type single-crystal CdTe exhibited a conversion efficiency of 11.7%.<sup>3</sup> However, a significant challenge was the high density of defects due to the lattice ( $\sim 10\%$ ) and thermal mismatch between CdS and CdTe. Because of this challenging problem, much of the effort focused instead on polycrystalline thin films due to their promise for creating an acceptable tradeoff between efficiency and low-cost manufacturing.<sup>4</sup> However despite extensive research, the highest reported efficiency for CdTe

solar cells is  $<17\%$  and has not improved much in over 13 years.<sup>5,6</sup>

Due to the difficulty of performing scientific study on random polycrystalline thin films much of the research has utilized a semi-empirical approach, and this has hampered advancement of fundamental understanding. Many studies have identified various efficiency loss mechanisms,<sup>7,8</sup> one of which is the nonuniformity of the crystals in polycrystalline films.<sup>2,9-12</sup> In this paper, the phrase “random polycrystalline” refers to the situation in which the morphology and crystal quality of the grains are uncorrelated or only slightly correlated. The term “nonuniformity” describes a wide variation in the morphology and crystal quality of the grains.

The structure of polycrystalline films has hampered technological development and scientific study in at least two ways. First, the grain boundaries create interdependencies between various parts of the device because they form an interconnected network within the thin film. This makes isolated study and development of each component of the device very difficult.<sup>10</sup> Grain boundaries give

(Received January 6, 2007; accepted June 5, 2007;  
published online September 19, 2007)

rise to a host of issues including; enhanced migration of dopants,<sup>8,10</sup> device shunting,<sup>13</sup> and high recombination velocities due to unpassivated surfaces. For example, isolated study and development of the back-contact is very difficult due to the effect that back-end processing has on the doping of CdTe in the bulk and at the CdTe/CdS interface.<sup>14</sup> Moreover, the enhanced migration of copper through grain boundaries has also been associated with device instability.<sup>15</sup>

Second, it is well known that inhomogeneity in cell electrical characteristics results in efficiency losses.<sup>16</sup> Nonuniformity is highly detrimental for two reasons. One is that the optimum performance of all CdTe grains is not achieved since each grain is different in size and shape. A second and more-insidious reason is that, because the diode current–voltage characteristic is exponential, poorly performing CdTe grains act as electrical loads to a relative large number of neighboring grains. This makes the device exponentially sensitive to small variations in localized film parameters.<sup>11</sup>

The need therefore exists to decouple the various parts of the device so that significant scientific understanding and technological development can be achieved. Recently, our group demonstrated a method to selectively grow CdTe, which we call the ordered polycrystalline approach.<sup>9</sup> Using this approach, we have now grown dense arrays of uniform CdTe mesas on CdS. We believe that this ordered structure has several advantages over random polycrystalline films. One important advantage is that precisely placed, uniform crystals and grain boundaries will decouple the interactions between different parts of the cells. This will enable the independent optimization of the various components of the cell. Another advantage is that, because the array will be highly uniform, losses attributed to nonuniformity will be greatly reduced.

In this paper, we present results of using the ordered polycrystalline approach to create dense arrays of CdTe/CdS heterostructures suitable for solar cells. The method shows promise for improving the morphological uniformity of the crystal grains. The fabrication procedure is explained. Results from various experiments that illustrate the relationship between processing and structure are presented. Future work will focus on modeling and measuring the electrical characteristics of the photodiode arrays.

## EXPERIMENTAL DETAILS

The fabrication procedure for the CdTe arrays consists of three fundamental steps: the deposition of CdS,<sup>9</sup> the deposition and patterning of a dielectric layer, and the selective-area deposition of CdTe. The polycrystalline CdS thin films were grown using a chemical-bath deposition method on commercially obtained indium tin oxide (ITO)-coated glass substrates. The chemical bath consisted of an aqueous

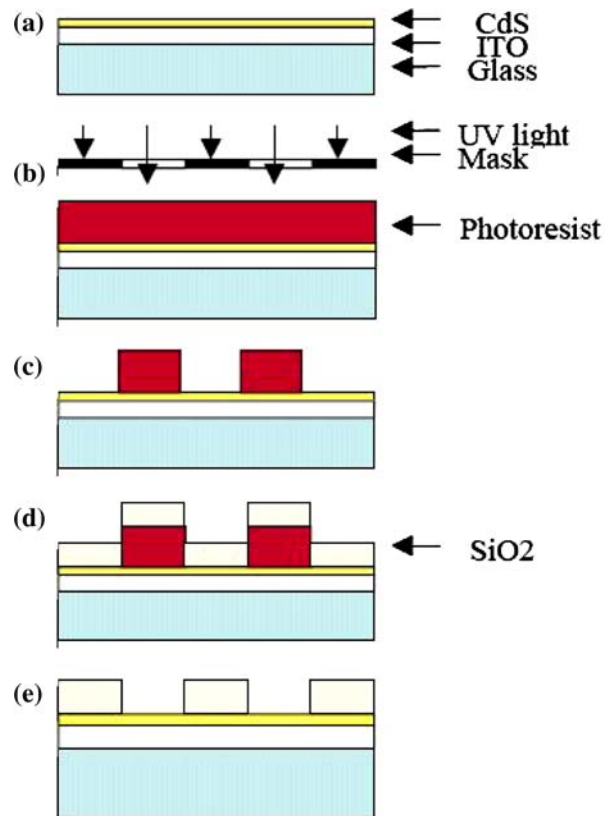


Fig. 1. Illustration of the process sequence for a negative photoresist SiO<sub>2</sub> substrate patterning: (a) glass/ITO/CdS substrate, (b) negative photoresist applied to the substrate and UV light exposure through the photomask, (c) sample after exposure and photoresist development, (d) silicon dioxide deposition, and (e) final structure following lift-off procedure.

solution of cadmium acetate, ammonium acetate, ammonium hydroxide, and thiourea in molar concentrations of 0.0007, 0.01, 0.15, 0.0012, respectively. The bath solution was heated to 88°C for a total time of 30 min. The thicknesses of the CdS films were 85 nm as measured by interferometry and scanning electron microscopy (SEM).<sup>17</sup>

The next step is the deposition and patterning of a SiO<sub>2</sub> layer. Dielectric layers such as SiO<sub>2</sub> and Si<sub>3</sub>N<sub>4</sub> have been shown to be effective growth mask layers for selective-area deposition.<sup>18,19</sup> In this study, a lift-off process was used to create the patterned SiO<sub>2</sub> layers on CdS. The basic process sequence is shown in Fig. 1. First, the CdS/ITO/glass substrates are coated with a negative photoresist and then patterned using a standard lithography process. The thickness of the photoresist was approximately 1,000 nm. Next, a 600-nm-thick layer of SiO<sub>2</sub> is deposited using electron-beam evaporation at 10<sup>-6</sup> Torr. After the SiO<sub>2</sub> film deposition, the sample was annealed at 145°C for 30 min to improve adherence of the SiO<sub>2</sub> to the CdS. Finally the photoresist was stripped to complete the lift-off process. The result is a patterned SiO<sub>2</sub> layer (growth mask) on CdS as shown in Fig. 2.

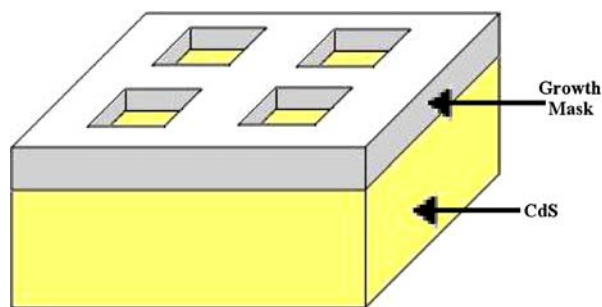


Fig. 2. Patterned dielectric layer (growth mask) on CdS. The ITO/glass is not shown in this figure.

The final step is the deposition of CdTe on the patterned sample using close-spaced sublimation.<sup>18,19</sup> In this study, the thickness of the CdTe was varied from 300 nm to 1,000 nm to study the evolution of the CdTe growth. Moreover, a lithographic mask with five regions corresponding to window opening sizes of 1, 1.5, 2, 2.5, and 3  $\mu\text{m}$  was used to study the effect of the patterning size on the selectivity of the CdTe growth. For each region, the pitch of the pattern was twice the window opening size. For example, the region with the window opening size of 3  $\mu\text{m}$  had a pitch of 6  $\mu\text{m}$ .

The temperature of the substrate ranged from 490°C to 520°C while the temperature of the source varied from 540°C to 570°C, always keeping a 50°C temperature difference between the source and substrate. The distance between the source and the substrate was set to 0.7 mm using glass spacers. The pressure was nominally 1 Torr with 5/6 partial pressure of He and 1/6 partial pressure of O<sub>2</sub>. The deposition time varied depending on the desired CdTe thickness.

## RESULTS AND DISCUSSION

Figure 3 is a plan-view SEM image of CdTe at the boundary between the patterned and planar growth areas of the sample. This figure clearly shows the effect of the patterned mask on the CdTe deposition; the area without patterning yields a random structure, whereas the patterned area results in an ordered array. The CdTe grows selectively on the CdS but not on the SiO<sub>2</sub> due to the differential surface mobility between the two surfaces. This is consistent with the report by Zhang and Bhat of CdTe grown on Si and GaAs.<sup>20</sup>

Figure 4 shows SEM images of selective-area depositions of CdTe, illustrating the effect of CdTe thickness and patterning size. Each column represents a distinct CdTe thickness of either 300, 750 or 1,000 nm from left to right. Each row corresponds to a different patterning pitch of 2, 3, 4, 5 or 6  $\mu\text{m}$ , respectively, from top to bottom. The magnification of all the images is the same, so differences can be appreciated better. In general, all the samples displayed good growth selectivity. However, note that

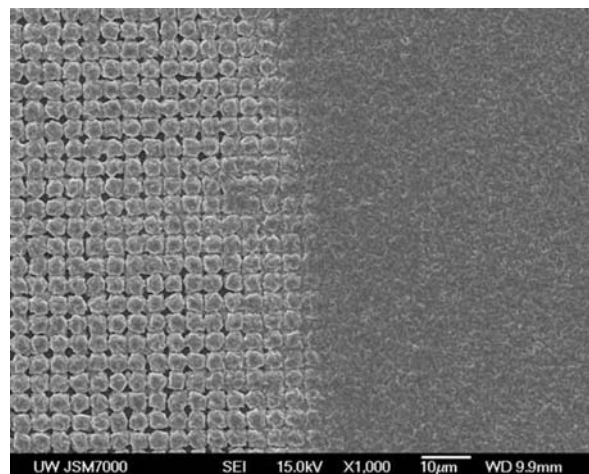


Fig. 3. Plan-view SEM image of the boundary between the patterned growth (left) and planar growth (right) of CdTe. This image clearly shows the effect of the patterned growth mask.

the samples with a pitch of 6  $\mu\text{m}$  showed significantly more superfluous nucleation of CdTe on SiO<sub>2</sub>, indicating that the diffusion length of Cd and Te adatoms is probably around 3  $\mu\text{m}$  (one-half the pitch). As expected, the samples with the densest films were the ones with smaller pitch and thicker CdTe layer. In fact, the sample with 1,000 nm of CdTe on a 2  $\mu\text{m}$  pitch shows the onset of coalescence between the CdTe islands. Moreover, the samples with the pitch of 2  $\mu\text{m}$  were the most uniform in size and shape.

Another interesting observation in this study was that the shape of the CdTe islands mimicked the shape of the opening in the SiO<sub>2</sub>. This is demonstrated in Fig. 5, where the diamond shape of the patterned SiO<sub>2</sub> was mimicked by the CdTe. Research on microlenses has shown that highly nonplanar features free from faceting can be produced through shadow-masked epitaxy. In this research, the shape of the lenses is controlled by the geometrical parameters of the mask.<sup>21</sup> The mask appears to alter the flux of the deposited material and this in turn governs the shape of the growing crystal, overriding the energetics of the crystallographic facets. This is very important since it shows that the ordered polycrystalline method can be used to control the size and shape of CdTe crystals.

Finally, a cross-sectional view of a CdTe island selectively grown on patterned SiO<sub>2</sub>/CdS/InSnO/glass with a 4  $\mu\text{m}$  pitch is shown in Fig. 6. A sample with a 2  $\mu\text{m}$  pitch with 300 nm of SiO<sub>2</sub> was contacted using a nitric-phosphoric etch followed by CdCl<sub>2</sub> treatment<sup>17</sup> and application of a graphite paste and anneal at 150°C for 30 min in air. Contrast in the CdTe is caused by the orientational differences of different crystal grains. Orientation contrast can also be seen in the InSnO layer, demarking crystal grains. Surface passivation of the CdTe grains is known to be an important processing

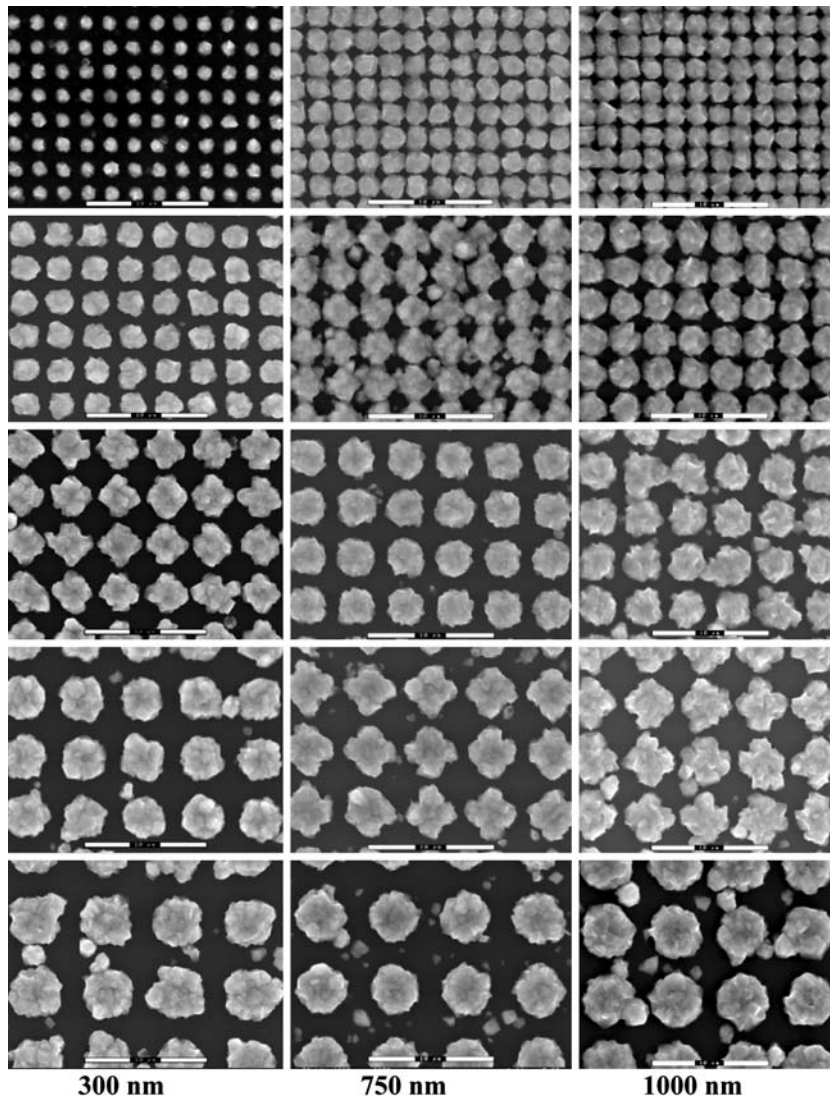


Fig. 4. Plan-view SEM images of ordered arrays of CdTe on CdS. The size of the patterning increases from top to bottom while the thickness of the CdTe increases from left to right. The smaller patterning sizes yield more uniform growth. All scale bars represent 10  $\mu\text{m}$ .

parameter of high-performance cells. Usually this is accomplished by heat treating the films in an oxygen-containing environment to create a tellurium-oxide surface layer. However, the tellurium-oxide layer has been suspected of being unstable. The proposed patterned structure will increase the interface area between the CdTe and  $\text{SiO}_2$  so the nature of this interface is very important. It is speculated that the  $\text{SiO}_2$  has the potential to passivate the CdTe surface similar to the way it passivates silicon in microelectronics.

The short-circuit current density of the sample in Fig. 6 was measured under AM1.5 conditions and found to be  $7 \text{ mA/cm}^2$  over an area of  $0.7 \text{ cm}^2$  ( $4.9 \text{ mA}$  was measured on a  $0.7 \text{ cm}^2$  contact). However, since the CdS/CdTe interface covers only one-fourth of the area (a simple geometrical calculation shows this), the actual current density through each of the windows was  $28 \text{ mA/cm}^2$ . To our knowledge,

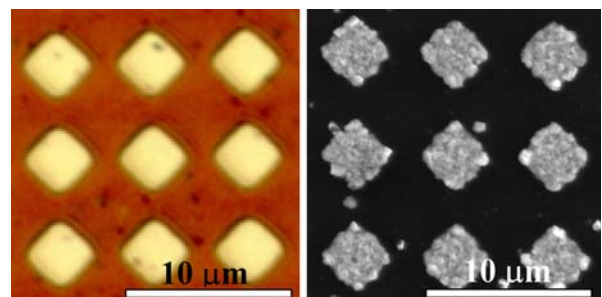


Fig. 5. Optical microscope images of a patterned  $\text{SiO}_2$  sample (left) and an SEM image of selective-area growth of CdTe (right). In both images, the features are diamond shaped, indicating that the growth mimics the shape of the pattern. Scale bars represent 10  $\mu\text{m}$ .

this is the highest reported current density for CdTe/CdS solar cells. This very high current density implies that the quantum efficiency is very high

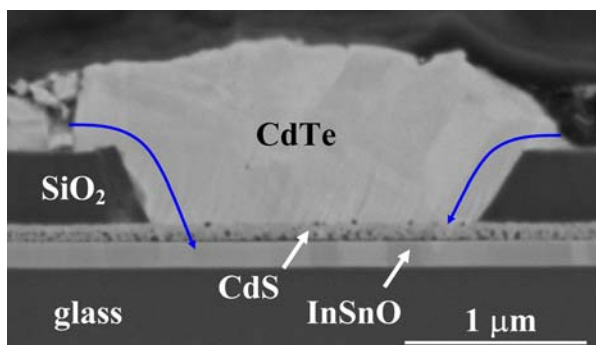


Fig. 6. Cross-sectional SEM image of a patterned CdTe/CdS heterostructure on an ITO/glass substrate. The arrows bending downward indicate a suspected funneling effect of the current. This current-concentrating effect could lead to performance improvement analogous to solar concentration.

and/or electrons are being generated throughout in the CdTe and then funneled through the SiO<sub>2</sub> openings as indicated by the blue arrows in Fig. 6. The combined effects of uniform crystals and current concentration could lead to significant performance gains.

## CONCLUSIONS

Structure, crystal perfection, and doping in semiconductors are the principal parameters that affect device characteristics. This is also true in polycrystalline solar cells. However, controlling the doping profile and structure uniformly in polycrystalline thin films is difficult due to the random nature of grains and grain boundaries. This prevents the desired optimum CdS/CdTe structure and doping from being achieved. The best that can be obtained is an average profile and structure with some degree of statistical nonuniformity.

The ordered photodiode array approach was proposed to overcome the problems inherent to random polycrystalline thin films due to the dramatic improvement in crystal uniformity. The approach consists of two basic steps: the deposition of a SiO<sub>2</sub> patterned dielectric layer and the selective-area deposition of CdTe. CdTe grains grow selectively on the CdS but not on the SiO<sub>2</sub> due to the differential surface mobility between the two surfaces. Furthermore, the CdTe mesa's size and shape mimics the shape of the window in the SiO<sub>2</sub>.

Measurements of the current density in the CdTe were high at 28 mA/cm<sup>2</sup>. This implies that either the quantum efficiency is very high or the electrons generated throughout the CdTe are being funneled through the SiO<sub>2</sub> opening. The former case implies very high crystal and interface quality. The latter phenomenon could lead to performance

improvements due to the current concentration that is taking place analogous to solar concentration.

Interestingly, the ordered polycrystalline technique can be used for indexing an array of polycrystalline grains of CdTe, which could be treated as separated diodes. By creating the indexed array, studies on individual grains can be explored such as doping concentration, defect density, *IV* and *CV* characterization for individual diodes, and the current funneling effect mentioned above. In addition, the indexing technique could be used potentially to study the effects of CdCl<sub>2</sub> treatment and Cu doping on each grain. In summary, the ordered polycrystalline approach has great potential for advancing the scientific understanding of CdTe-based solar cells and increasing their efficiency. The approach is generic and could be applied to other material systems.

## ACKNOWLEDGEMENTS

Partial support for this work was provided by generous grants from the Texas Instruments Foundation and the National Renewable Energy Laboratory (Contract #ACQ-4-33623-02).

## REFERENCES

1. R. Birkmire and E. Eser, *Annu. Rev. Mater. Sci.* 27, 625 (1997).
2. K. Durose, P.R. Edwards, and D.P. Halliday, *J. Cryst. Growth* 197, 733 (1999).
3. S. Ikegami, N. Nakayama, H. Matsumoto, K. Yamaguchi, H. Uda, H. Taniguchi, M. Yoshida, and T. Yamashita, *Natl. Tech. Rep. (Japan)* 24, 361 (1978).
4. Robert W. Birkmire, *Sol. Energ. Mater. Sol. Cell.* 65, 17 (2001).
5. R. Noufi and K. Zweibel, World Conference on Photovoltaic Energy Conversion, Waikoloa, Hawaii, May 9, 2006.
6. D. Zubia, unpublished.
7. J.R. Sites, *Sol. Energ. Mater. Sol. Cell.* 75, 243 (2003).
8. H.C. Chou, et al., *Mater. Chem. Phys.* 43, 178 (1996).
9. J. Terrazas, A. Rodriguez, C. Lopez, A. Escobedo, F. Kuhlmann, J. McClure, and D. Zubia, *Thin Solid Films* 490, 146 (2005).
10. A. Rohatgi, et al., *13th NREL Photovoltaics Program Review* 353, 368 (1996).
11. V.G. Karpov, A.D. Compaan, and D. Shvydka, *Appl. Phys. Lett.* 80, 4256 (2002).
12. V.G. Karpov, A.D. Compaan, and D. Shvydka, *Phys. Rev. B* 69, 045325 (2004).
13. D. Zubia (Thesis, University of Texas at El Paso, 1993).
14. D.H. Levi, L.M. Woods, D.S. Albin, T.A. Gessert, D.W. Niles, A. Swartzlander, D.H. Rose, R.K. Ahrenkiel and P. Sheldon, *Twenty-Sixth Photovoltaic Specialist Conference*, Anaheim CA, September 30–October 3, 1997, pp. 351–354.
15. K.D. Dobson, I. Visoly-Fisher, G. Hodes, and D. Cahen, *Sol. Energ. Mater. Sol. Cell.* 62, 295 (2000).
16. P.N. Gibson, M.A. Baker, E.D. Dunlop, M.E. Ozan, D. Lincot, M. Froment, and G. Agostinelli, *Thin Solid Films* 387, 92 (2001).
17. A. Rodriguez (Thesis, University of Texas at El Paso, 2005).
18. J. Terrazas (Thesis, University of Texas at El Paso, 2005).
19. C. Lopez (Thesis, University of Texas at El Paso, 2005).
20. R. Zhang and I. Bhat, *J. Electron. Mater.* 29, 765 (2000).
21. G.M. Peake, S.Z. Sun, and S.D. Hersee, *J. Electron. Mater.* 26, 1134 (1997).